NOVEL ANTIFREEZE PROTEIN CONSTRUCTS FOR IMPROVED ACTIVITY

ÖZGE CAN

Bachelor of Science in Chemical Engineering

Ege University

June 2001

Master of Science in Chemical Engineering

Izmir Institute of Technology

June 2004

Submitted in partial fulfillment of requirements for the degree

DOCTOR OF ENGINEERING IN CHEMICAL ENGINEERING

at the

CLEVELAND STATE UNIVERSITY

December 2008

This dissertation has been approved for the Department of Chemical Engineering and the College of Graduate Studies by

_____

Dr. Nolan B. Holland
Department of Chemical Engineering
Cleveland State University

_____

Date

_____

Dr. Orhan Talu
Department of Chemical Engineering
Cleveland State University

_____

Date

_____

Dr. Surendra N. Tewari
Department of Chemical Engineering
Cleveland State University

_____

Date

_____

Dr. Rolf Lustig
Department of Chemical Engineering
Cleveland State University

_____

Date

_____

Dr. Jacqueline Vitali
Physics Department
Cleveland State University

_____

Date

ACKNOWLEDGMENTS

I would like to express my deepest gratitude to my academic advisor Dr. Nolan B. Holland for his invaluable help, support and understanding during my thesis study. I am grateful for his patience, creative advice and our brain storming discussions even at our long road trips to the scientific conferences. He taught me to develop skills to lead and perform a successful research which I am sure that will help me throughout my career. I have learned too much from him and it has been a pleasure and great experience working under his supervision.

I would like to thank Dr. Sakae Tsuda at the Hokkaido National Industrial Research Institute, Japan for kindly providing type III antifreeze protein genes.

I would like to thank Dr. Art Heuer at the Case Western Reserve University for kindly providing us the nanoliter osmometer and to Mr. Alan McIlwain for his generous technical support related to the osmometer.

I would like to thank Dr. Mark Ruegsegger at the Ohio State University for his valuable contributions to the bioconjugation studies.

My sincere thank to Dr. Orhan Talu for his guidance, support and precious suggestions through the course of my research as well as during my teaching assistance for unit operations laboratory. I would like to acknowledge my dissertation committee members Dr. D.B. Shah, Dr. Surendra N. Tewari, Dr. Rolf Lustig and Dr. Jacqueline Vitali for being on my committee and for their valuable contributions to my thesis study.

I would like to thank Ali Kaddah, Jim Barker, David Epperly for their generous help, they were always there when I needed them.

I would like to thank all my colleagues, Sarah Milliron, Pavani R. Bejjanki, Suresh Essampally, Ali Ghoorchian and James Cole for their friendship and valuable insights. I also would like to thank our summer intern Mark Nasca for his help and valuable effort in the laboratory for the last two summers.

I would like to give my special thanks to Ms. Becky Laird and Ms. Darlene Montgomery for their constant motivation and help and for making my time at Cleveland State University an unforgettable one.

Finally, I would like to send my special gratitude and love to my family, and especially to my wife and colleague, Dr. Asli Ertan Can, for being there with me and for her endless love and great support.

NOVEL ANTIFREEZE PROTEIN CONSTRUCTS FOR IMPROVED ACTIVITY

ÖZGE CAN

ABSTRACT

Many organisms are exposed to subzero temperatures in nature and can survive these temperatures by the effect of antifreeze proteins (AFPs), which inhibit ice crystal growth and change the morphology of ice crystals. Although the effects of these proteins, such as recrystallization inhibition, ice growth inhibition, and crystal habit changes, are known, a conclusive description of the protein-ice crystal interaction including interaction energy, surface coverage, and lifetime of adsorbate has been elusive.

In this study, different antifreeze protein constructs are designed and expressed such that they can be conjugated to polymers to increase the thermal hysteresis activity especially at low concentrations. Trimers of these proteins are also constructed using a foldon domain attached to their C-terminus. New constructs of type I and type III antifreeze proteins yield significantly higher thermal hysteresis activities than the native protein.

Furthermore, we determine the binding equilibrium constant for a type III fish antifreeze protein and the relationship between thermal hysteresis and surface coverage for this protein. This is possible using experimental data from a two-domain antifreeze protein and its related single domain protein. The classical Langmuir isotherm is used to

describe the equilibrium exchange of the single domain type III AFP molecules at the ice crystal surface, while a modification of the Langmuir isotherm is derived to describe the adsorption of the two-domain AFP. Because the protein adsorption is governed by different isotherm relationships, there are two independent data sets allowing the determination of the two unknowns of surface coverage and binding energy. The data yield a binding equilibrium constant of 1.9 mM^{-1} for the type III AFP-ice interaction. The analysis results in a relationship between surface coverage and thermal hysteresis, as well as kinetic equations of the adsorption of the proteins onto the ice surface.

TABLE OF CONTENTS

LIST OF FIGURES

LIST OF ABBREVIATIONS

AFP	Antifreeze protein
AFGP	Antifreeze glycoprotein
RD3	Two domain type III AFP from Antarctic eel pout
RD3N	N-domain RD3
RD3CCys	C-domain RD3 and its linker having a cysteine at the N-terminus
PAA	Linear chain polymer polyallylamine
RD3CCysrxn	RD3CCys reacted with PAA
foldon	Trimerization domain from bacteriophage T4 fibritin
linker	9 residue linker used in foldon constructs
RD3Nfoldon	RD3N trimer
T1D	Type I AFP composed of 5 repeats of 11 amino acids
T1N	Genetically modified version of T1D
T1Nrxn	T1N reacted with PAA
T1Dfoldon	T1D trimer
EGFP	Green fluorescence protein
nfe8EGFPCys	One-domain type III AFP with EGFP and a cysteine
nfe8EGFPCysrxn	nfe8EGFPCys reacted with PAA
HPLC	High pressure liquid chromatography
PCR	Polymerase chain reaction
θ	Surface coverage
K	Equilibrium constant
C	Protein concentration in solution
ΔG^o	Gibbs free energy
R	Universal gas constant
T	Temperature
k_a	Adsorption rate constant
k_d	Desorption rate constant
t	Time
tk_d	Dimensionless time

CHAPTER I

INTRODUCTION

1.1 Overview

Many organisms are exposed to subzero temperatures in nature. There are various places in which this exposure may occur at night and also at high altitudes in equatorial regions. Fish in the Antarctic Ocean have been living for approximately 25 million years and the important fact is that they have been showing rapid reproduction and growth indicating how well they have adapted to cold environment [1]. An interesting and complex adaptation to life in those challenging environments is the expression of antifreeze proteins (AFPs) that inhibit ice crystal growth [2]. The nucleation of ice crystals in cells and tissues will typically occur first in the extracellular fluid before intracellular fluids freeze. This naturally protects cells and tissues from freezing at temperatures slightly below the freezing point [3].

Antifreeze glycoproteins were first found in Antarctic teleost fish 30 years ago by Art DeVries and his colleagues. Soon after this discovery, several other species of antifreeze proteins were identified [4]. Antifreeze proteins allow organisms to survive at

subzero temperatures or at temperatures lower than the freezing point of their bodily fluids by inhibiting ice crystal growth. This phenomenon gave rise to many studies in order to gain more information as to how they prevent the ice crystal growth [5]. There have been several theories some of which have been experimentally proven and some still remain as a question [6]. However the exact mechanism is not known, the major role of antifreeze proteins in ice binding is suggested as hydrophobic interactions, hydrogen bonding and van der Waals interactions which are required for the optimal surface-surface complementarity [6-9]. AFPs bind to specific planes of the ice surface, which in turn stops subsequent growth at temperatures below the colligative melting point. The interaction of AFPs with the ice crystal causes thermal hysteresis, which is a difference between freezing and melting temperatures. AFPs also prevent the redistribution of the water between ice crystals and the solution referred to as ice recrystallization [10].

1.2 Significance and applications

There are numerous situations in which appropriate preservation of the tissues or organs is needed to provide sufficient time for transplantation. Heart and liver transplantation for example are traditional surgical techniques for the treatment of end stage organ failures [11, 12]. The storage time for a donated heart or liver is limited to 5 to 12 hours with current preservation techniques. This does not provide sufficient time for optimizing donor-recipient tissue matching and causes significant challenges in the organ transportation process [13]. Additional promise for the use of cellular therapy for treatment of heart disease often requires long term storage of cells and tissues. When cellular solutions freeze, cryopreservation becomes unsuitable due to damage caused by

ice formation that disrupts cell membranes or causes osmotic stress by naturally increasing salt concentration in the solution [11]. Thus, it is important to investigate the storage (cryopreservation) of cells, tissues, blood, and organs for increasing the success in the treatment of cardiovascular and other diseases [2, 10, 11, 14, 15]. One promising approach in improving the survival of cells after cryopreservation is by using antifreeze proteins as an additive.

In addition to the cryogenic storage of cells and tissues, there are also various places in petrochemical processes in which the effective heat transfer is required to reduce the cost of the processes. Heat transfer equipments such as heat exchangers are the heart of the petrochemical processes and the effectiveness of such processes is significantly dependent on the efficient heat transfer throughout the various petrochemical systems.

Using ice slurry systems is of great interest because of the latent heat phenomena of the ice that is observed during ice melting [16-25]. However, it is crucial to overcome the difficulties observed during transportation of ice slurry such as the ice crystal growth which can cause clogging of pipelines reducing their effectiveness [21, 26, 27]. It is extremely important to find new functionally thermal fluids or the modifications of the existing ones to overcome these challenges [23, 24, 28-30]. One promising approach in improving the utilization of ice slurry systems is using antifreeze proteins (AFPs) as an additive to obtain an efficient heat transfer fluid for a particular application in the petrochemical industry [19, 21, 22, 25, 31, 32].

Creating superior AFP constructs which would have increased thermal hysteresis activities especially at low concentrations would make it easier and economical to use

them as an additive in these systems. In the light of the developing bioconjugation technology, designing novel synthetic materials that are suitable to use in such applications is very promising.

1.3 AFP structures

Antifreeze proteins (AFPs) are ice-binding proteins found in various organisms (such as fish, insects, and plants) exposed to freezing conditions [9]. Although AFPs are structurally diverse, they typically present a relatively large, flat and slightly hydrophobic surface for binding to ice [9, 33-36]. Amino acid composition varies considerably both between species and sometimes within species. Also, they have a wide range of molecular weights from 5 kDa for a type I fish AFP to 36 kDa for AFP from winter rye [37]. Their structural diversity together with an inability to examine the AFP-ice interaction directly, has made structure function studies difficult [9]. AFPs generally display well defined folds and conformations. Their structures range from the single α-helices of type I AFP, to the globular types II and III AFPs (Figure 1.1). Type I AFP shows striking regularities in the positioning of suspected ice-binding motifs, while types II and III AFPs show no obvious repetitive components on their surfaces. Indeed, these proteins appear to share little in common other than their defining characteristic of ice-growth inhibition. The type I AFP is a single α-helical fold which is slightly curved amphiphilic fold. In this helical structure, there is a large proportion of alanine residues [38]. Compared to the other AFPs, there is a more detailed structure for the type III AFPs. Ice binding sites are readily determined by site directed mutagenesis and found to

be relatively hydrophobic [39]. Thus, it is important to note that hydrophobic residues on the side chain play important role as well as their packing strength.

Type III AFP is a 7 kDa globular protein found in Antarctic eel or ocean pouts and is comprised of around 65 amino acids [35]. As a result of high resolution X-ray and NMR studies, it is found that type III AFP has a compact fold with several β strands and one helical turn and a flat hydrophobic surface to bind to the ice crystal [3, 40-42]. Ice binding models of type III AFP suggest that this protein adsorbs to the prism plane of the ice crystal [43, 44]. There have been various isoforms of this protein studied. One of them, RD3, is unique because it is comprised of two type III AFP domains connected by flexible nine-residue linker [45]. The two domains are free to bind to the ice surface independently [46], resulting in larger thermal hysteresis than the single domain proteins at low concentrations [47].

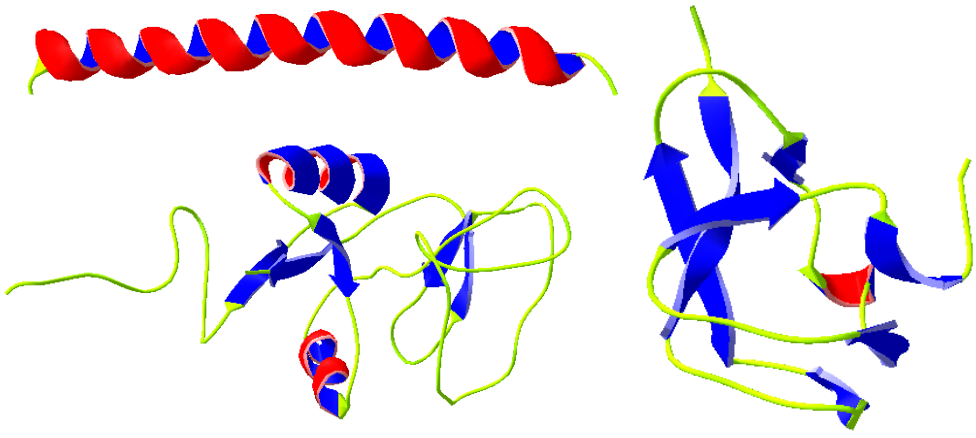

Figure 1.1. Antifreeze protein structures. Counter clockwise from top left: Type I AFP from winter flounder, Type II AFP from sea raven, and Type III AFP from ocean pout. PDB IDs are 1WFA [36], 2afp [48] and 1ucs [49], respectively. Figures were produced using DeepView/Swiss-PdbViewer software program [50].

1.4 Current trends on AFP research

Even though AFPs comprise a structurally diverse class of proteins, they have in common the ability to bind to ice and inhibit its growth. This action at ice-solution interface leads to a lowering of the nonequilibrium freezing point below the melting point, referred to as thermal hysteresis. Based on the assumption that AFPs interact with ice through adsorption to specific planes, this would indicate that as long as the supercooling is below a critical value, there will be sufficient amount of time for the AFP to align along the energetically favorable direction on the appropriate crystal plane. There might however be AFP molecules adsorbing to the surface occasionally but these will not be able to completely inhibit crystal growth [29]. AFPs are incorporated within the ice when it freezes because of their affinity for its surface. These AFPs can act as recrystallization inhibitors even in the frozen state by inhibiting the growth of large ice crystals at the expense of small ones, particularly when ice approaches the melting temperature and becomes more fluid [51]. Recrystallization takes place most rapidly at temperatures where ice slurries are used that are just below freezing and during warming from the glassy state. Extremely low concentrations (100 μg/L) of AFP are effective in inhibiting ice recrystallization [21]. Recrystallization inhibition has been shown to occur in the presence of AFPs performed [2, 21, 22, 52-55].

There have been several studies in the literature in which they have investigated the ice binding mechanism of the AFPs [41, 56-62]. At the first glance it seemed like hydrophilic residues on the surface of the protein were causing the ice binding activity because when they changed the hydrophilic sites using site directed mutagenesis they obtained 90% loss of activity and they thought the mismatch between the ice binding site

of the protein and the ice caused reducing the strength of the hydrogen bond [56]. Although hydrogen bonding was thought to be the primary ice binding mechanism previously [43], there have been other factors such as steric complementarity of the protein, van der Waals interactions at the ice protein interface, etc. It appears that polar side chains of the protein are not surface accessible so that they can not form efficient hydrogen bonds. Another factor inhibiting hydrogen bonding is that limited amount of water molecules in the ice surface have also limited ability to find protein molecules in the ice surface to hydrogen bond.

Other research groups suggested that this loss of activity was the result of the steric interference with the docking of the AFP and the ice [4]. Effects of steric mutations were also investigated by Deluca et al., in 1998 by replacing the Ala16 with the larger side chains and they found that there are multiple causes for the loss of the thermal hysteresis activity and the ice morphology including the tightness of the side chain packing and the rigidity of the ice binding surface. These studies were extended by other groups and the major role in ice binding was proposed as hydrophobic interactions, hydrogen bonding and van der Waals interactions which are required for the optimal surface-surface complementarity [7, 8].

Chao et al. studied the effect of mixing different types (type I, type II and type III) of AFPs on the thermal hysteresis activity. Mixtures of these proteins produced different ice crystal morphologies but did not affect the thermal hysteresis activity. They suggested that these proteins are independently active and do not require protein-protein interactions for binding to the ice [63].

Kristiansen et al. investigated the effect of salt concentration in the solution on the thermal hysteresis activity. They suggested that the salts present in the solution decreases the solubility of the proteins around the ice crystal leading to the accumulation of the AFPs available for adsorption. This effect is explained by so-called salting out effect [64]. However, the ability of the proteins to bind to the ice crystal in the insoluble stage remains unclear.

1.5 AFPs in cell/organ preservation

There are several studies in which they have used antifreeze proteins in cell or organ preservation. Chao et al. investigated the inflIuence of type III AFP mutants on hemolysis of cryopreserved red cells [14]. They used different types of AFPs which were preliminarily purified and their antifreeze activities were measured as thermal hysteresis. Then, they collected human blood from healthy volunteers which was processed to obtain red cells then were cryopreserved. Samples were thawed in air at room temperature, which leads to very slow warming. They concluded that the relative thermal hysteresis activity of the type III protein and the mutant directly correlates with their capacity to inhibit ice recrystallization and to protect red cells during a freeze-thaw cycle. They also supported their hypothesis by another study performed by Knight and Duman, 1986, that inhibition of ice recrystallization by AFPs can help cells survive during freezing and thawing [54].

Amir et al. in 2003 were first to demonstrate successful subzero cryopreservation of mammalian hearts using AFP I and AFP III in an in vivo heterotopic heart transplantation model [13]. All hearts preserved at subzero temperatures using AFP I or

AFP III survived showing excellent viability. They concluded that subzero preservation of mammalian hearts using type I and type III AFPs is feasible.

In another study performed by Amir et al. in 2004, they aimed to evaluate whether lowering the temperature can increase the preservation time of a rat heart and whether prolonged subzero preservation using AFPs improves the viability of harvested hearts compared to hearts preserved using standard techniques at 4°C [12]. They concluded that their results show a clear benefit of subzero nonfreezing storage of rat hearts using AFPs. They were able to demonstrate that using AFPs improves survival in subzero preservation of rat hearts.

1.6 AFPs with increased thermal hysteresis activities

In regard to increasing thermal hysteresis activity, superior AFPs have been investigated by a number of researchers. HPLC6 is the most extensively characterized type I AFP, which has three repeats of 11 amino acid residues [65]. Chao et al. investigated one of the longer type I serum AFPs in winter flounder plasma. This construct was named as AFP9 and had four repeat sequence. They found that this longer protein is more active than its shorter isoform even tough it has fewer ice binding residues in its structure. They suggested that longer size would have a positive effect increasing the thermal hysteresis activity [66]. After this discovery of the larger AFP in winter flounder species, which is much more active than the type I AFPs, the same group found another longer AFP in American plaice with a molecular weight of approximately 17 kDa. This protein is five times longer than the 3 repeat type AFP and exhibited

significant thermal hysteresis activity even at low concentrations, i.e. 2.2 ^{o}C at 0.4 mg/ml [67, 68].

The improved thermal hysteresis activity was not only studied for type I AFPs. In a study performed by Miura et al., they showed the enhanced activitiy of the type III dimer connected by a nine residue linker [47]. They compared the activity of the monomer of the same protein with its dimer and found that the dimer was 2 times as active as the monomer. This enhancement was even more pronounced yielding thermal hysteresis activities as much as 6 times greater than the monomer for lower concentrations. This effect was explained by the assumption that the average distance between the dimer molecules is smaller than that of the monomers. Hence, in order to saturate the ice surface and stop the ice growth, relatively small amount of dimer would be needed as compared to the monomer. More detailed investigation of the increased activity of the type III dimers was presented in another study [61]. They showed that the recombinant dimer type III AFP from Antarctic eel pout is twice as active as its monomer. However, when they inactivated one of the domains, its activity was reduced to 1.2 fold than that of the monomer. When two monomers were linked through a disulfide bond such that two domains could not bind to the ice surface simultaneously, the dimer was again only 1.2 times as active as its monomer. These findings were used to conclude that the enhanced activity of the dimer results from the ability of the two domains of the dimer to bind to the ice surface at the same time by doubling the ice binding surface area. The increased thermal hysteresis activity of type III dimers was further investigated by creating multimers (tandem repetition of dimers, trimers and

tetramers) of the various combinations of the monomers [69]. They found that as the size of the molecule increases, thermal hysteresis activity also increases.

Similar type of studies was carried out using insect AFPs by adding and deleting coils from the structure of the protein. It has been shown that the enhanced activity of the longer insect AFPs results from the greater size and especially the greater ice surface binding area [70, 71].

1.7 Theories on AFP/ice interactions

Among AFPs, there is a considerable variance in thermal hysteresis activity. For example, hyperactive insect (*Tenebrio molitor*) AFP [72] has a thermal hysteresis activity of 4.1˚C at a concentration of 150 μM, whereas for the same concentration, two-domain type III (RD3) [69] and type I (winter flounder) [73] AFPs can only depress freezing point by 0.25˚C and 0.17˚C, respectively.

Although numerous studies have been performed to investigate the interactions between AFPs and the ice crystal, an explicit description of the interaction has been elusive [21, 74, 75]. In developing a model of the protein-ice interaction, two seemingly contradictory experimental observations are particularly important: irreversible adsorption of AFPs to ice and a concentration dependence of thermal hysteresis activity. The predominant model describing thermal hysteresis is based on an adsorption inhibition mechanism derived using the Kelvin effect [76]. By adsorbing to the ice surface irreversibly, AFPs are thought to prevent ice crystal growth by increasing curvature of the exposed ice surface, which makes further ice growth energetically unfavorable [6, 44]. This is consistent with the observation of irreversible adsorption

using fluorescence microscopy [77]. However, it has been difficult to reconcile irreversible adsorption with the concentration dependence of thermal hysteresis. Other theories have been developed to account for the concentration dependence of thermal hysteresis, but are based on a reversible equilibrium between AFP and ice at all temperatures [62, 78, 79], which is inconsistent with the experimental observations described above.

One recent model presented by Kristiansen and Zachariassen accounts for both irreversible adsorption and concentration dependence of thermal hysteresis [6]. According to this model, at the bulk melting point there is a reversible equilibrium distribution of AFP molecules between the ice-water interfacial region and bulk water phase, resulting in the concentration dependence of thermal hysteresis. At temperatures lower than the melting point AFP molecules become irreversibly adsorbed onto newly formed ice crystal surfaces. This illustrates the possibility of both a reversible and irreversible adsorption by AFPs at different stages of ice formation.

To describe the reversible adsorption, it is important to determine the energetics of the AFP adsorption to the ice crystal surface. However, it is almost impossible to determine the binding energy of the AFP with traditional experimental methods because of the dynamic nature of the ice-water interface. The concentration dependence of thermal hysteresis is one measurement that is readily available, but the relationship between thermal hysteresis and binding energy is not evident. Experimental difficulties in AFP research have made simulations and analytical models necessary to overcome this challenge [62, 75, 80, 81]. There have been energy minimization, molecular dynamics and molecular simulation studies to determine the binding face of the AFPs by

calculating binding energies of individual possible binding sites [39]. However, there is a great difference between calculated energies likely owing to the level of complexity of the models used. Winter flounder AFP-ice interaction energy was found to be 84 kcal/mol in vacuo [82] and 157 kcal/mol in water [83] using energy minimization and molecular dynamics simulations. On the other hand, AFP/ice interaction energy has been calculated as low as 4.9 kcal/mol in terms of Gibbs free energy for winter flounder AFP using Monte Carlo simulations [62]. Furthermore, interaction energies of several hundreds of kilocalories per mole were calculated for different patches of the ice binding surfaces of type III AFP [39].

Determination of the surface concentration of AFPs on the ice crystal has similar difficulties. However, there have been some attempts to estimate AFP concentration at the ice crystal surface employing different methods such as fluorescence microscopy [77] or scanning tunneling microscopy [29]. Both studies indicated that AFPs bind to the ice crystal surface at monolayer or submonolayer coverage. In support of these data on adsorption onto ice surfaces, recent neutron reflection study also showed that type III AFP adsorbs as a single layer onto a hydrophilic SiO_2 substrate [84]. Although the use of SiO_2 as an ice crystal mimic is limited due to different crystal lattice dimensions, this does provide insight into the general adsorption behavior of the protein.

1.8 Oligomerization domains

Oligomerization domains such as collagen triple helices and coiled coils make up the subunit assembly of a large number of proteins [85]. The alpha helical coiled coil is the most abundant subunit oligomerization motif found in proteins [86, 87]. Fibritin from

T4 bacteriophage is a triple helical coiled coil and it folds into this structure by the help of the foldon domain, which has been found to be necessary for the formation of the triple stranded coiled coil structures as a result of the mutagenesis studies [88, 89].

The addition of oligomerization domains to the functional proteins is very advantageous in most instances especially where the stabilization of the different domains is needed [88]. Oligomerization domains also introduce high binding strength by enforcing increased local concentration of the molecules that are attached to them [87, 89].

1.9 Bioconjugation

This section introduces a brief description of bioconjugation reactions, molecules and reagents that were used in this study. Bioconjugation is an emerging field in life sciences and has become an important tool in pharmaceutical and materials science [90-93].

Bioconjugation is a technique to form a novel molecule composed of one or more components (nano particles, proteins, polymers, antibodies, etc.) having functional groups that have compatible chemistries [94, 95]. Proteins are composed of amino acids that are polymerized together by forming peptide (amide) bonds. Amino acids form the backbone which constitutes central carbons and each central carbon is bound to a hydrogen molecule and a side chain. The sequence and the properties of the amino acids in the protein determine the structure and the function. Amino acids contain an amino group and a carboxyl group (Figure 1.2). There are 20 common amino acids found in nature, and they contain a specific side chain which determines the particular chemical

structure, charge, hydrophilicity, hydrogen bonding capability and reactivity [96]. Side chains do not participate in polypeptide formation reactions and are free to interact with their environment limited by the folded structure of the protein.

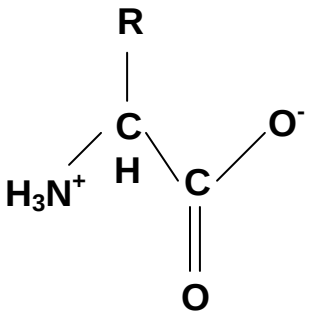

Figure 1.2. Amino acid structure. An amino acid consisting of a primary amine, a carboxylic acid group, and a side group. At physiological pH, the amine group is protonated and carries a positive charge and carboxylate is ionized and has a negative charge.

In order to successfully conjugate two molecules it is necessary to determine the chemical and physical characteristics of the molecules to be conjugated [96]. Isoforms of a molecule of interest can also be engineered to obtain a suitable functional group that has active sites which are reactive towards a crosslinker or a reagent that is tended to use in these reactions. In fact, in most cases this modification is necessary to create a compatible chemistry between the reagent and the target molecule. These reagents are generally commercially available and provide a solid support to almost every biological molecule such as peptides, proteins, oligonucleotides, lipids and organic compounds [96].

The major challenge in these studies is the difficulty of introducing site specific functional groups to the reaction scheme [91, 95]. Proteins generally contain multiples of

the same functional group that is intended to be used in the conjugation reactions. This may not be a problem in some instances where it is known that some of these residues are buried in the protein's folded structure and are not accessible for the reaction [97]. Hence, in order to overcome the difficulties related to the site specific bioconjugation, knowledge of the primary and secondary structures of the protein is required. Consequently, selecting less abundant amino acid as a target residue plays an important role in site directed bioconjugation. Among amino acids, tryptophan and cysteine residues are the most valuable targets in terms of their natural scarcity [98]. Dithiothreitol (DTT) can be used to disrupt disulfide bond formation, hence providing more cysteine residues available for bioconjugation reactions and preventing formation of unwanted chemical structures. However, care should be taken to account for biological activity of the molecule. Because, excessive addition of DTT into the reaction sometimes leads to disruption of the three dimensional structure of the protein and hence the possibility of the requirement of disulfide bonds for a specific biological activity should be considered [99]. Thiol groups present in cysteine residue are reactive towards several reagents such as maleimides and vinyl sulfones [100, 101]. The reaction of thiol groups at neutral pH produces irreversible thioester bonds which are stable under the reaction conditions [102]. Maleimides have double bonds which react with sulfhydryl groups to form stable thioether bonds. These molecules are generally used as heterobifunctional reagents which carry another functional group that is reactive towards another target molecule [100]. Heterobifunctional reagents are used in two-step reactions. Reagent is first reacted with one of the target molecules and then is reacted with the other. Having a reagent with two functional groups is advantageous because they are generally designed to have a linker

between the two functionalities which can be changed to improve reaction conditions such as solubility [103].

The modification of carboxylic acid groups that are present in the carboxy-terminus of the proteins is one of the most commonly used conjugation techniques [90]. Reactions of these groups with amines can be accomplished by introducing N-hydroxysuccinimide (sulfo-NHS) ester which is water soluble and reactive towards a carboxylate in the presence of carbodiimide EDC [90, 104]. The water soluble carbodiimide can be used to form active ester bonds with the carboxylate groups using NHS. The addition of sulfo-NHS to EDC reactions is advantageous for increasing the solubility and stability of the active intermediate, which reacts with the target amine molecule [105].

1.10 Scope of the thesis

The ultimate goal of this work is to better understand ice crystal growth inhibition of AFPs so that more effective cryopreservative or ice slurry additives can be made. The work in this thesis uses thermal hysteresis measurements of different antifreeze protein constructs and relates these measurements to the kinetics and thermodynamics of adsorption.

For this, several antifreeze protein constructs are designed to improve the thermal hysteresis activity. These constructs are engineered using site directed mutagenesis techniques and proteins are expressed in *E.coli* expression systems. Site directed bioconjugation techniques are used to create superior antifreeze molecules and are characterized using various methods such as thermal hysteresis measurements,

fluorescence microscopy, polyacrylamide gel electrophoresis, reverse phase and size exclusion HPLC and circular dichroism spectroscopy.

In addition, Langmuir adsorption isotherm models are used to relate thermal hysteresis and surface coverage values of single-domain and two-domain type III AFP using previously published thermal hysteresis versus concentration data [61]. Surface coverage and binding energy are determined by fitting two independent thermal hysteresis data sets with the classical Langmuir isotherm and a modified isotherm for the one- and two-domain proteins, respectively. Such a comparison is possible because all of the domains have identical structures and should have equivalent binding energies. This study is also extended to trimers (three-domain AFPs) that are designed to improve the thermal hysteresis activity. We first describe the model systems with the governing equations, then derive the isotherms, and finally use these with our experimental data to relate thermal hysteresis with surface coverage.

CHAPTER II

EXPERIMENTAL

This section introduces detailed information about the protein constructs that have been designed, prepared and characterized in this study. There are mainly two groups of AFPs which have distinct structural properties such as alpha helicity and size. One class of AFP that was studied in detail is type I AFP.

We have produced T1D, which is an α-helical protein composed of five repeats of 11 amino acids following a protocol given by Solomon et al., 1999 [106]. Another construct, T1N, which is an isoform of T1D was designed and produced by site directed mutagenesis for carboxy-terminus bioconjugation to a polyamine by removing the acidic residues in T1D. This reaction product is presented in Figure 2.1, where T1N is attached to the PAA, which is a linear chain polymer with amine groups attached to its backbone. A monomer making up PAA is also shown as an inset.

In order to make trimers of T1D, we have used foldon domain, which keeps three domains in close proximity and folds them such that they form trimers [85, 88, 89]. This trimer sample, T1Dfoldon, was designed using a modified T1D gene that was attached to

the foldon domain with a linker between them. This construct is presented in Figure 3.1, where foldon domain forms a triple helix keeping the three T1D molecules as a trimer.

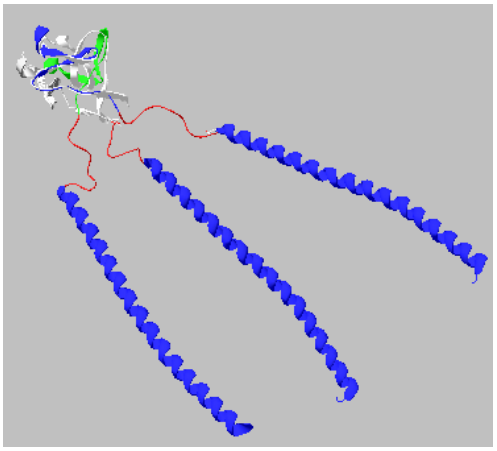

Figure 2.1. Schematic diagram showing the T1Dfoldon. Foldon domain and T1N were produced from PDB IDs 1NAY [89] and 1WFA [36], using DeepView/Swiss-PdbViewer software program, respectively [50]. Red region represents the linker.

Another protein construct was prepared using RD3, which is a two-domain type III AFP connected via 9-residue linker. Experiment sets were designed to isolate RD3N, which is the N-domain of the RD3, and this gene was modified such that it can be attached to the foldon domain having a linker. This construct was named as RD3Nfoldon and presented in Figure 2.2.

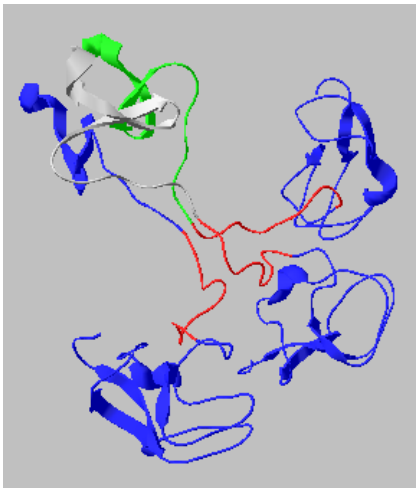

Figure 2.2. Schematic diagram showing the RD3Nfoldon. Foldon domain and N-domain RD3 were produced from PDB IDs 1NAY [89] and 1c8a [47], using DeepView/Swiss-PdbViewer software program, respectively [50]. Red region represents the linker.

Two more type III AFPs were prepared, which are named as RD3CCys and nfe8EGFPCys. RD3CCys is the C-domain RD3 with its linker. Cysteine residue was placed at the N-domain before the linker for site directed bioconjugation of this sample to a polyamine. nfe8EGFPCys is a single domain type III AFP and it was obtained using the gene for His-nfeAFP8-EGFP, which has His-tag (used aid protein purification process), nfeAFP8 (an isoform of type III AFP from Notched-fin eelpout, which lives off the north east coast of Japan) and EGFP (green fluorescence protein used to visualize where the protein binds to the ice crystal). The gene for His-nfeAFP8-EGFP was modified such that His-tag was removed and a cysteine residue was added to the C-terminal domain after EGFP for bioconjugation purposes.

In all procedures oligonucleotides (primers) were ordered from Invitrogen and the restriction endonucleases from New England Biolabs. Detailed descriptions of these procedures are given in the following sections.

2.1 Synthesis and cloning of the genes

E. coli strain BL21 Star (from Invitrogen) was used as the cloning and the expression host strain. In all cloning experiments, pET20b was used as an expression plasmid (Novagen Inc.).

The procedure for obtaining the gene for T1D (rAFP in their case) was previously described by Solomon et al., 1999 [106]. We have used a slightly modified version of their technique to obtain the sequence for T1D which was designed to have 5 repeats of the 11 amino acid repeat units from type I AFP winter flounder (*Pseudopleuronecta americanus*),

MDTASDAAAAAALTAANAAAAAALTAANAAAAAALTAANAAAAAAL

TAANAAAAAALTAR

Briefly, four primers were used two of which included the major portion of the sequence (1000 and 2000) that was extended using the two other shorter primers (1001short and 2002short) according to the overlap extension technique.

*Short Primers (*5′ to 3′):

1001short: CCCCCCCCATATGGACACTGCCTCTGACG
2002short: GCGCGGATCCTATTACCGTGCTGTCAAGGCC

*Template Primers (*5′ to 3′):

1000 (5′ to 3′):
ACTGCCTCTGACGCCGCAGCTGCTGCAGCACTGACAGCGGCTAATGCTGCTGCAGCAGCA
GCTTTGACTGCAGCGAACGCTGCAGCCGCAGCTGCACTC

2000 (5′ to 3′):
CAAGGCCGCGGCCGCCGCCGCATTTGCGGCAGTCAGAGCAGCAGCTGCAGCTGCATTGGC
AGCGGTGAGTGCAGCTGCGGCTGCAGCG

ACTGCCTCTGACGCCGCAGCTGCTGCAGCACTGACAGCGGCTA
CCCCCCCCATATGGACACTGCCTCTGACG ---------->

ATGCTGCTGCAGCAGCAGCTTTGACTGCAGCGAACGCTGCAGCCGCAGCTGCACTC
GCGACGTCGGCGTCGACGTGAGTGG

CGACGGTTACGTCGACGTCGACGACGAGACTGACGGCGTTTACGCCGCCGCCGGCGCCG
<---------- CCG
GAAC
GAACTGTCGTGCCATTATCCTAGGCGCG

PCR amplifications were carried out in a 50 µl reaction volume using a thermal cycler (Thermo Electron Corp.) and reactions contained 0.01 µM template primers, 1.25 µM short primers, nuclease free water and 1x PCR master mix obtained from Promega Corp. Amplified DNA was run on a 2% agarose gel in TAE buffer (40 mM Tris acetate, 2 mM EDTA, pH 8.5) at 80 V.

After agarose gel electrophoresis, DNA samples were purified using a gel extraction kit (Qiagen Inc.) and samples were eluted in double distilled water. The purified insert DNA and the pET20b expression vector were 10 fold over digested in a double digestion reaction using NdeI and BamHI restriction endonucleases. Digestion products were run on an agarose gel and purified (Promega), which were then used to be ligated. 1X Quick ligase buffer (New England Biolabs, Inc.) was used in five minute ligation reaction including approximately 50 ng of the vector DNA and approximately 10 fold molar excess of the insert DNA. 10 µl of ligated products were transformed using BL21 Star (Invitrogen) competent cells on agar plates having LB (Lysogeny broth) medium and 100 µg ampicilin. After overnight transformation, colonies were selected

and plasmid DNA was purified from 5 ml overnight cultures using Qiagen Miniprep kit. Samples were then screened using PCR and sent for DNA sequencing. DNA sequencing of the T1D and T1N samples were carried out at the Cleveland State University Genomics Laboratory in the Department of Chemistry. Samples were sequenced using T7 forward primer. One plasmid was designated as T1D. The DNA sequence for T1D is as follows:

ATGGACACTGCCTCTGACGCCGCAGCTGCTGCAGCACTGACAGCGGCTAATGCTGCTGCA
GCAGCAGCTTTGACTGCAGCGAACGCTGCAGCCGCAGCTGCACTCACCGCTGCCAATGCA
GCTGCAGCTGCTGCTCTGACTGCCGCAAATGCGGCGGCGGCCGCGGCCTTGACAGCACGG

In order to conjugate this protein to a polyallyamine through its carboxy terminus, we have modified T1D by replacing the two acidic residues at the N-terminus. This modified protein was named as T1N and an analogous procedure was used to create the gene for producing T1N except that a slightly modified forward extension primer was designed to replace aspartic acid residues with asparagines.

Short Primers (5′ to 3′):

1001N: CCCCCCCCATATGAACACTGCCTCTAACGCCGC
2002short: GCGCGGATCCTATTACCGTGCTGTCAAGGCC

*Template Primers (*5′ to 3′):

1000 (5′ to 3′):
ACTGCCTCTGACGCCGCAGCTGCTGCAGCACTGACAGCGGCTAATGCTGCTGCAGCAGCA
GCTTTGACTGCAGCGAACGCTGCAGCCGCAGCTGCACTC

2000 (5′ to 3′):
CAAGGCCGCGGCCGCCGCCGCATTTGCGGCAGTCAGAGCAGCAGCTGCAGCTGCATTGGC
AGCGGTGAGTGCAGCTGCGGCTGCAGCG

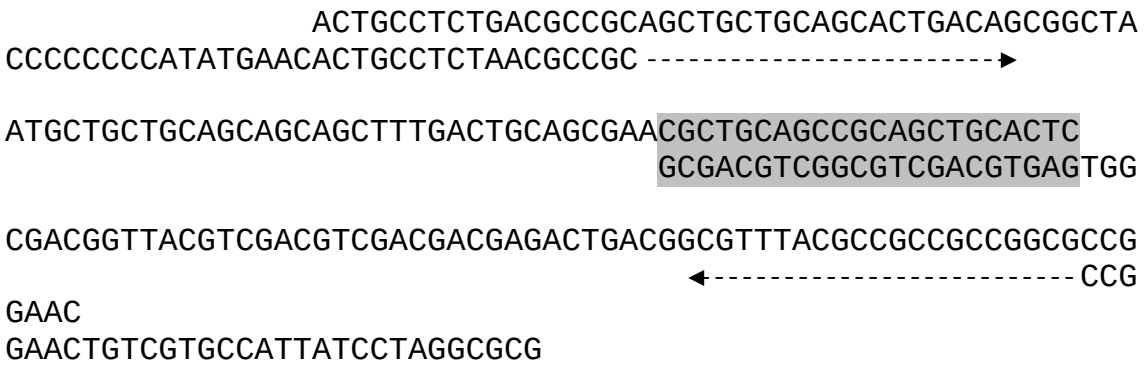

A similar procedure was used in PCR reactions and cloning the T1N gene, which is given as:

ATGAACACTGCCTCTAACGCCGCAGCTGCTGCAGCACTGACAGCGGCTAATGCTGCTGCA

GCAGCAGCTTTGACTGCAGCGAACGCTGCAGCCGCAGCTGCACTCACCGCTGCCAATGCA

GCTGCAGCTGCTGCTCTGACTGCCGCAAATGCGGCGGCGGCCGCGGCCTTGACAGCACGG

TAATAG

Corresponding amino acid sequence for T1N is as follows (mutated sites are highlighted):

MNTASNAAAAAALTAANAAAAAALTAANAAAAAALTAANAAAAAAL

TAANAAAAAALTAR

In order to incorporate T1D into the plasmid having a foldon domain and a linker, we have designed a system of procedures. T1D was modified in a 50 µl PCR reaction using two primers that were designed to add a SfiI recognition site at the 3′ end [107].

In the first step of the plasmid preparation, SfiI endonuclease recognition site was created and inserted into pET20b vector so that each time we wanted to incorporate a

new gene into the vector we would have to single digest the vector with SfiI endonuclease. In the below sequence, the inner piece (highlighted portion in the inner piece shows the SfiI recognition site) was annealed and ligated into a pET20b plasmid that had been double digested with NdeI and EcoRI endonucleases (cut sites are highlighted).

CATATGAGCAAAGGGCCGGGCTGGCCGTGATAATTC
GTATACTCGTTTCCCGGCCCGACCGGCACTATTAAG

NdeI ***EcoRI***

In the annealing process, 0.8 μM forward and reverse primers were used in a 50 μl reaction volume having 1X quick ligase buffer and nuclease free water (New England Biolabs, Inc.). Reaction mixture was heated at 94 ^{o}C for 5 minutes and then slowly cooled down to room temperature at a rate of 1 ^{o}C/ min using a thermocycler (Thermo Electron Corp.). The sample was directly ligated into a pET20b vector which was double digested with NdeI and EcoRI and purified by gel electrophoresis.

Foldon was also produced by annealing, using primers that were designed to form a foldon domain and have a SfiI recognition site. Annealed forward and reverse primer sequences are shown below. Highlighted ends represent the SfiI cut sites.

TGGCCGGGTTACATCCCGGAAGCTCCGCGTGACGGTCAGGCTTACGTTCGTAAAGA
CCGACCGGCCCAATGTAGGGCCTTCGAGGCGCACTGCCAGTCCGAATGCAAGCATTTCT

CGGTGAATGGGTTCTGCTGTCTACCTTCCTGTGATAAGGC
GCCACTTACCCAAGACGACAGATGGAAGGACACTATT

Annealed foldon primers were directly ligated to pET20b vector that was single digested with SfiI. After single digestion, sample was dephosphorylated using Antarctic

Phosphatase (New England Biolabs). In a 30 minute reaction at 37 ^{o}C, Antarctic Phosphatase helps to catalyze the removal of 5′ phosphate groups from DNA and it is used to prevent self ligation of the digested DNA. In the absence of the 5′ phosphoryl termini required by ligases, they cannot self-ligate. Hence, dephosphorylation is used to decrease the vector background in cloning. Digested and dephosphorylated vector was run on an agarose gel and then purified, which was then used to be ligated with annealed foldon gene.

The next step was to produce a linker and incorporate it into the vector having a foldon domain and a SfiI recognition site. Forward and reverse linker primers were designed and annealed using the same procedure as described above. Annealed linker has a DNA sequence shown in below sequence with SfiI cut sites highlighted.

```
    TGGCCGGACGGTACCACCTCCAAAGGC
CCGACCGGCCTGCCATGGTGGAGGTTT
```

In order to insert annealed linker, pET20b vector having a foldon domain and a SFiI cut site was single digested with SfiI. After single digestion, vector was dephosphorylated at 37 ^{o}C for 30 minutes and run on an agarose gel and then purified. Annealed linker was directly ligated into the vector.

The resulting portion of the vector pET20b (shown as a single piece of DNA from 5′ to 3′) having a foldon domain, a linker and a SfiI recognition site is as follows:

```
CATATGAGCAAAGGGCCGGGCTGGCCGGACGGTACCACCTCCAAAGGCTGGCCGGGTTAC
ATCCCGGAAGCTCCGCGTGACGGTCAGGCTTACGTTCGTAAAGACGGTGAATGGGTTCTG
CTGTCTACCTTCCTGTGATAAGGC
```

Sequence starts with the NdeI recognition site (first highlighted section in light gray) and continues with the SfiI recognition site (highlighted as dark gray), a linker which starts right after the SfiI recognition site and highlighted as light gray. The rest of the sequence corresponds to the foldon domain.

In the following step, T1D was modified in order to include a SfiI recognition site at 3′ end of the gene. For this, two primers (shown below), T7 forward universal primer (New England Biolabs) and a designed Sfi typeI reverse were used in 50 µl PCR reaction as described above.

T7 forward: TAATACGACTCACTATAGGG
Sfi typeI reverse: CCAAAAAAAGGCCAGCCCGGCCGTGCTGTCAAG

Modified T1D having a SfiI recognition site and the plasmid with foldon and linker were double digested with NdeI and SfiI endonucleases and separated by agarose gel electrophoresis and then purified. Purified insert and vector DNA were then ligated back together following the same procedures as described above. In all cases, after transformations were plated overnight, colonies were selected and plasmid DNA was purified from 5 ml overnight cultures using Qiagen Miniprep kit. Samples were then screened using PCR and sent for DNA sequencing. A sample of each was stored in -80 ^{o}C freezer as a frozen stock (500 µl overnight culture in 500 µl 50% glycerol solution) for future use. DNA sequencing for all of the samples except T1D and T1N was carried out at the Cleveland Clinic Genomics Core. The amino acid sequence of the T1Dfoldon is as follows (the linker and the foldon domains are highlighted as light and dark gray, respectively):

MDTASDAAAAAALTAANAAAAAALTAANAAAAAALTAANAAAAAALTAANAAAAA
ALTARPGWPDGTTSKGWPGYIPEAPRDGQAYVRKDGEWVLLSTFL

Type III AFP constructs were prepared using a two-domain type III AFP from antarctic eel pout (*Rhigophila dearborni*), which is named RD3 [47]. This gene was used as a template DNA in a PCR reaction with forward and reverse primers namely, T7 Forward and Reverse RD3N SfiI.

Reverse RD3N SfiI: CCCAAAGGCCAGCCCGGCCATTCGTAGTTTTT

This reaction produces two bands; one at 595bp and the other at 295bp. Lower band was removed and purified from the agarose gel to get the N domain RD3 gene. However, the lower band needed to be amplified to obtain enough DNA for cloning. Hence, the lower piece was used as a template in another PCR reaction to amplify the DNA.

The sequence of the lower band is:

TAATACGACTCACTATAGGGAGACCACAACGGTTTCCCTCTAGAAATAATTTTGTTTAAC
TTTAAGAAGGAGATATACATATGAATAAAGCTTCCGTTGTTGCTAACCAGCTGATCCCGA
TCAACACCGCTCTGACCCTGATCATGATGAAAGCTGAAGTTGTTACCCCGATGGGTATCC
CGGCTGAAGAAATCCCGAACCTGGTTGGTATGCAGGTTAACCGTGCTGTTCCGCTGGGTA
CCACCCTGATGCCGGACATGGTTAAAAACTACGAATGGCCGGGCTGGCCTTTGGG

After digesting the lower band with NdeI and SfiI endonucleases, DNA becomes:

TATGAATAAAGCTTCCGTTGTTGCTAACCAGCTGATCCCGATCAACACCGCTCTGACCCT
GATCATGATGAAAGCTGAAGTTGTTACCCCGATGGGTATCCCGGCTGAAGAAATCCCGAA
CCTGGTTGGTATGCAGGTTAACCGTGCTGTTCCGCTGGGTACCACCCTGATGCCGGACAT
GGTTAAAAACTACGAATGGCCGGGC

The above piece was ligated to the plasmid having foldon, linker and SfiI recognition site that is double digested with NdeI and SfiI endonucleases.

The resulting sequence for Rd3Nfoldon is as follows (the linker and the foldon domains are highlighted as light and dark gray, respectively):

MNKASVVANQLIPINTALTLIMMKAEVVTPMGIPAEEIPNLVGMQVNRAVPLGTTLMPDM

VKNYEWPGWPDGTTSKGWPGYIPEAPRDGQAYVRKDGEWVLLSTFL

Another type III AFP construct, RD3CCys was produced similarly from the RD3 gene. RD3 was used as a template in a 50 µl PCR reaction with forward and reverse primers, RD3CCysForward and Reverse 20b, respectively.

RD3CCysForward: GGATATCATATGTGCACCACCTCCCCGGGTCTG

Reverse 20b: AATTGCAAGCTTGTCGACG

After the PCR reaction, both insert and the vector (pET20b) were double digested using BamHI and NdeI endonucleases and then purified. These pieces were ligated to each other to form RD3CCys, which has a DNA sequence of:

CATATGTGCACCACCTCCCCGGGTCTGAAATCCGTTGTTGCTAACCAGCTGATCCCGATC
AACACCGCTCTGACCCTGGTTATGATGAAAGCTGAAGAAGTTTCCCCGAAAGGTATCCCG
TCCGAAGAAATCTCCAAACTGGTTGGTATGCAGGTTAACCGTGCTGTTTACCTGGACCAG
ACCCTGATGCCGGACATGGTTAAAAACTACGAATAG

The corresponding amino acid sequence for RD3CCys is given as:

CTTSPGLKSVVANQLIPINTALTLVMMKAEEVSPKGIPSEEISKLVGMQVNRAVYLDQTL

MPDMVKNYE

Dark gray highlighted C represents the cysteine residue on the N-terminus, while the inner light gray highlighted region is the linker designed to have a space between the protein and the cysteine residue. The rest of the sequence is the C-domain of the RD3.

One other construct was nfe8EGFPCys, which is an isoform of type III AFP and it was obtained using the gene for His-nfeAFP8-EGFP (His-tag, nfeAFP8 and EGFP) [108]. Green fluorescence protein is used to visualize where the protein binds to the ice

crystal. The gene for His-nfeAFP8-EGFP was modified such that His-tag was removed and a cysteine residue was added to the C-terminal domain after EGFP for bioconjugation purposes.

The original DNA sequence for nfe8EGFPCys is as follows (His-tag region is highlighted in the below sequence):

CATATGCACCACCACCACCACCACAACCAGGCGTCCGTGGTGGCCAACCAGC
TGATCCCCATAAATACTGCCCTGACTCTGGTGATGATGAGGGCGGAGGTGGT
CACCCCAATGGGCATCCCCGCCGTGGACATTCCCCGATTAGTCTCAATGCAA
GTGAACAGGGCAGTGCCGTTGGGCACAACCCTCATGCCAGAGATGGTGAAAG
GGTACACCCCGGCTGAATTCGAAATCACTAGTGAATTCGATATCAAGCTTATC
GATACCGTCGACCTCGACATGTCTAAAGGTGAAGAATTATTCACTGGTGTTGT
CCCAATTTTGGTTGAATTAGATGGTGATGTTAATGGTCACAAATTTTCTGTCT
CCGGTGAAGGTGAAGGTGATGCTACTTACGGTAAATTGACCTTAAAATTTATT
TGTACTACTGGTAAATTGCCAGTTCCATGGCCAACCTTAGTCACTACTTTCGG
TTATGGTGTTCAATGTTTTGCGAGATACCCAGATCATATGAAACAACATGACT
TTTTCAAGTCTGCCATGCCAGAAGGTTATGTTCAAGAAAGAACTATTTTTTTC
AAAGATGACGGTAACTACAAGACCAGAGCTGAAGTCAAGTTTGAAGGTGAT
ACCTTAGTTAATAGAATCGAATTAAAAGGTATTGATTTTAAAGAAGATGGTA
ACATTTTAGGTCACAAATTGGAATACAACTATAACTCTCACAATGTTTACATC
ATGGCTGACAAACAAAAGATGGTATCAAAGTTAACTTCAAATTAGACACAAC
ATTGAAGATGGTTCTGTTCAATTAGCTGACCATTATCAACAAAATACTCCAAT
TGGTGATGGTCCAGTCTTGTTACCAGACAACCATTACTTATCCACTCATCTGC
CTTATCCAAAGATCCAAACAAAAGAGAGACACATGGTCTTGTAAAATTTGTT
ACTGCTGCTGGTATTACCATTGGTATGGATGAATTGTACAAATAGTCGAGAAT
CCATCACACTGGCGGCCGCTCGAGCCCACCACACCACCTCTGAGATCTGCTG
CTACTAAGCCCGAAGGAATTGAGTGGCTGCTGCACGTTAACAATACAGCTAC
CCCTTGGGCCTCAAACGTTTTGAGGGTTTTGTTAAGGCGTATTATTCGATTGT
CTATGGACACCTCTTCGCCCTTAATCCGCGGTGAGCGTTCACCACTTC

The forward and reverse primers were designed to remove the His-tag.

AseI nfe8EGFP Forward: GGGAAAATTAATGAACCAGGCGTCCGTGGTG

BamHI nfe8EGFP Cys Reverse: CCCCGGATCCCTAGCATTTGTACAATTCATCC

After performing PCR reaction with forward and reverse primers, the DNA of interest became as follows (AseI, NdeI and BamHI recognition sites were highlighted in order):

GGGAAAATTAATGAACCAGGCGTCCGTGGTGGCCAACCAGCTGATCCCCATAAATACTGC
CCTGACTCTGGTGATGATGAGGGCGGAGGTGGTCACCCCAATGGGCATCCCCGCCGTGGA
CATTCCCCGATTAGTCTCAATGCAAGTGAACAGGGCAGTGCCGTTGGGCACAACCCTCAT
GCCAGAGATGGTGAAAGGGTACACCCCGGCTGAATTCGAAATCACTAGTGAATTCGATAT
CAAGCTTATCGATACCGTCGACCTCGACATGTCTAAAGGTGAAGAATTATTCACTGGTGT
TGTCCCAATTTTGGTTGAATTAGATGGTGATGTTAATGGTCACAAATTTTCTGTCTCCGG
TGAAGGTGAAGGTGATGCTACTTACGGTAAATTGACCTTAAAATTTATTTGTACTACTGG
TAAATTGCCAGTTCCATGGCCAACCTTAGTCACTACTTTCGGTTATGGTGTTCAATGTTT
TGCGAGATACCCAGATCATATGAAACAACATGACTTTTTCAAGTCTGCCATGCCAGAAGG
TTATGTTCAAGAAAGAACTATTTTTTTCAAAGATGACGGTAACTACAAGACCAGAGCTGA
AGTCAAGTTTGAAGGTGATACCTTAGTTAATAGAATCGAATTAAAAGGTATTGATTTTAA
AGAAGATGGTAACATTTTAGGTCACAAATTGGAATACAACTATAACTCTCACAATGTTTA
CATCATGGCTGACAAACAAAAGAATGGTATCAAAGTTAACTTCAAAATTAGACACAACAT
TGAAGATGGTTCTGTTCAATTAGCTGACCATTATCAACAAAATACTCCAATTGGTGATGG
TCCAGTCTTGTTACCAGACAACCATTACTTATCCACTCAATCTGCCTTATCCAAAGATCC
AAACGAAAAGAGAGACCACATGGTCTTGTTAGAATTTGTTACTGCTGCTGGTATTACCCA
TGGTATGGATGAATTGTACAAATGCTAGGGATCCGGGG

The above DNA was double digested with AseI and BamHI and ligated to the pET20b vector, which was double digested with NdeI and BamHI. Since, there is a NdeI recognition site in the middle of the sequence, we have chosen another endonuclease, AseI to digest 5′ end of the insert DNA. This is possible because, NdeI and AseI have common overhangs but different recognition sites. Purified insert and vector were then ligated back together to form nfe8EGFPCys, which has an amino acid sequence as follows:

MNQASVVANQLIPINTALTLVMMRAEVVTPMGIPAVDIPRLVSMQVNRAVPLGTTLMPEM
VKGYTPAEFEITSEFDIKLIDTVDLDMSKGEELFTGVVPILVELDGDVNGHKFSVSGEGE
GDATYGKLTLKFICTTGKLPVPWPTLVTTFGYGVQCFARYPDHMKQHDFFKSAMPEGYVQ
ERTIFFKDDGNYKTRAEVKFEGDTLVNRIELKGIDFKEDGNILGHKLEYNYNSHNVYIMA
DKQKNGIKVNFKIRHNIEDGSVQLADHYQQNTPIGDGPVLLPDNHYLSTQSALSKDPNEK
RDHMVLLEFVTAAGITHGMDELYKC

The above sequence for nfe8EGFPCys starts with nfe8 (first highlighted section) at the N-terminus followed by the green fluorescence protein (middle highlighted section) and a cysteine residue (highlighted as dark gray) at the C-terminus.

2.2 Protein expression and purification

Overnight cultures of T1D and T1N in 5 ml LB medium were used to inoculate 1L cultures having 100 µl ampicilin. Samples were induced with isopropyl-β-D-thiogalactopyranoside (IPTG) (Thermo Fisher Scientific Inc.) after optical cell density has reached a value of 0.6 that was measured using a UV spectrophotometer (Thermo Electron Corp.) at 600 nm. Induced samples were shaken in an incubator at 37 ^{o}C for 6 hours. Time course of the 1 ml samples that were taken before induction and every hour after induction was monitored by polyacrylamide gel electrophoresis (10-20 % tris-glycine). Samples were centrifuged at 14000 rpm using a microcentrifuge and supernatant was discarded. Pellets were resuspended in 100 µl BPER (Pierce) and centrifuged again to separate soluble and insoluble fractions. 20 µl samples were run on the Tris-glycine gel at 80 Volts for two hours. Then it was stained using GelCode Blue staining reagent (Pierce) and then destained according to the protocol given in the manufacturer's manual. It was observed that both proteins were primarily in the insoluble fractions.

T1D and T1N samples were purified using ethanolic extraction according to the protocol given in Solomon and Appel, and dialyzed against 100 mM ammonium bicarbonate using 1000 Da cutoff membrane and then lyophilized for further experiments [106].

The other proteins were expressed as discussed above and purified using a detergent, BPER (Pierce) following the manufacturer's protocol followed by denaturation in 6 M Guanidine hydrochloride. Samples were refolded in buffer (50 mM K_2PO_4 and 100 mM NaCl) for 3 days at 4^oC. A detailed protein purification protocol is given in Appendix (A5).

Reverse phase HPLC was run using Shimadzu HPLC system for T1D and T1N to ensure the purity of the proteins. Two different solutions (solution A: 950 ml double distilled water, 50 ml acetonitrile (HPLC grade, Sigma-Aldrich), 1 ml TFA and solution B: 600 ml acetonitrile, 300 ml isopropanol, 100 ml double distilled water, 0.75 ml TFA) were pumped to the C18 column (150x10 mm) (Restek) with 0.5% gradient of 85% to 100% solution B between 6 and 36 minutes followed by 100% solution B for an additional 5 minutes to ensure that the proteins were eluted from the column.

2.3 Molecular weight determination

Molecular weight of the samples was determined by mass spectroscopy as 5108.6 and 5105.6 Da for T1D and T1N, respectively. These results were in accordance with the weights calculated from the primary sequence. Samples were analyzed at the University of Oklahoma Health Sciences Center (Molecular Biology Proteomics Facility). The size of the other samples was determined using polyacrylamide gel electrophoresis.

2.4 Protein concentration determination

Concentration of the concentrated master solutions of T1D and T1N were determined by amino acid analysis. Highly hydrophobic, lyophilized protein was

resuspended in 10% acetic acid and dialyzed against 0.4% acetic acid and 30 mM ammonium bicarbonate (pH 4.6) for buffer exchange. Samples were analyzed at the University of Oklahoma Health Sciences Center (Molecular Biology Proteomics Facility). Both protein samples, containing 100 µl of approximately 1mg/ml solution of TID or TIN, were transferred to hydrolysis tubes and then the sample container vials were rinsed with 80 µl of 33% acetonitrile and then 80 µl of 30% acetic acid. The samples were Speed-Vac dried, 6 N HCl was added and the tubes were vacuum sealed and hydrolyzed at 110^{o}C for 20 hrs. Post-hydrolysis, 50 nanomoles of β-(2-Thienyl)-DL-Alanine internal standard was added and the hydrolysate was vacuum-centrifuged to dryness. The hydrolysate was redissolved in 200 µl of 0.01 N HCl and passed through a 0.45 µm filter with centrifugation.

For the other proteins, concentrations were determined by calculating the molar extinction coefficients by following the procedure given by Gill and Hippel [109]. Briefly, the molar extinction coefficient of a denatured protein in 6M guanidine hydrochloride (GdnHCl) is calculated by using the number of the absorbing residues in the protein amino acid sequence. The model compounds that have a distinctive absorbance at a specific UV wavelength (276-282 nm) are tryptophan, tyrosine and cysteine for which the molar extinction coefficients have been measured previously [109]. The molar extinction coefficient of a denatured protein in $(M.s)^{-1}$ is given by:

$$\varepsilon_{M,Gdn.HCl} = a\varepsilon_{M,Tyr} + b\varepsilon_{M,Trp} + c\varepsilon_{M,Cys} \qquad \textbf{(2.1)}$$

In equation 2.1, $\varepsilon_{M,Tyr}$, $\varepsilon_{M,Trp}$, and $\varepsilon_{M,Cys}$ are the molar extinction coefficients of tyrosine, tryptophan, and cysteine, respectively. The coefficients a, b, and c are the number of each residue per protein molecule.

In order to determine the molar extinction coefficient of the native protein, native and denatured (in 6M GdnHCl) protein solutions with the same concentrations were prepared. Then, the concentration of the denatured protein, which was experimentally the same as the native protein was calculated using the UV absorbance measured at 280 nm according to equation 2.2.

$$C_{den} = Abs_{Gdn.HCl} / \varepsilon_{M,Gdn.HCl} \quad \textbf{(2.2)}$$

Where, $Abs_{Gdn.HCl}$ is the UV absorbance measured for the denatured protein at 280 nm. Equation 2.3, which is similar to the equation 2.2 is also valid for the native protein:

$$C_{nat} = Abs_{nat} / \varepsilon_{M,nat} \quad \textbf{(2.3)}$$

In the final step, the molar extinction coefficient of the native protein was calculated by equating the concentration terms in the above equations. The resulting equation becomes (equation 2.4):

$$\varepsilon_{M,nat} = (Abs_{nat})(\varepsilon_{M,Gdn.HCl}) / (Abs_{Gdn.HCl}) \quad \textbf{(2.4)}$$

This procedure was repeated for five times for each protein at each concentration and a calibration curve was constructed to ensure the linearity of the absorbance values with respect to concentration.

2.5 Antifreeze protein/polymer bioconjugates

In the T1N/polyallylamine reaction, 5 µl polyallylamine (Sigma-Aldrich) (20 w% in water) was mixed with 24 µl EDC (1-Ethyl-3-[3-dimethylaminopropyl]carbodiimide hydrochloride) (Sigma-Aldrich) and 10.9 µl sulfo-NHS (n-hydroxysulfosuccinimide) (Sigma-Aldrich) in 300 µl 0.4% acetic acid, 30 mM ammonium bicarbonate [96]. T1N

(0.3 mM, which is approximately 13 molar excess of the polymer) was added to the reaction mixture in a round bottom volumetric flask and stirred using a small magnet for 2 hours at room temperature. A schematic diagram of the reaction product is given in Figure 2.3. After reaction is completed, unreacted impurities were removed by dialysis using 3500 MW cutoff Spectra/Por dialysis membrane.

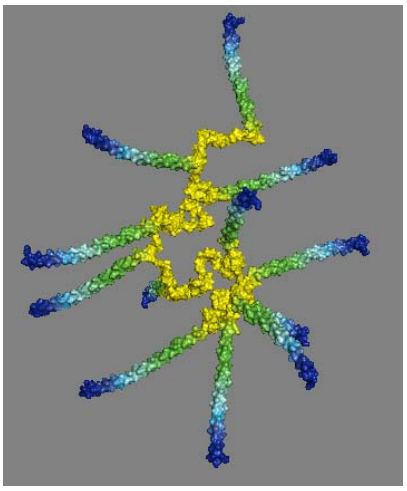

Figure 2.3. Schematic diagram representing T1N/PAA reaction product. T1N was produced from PDB ID 1WFA [36], using DeepView/Swiss-PdbViewer software program [50]. PAA (17 kDa) was produced using PyMOL version 0.99.

RD3CCys and nfe8EGFPCys were also reacted to the polyallylamine but using a different reaction scheme in a two step process. These molecules were designed to have only one cysteine residue at either 5′ or 3′ end for site directed conjugation. NHS-PEG6-Maleimide crosslinker (Thermo Scientific) was used in the conjugation reactions (Figure 2.4). Polyethylene glycol linker between heterobifunctional linker is used to improve solubility of the conjugated product [96].

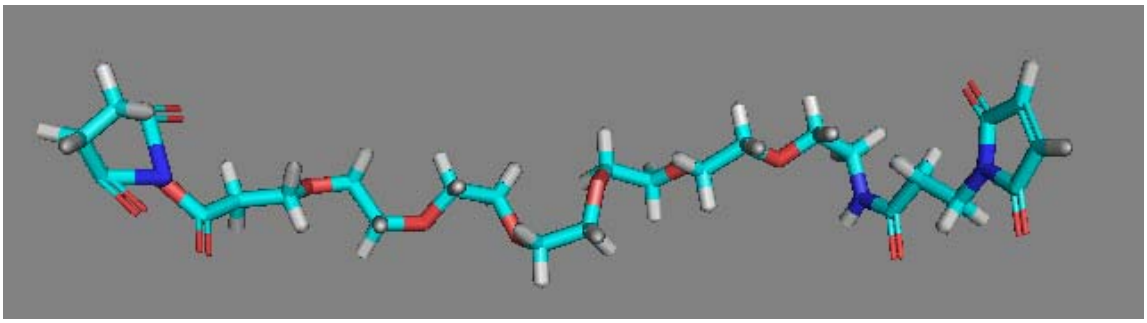

Figure 2.4. NHS-PEG_6-Maleimide (N-hydroxysuccinimidyl-([N-maleimidopropionamido]-hexaethyleneglycol) ester) produced using PyMOL version 0.99.

First, 1 mM crosslinker was reacted with PAA in 10 fold molar excess. 8.5 µl PAA (20 w% in water) and 4 µl 250 mM crosslinker were mixed in 1 ml PBS (phosphate buffered saline) and 2 mM EDTA, pH 7.2 in a round bottom flask and incubated at room temperature for 30 minutes by stirring. EDTA (calcium chelator) was added to the solution to prevent metal catalyzed disulfide bond formation.

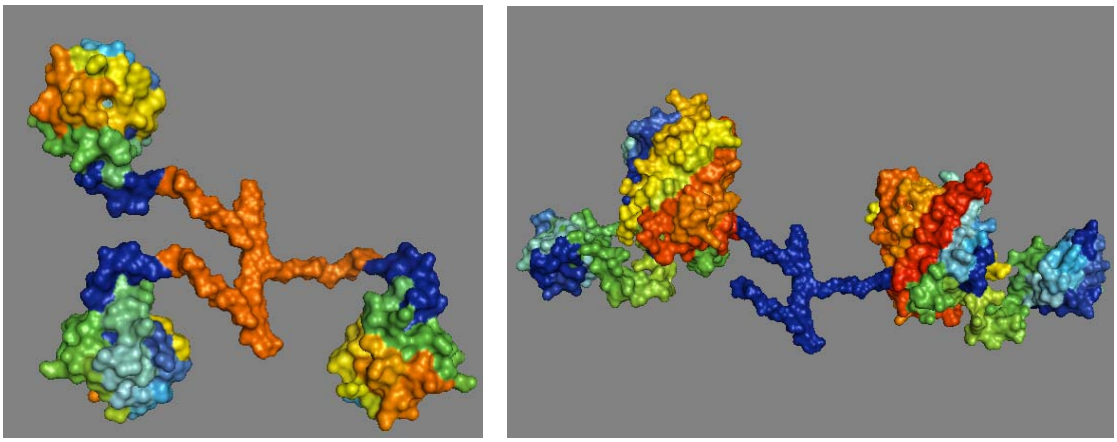

Figure 2.5. Schematic representation of RD3CCys/PAA (left) and nfe8EGFPCys/PAA (right) reactions. EGFP and C-domain RD3 were produced from PDB IDs 2oky [110] and 1c8a [47], using DeepView/Swiss-PdbViewer software program, respectively [50]. A short segment of PAA was produced using PyMOL version 0.99.

In a separate vessel, 5 mM Tris[2-carboxyethyl] phosphine (TCEP from Thermo Scientific) was added to the RD3Ccys and nfe8EGFPCys protein solutions to prevent the formation of dimers through disulfide bonds between cysteine residues. Protein samples were reacted with TCEP for reducing disulfide bonds for 1 hour and then dialyzed against the conjugation buffer (PBS, 2 mM EDTA, pH 7.2).

After the first reaction was completed, 200 µl of reacted PAA and 0.4 mM protein solution were mixed in the same conjugation buffer (1 ml total solution volume) and reacted at room temperature for 2 hours and then stored at 4^{o}C.

2.6 Size exclusion HPLC

A 500 µl aliquot of the reaction mixture was loaded to the 20 ml Bio-scale size exclusion column (Bio-Rad Laboratories, Inc.) filled with Toyopearl HW-55F resin (Tosoh Corp.). Column was filled with the resin according to the manufacturers' instructions. Reaction buffer solution was pumped to the HPLC (Shimadzu) column in the down-flow mode at a flow rate of 1 ml/min and UV absorbance values were recorded at 230 and 280 nm at the same time reaction mixture injected to the column. Samples were collected from the column outlet at every minute to be analyzed later.

2.7 Thermal hysteresis experiments

The interaction of AFPs with the ice crystal results in thermal hysteresis, which is the difference between freezing and melting temperatures. Thermal hysteresis activity was measured using a home made nanoliter osmometer (Laboratory of Art Heuer at CWRU) attached to an optical microscope (Olympus) as previously described (Figure 2.6) [73]. Briefly, a single drop of protein solution was suspended in oil. The droplet was flash frozen at around -40 ^{o}C and, upon increasing the temperature to the melting point, was thawed slowly (approximately 0.2 ^{o}C/min) until a single ice crystal was obtained. After obtaining a single ice crystal, solution was cooled at a rate of 0.01 ^{o}C/min. The temperature at which the crystal grows was recorded as the freezing temperature. The difference between these two temperatures was taken as the thermal hysteresis [22, 43, 60]. Morphological changes of the ice crystal structure in the presence of AFPs were also investigated using optical microscopy and a digital camera.

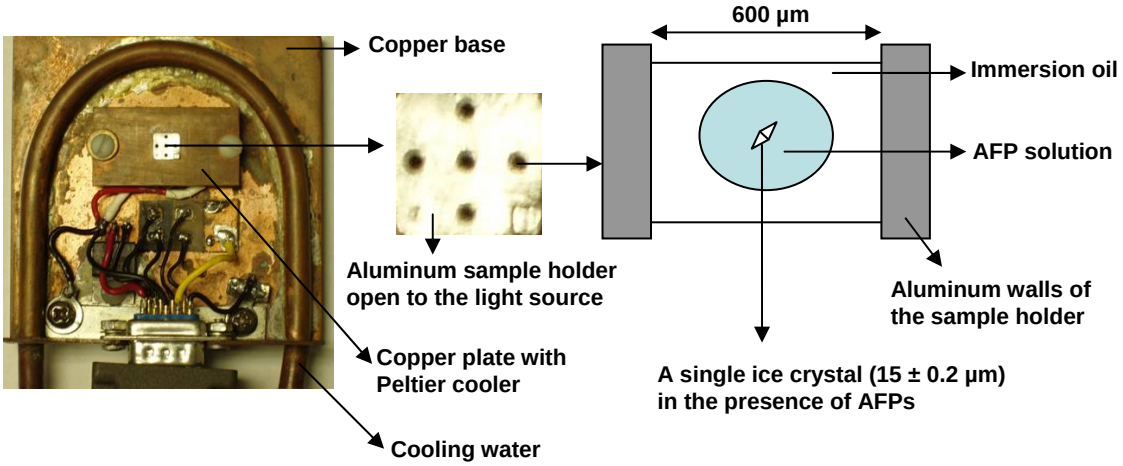

(A) (B) (C)

Figure 2.6. (A) General view of the nanoliter osmometer, (B) Top view of the aluminum sample holder, (C) Side view of the one hole of the sample holder including oil and sample in it.

The sample holder has 5 holes which are 600 µm in diameter (Figure 2.6). A droplet of immersion oil (Cargill, type B from Thermo Fisher Scientific) was placed into one of the holes of the nanoliter osmometer using a custom-built injector composed of a glass pipette, a small tubing, a glass Pasteur pipette and a bulb. Glass pipette was made using a pipette puller by optimizing the parameters such as temperature and pulling speed in order to create a tip around 10 µm in diameter which is the appropriate tip size for this system. Approximately, 14 nl of the protein solution, which corresponds to a spherical droplet size of 300 µm in diameter was injected into the immersion oil. It is very important that the solution is not contacted with the aluminum walls of the sample holder and is not exposed to air to prevent any possible ice crystal nucleation. Automatic nanoliter injector (Drummond Scientific) with a 3D manipulator was used along with the glass micropipettes in order to inject the protein sample. Automatic injector provides accurate and reproducible injection volumes. Glass micropipettes were filled with

immersion oil to provide even more consistency in the sample size. Since, oil is incompressible, the automated plunger moving towards the tip of the glass micropipette only works to inject the sample of interest without compressing the air inside the pipette.

The other major issue is to prevent the condensation occurring on the sample stage caused by the humid air in the laboratory while cooling. This was prevented using a setup including a pump connected to desiccant filled column to produce dry air being sent onto the sample holder. The microscope was sealed from the environment using a plastic bag to keep the dry air inside.

2.8 Circular dichroism spectroscopy studies

CD spectra were measured using a circular dichroism spectrometer (Aviv) for purified T1D, T1Dfoldon and RD3Nfoldon samples in the Physiology and Biophysics Department at Case Western Reserve University. Samples were analyzed in single runs at 25 ^{o}C between 190 to 250 nm. α-helicity of the T1D and the characteristic folding of the foldon constructs were investigated.

CHAPTER III

RESULTS AND DISCUSSION

3.1 Expression and purification of the proteins

This section introduces the results and discussion regarding the expression and purification of the recombinant type I and type III antifreeze proteins used in this study.

3.1.1 Expression and purification of T1D and T1N

T1D was designed to contain five repeats of the 11 amino acid repeat units from winter flounder [106]. The sequence of the gene to code for T1D was designed to form long synthetic oligonucleotides in the correct register during PCR reactions. Since this gene includes repetitive units, special care must be taken when designing the primers to prevent misannealing in PCR reactions. The four oligonucleotides were amplified by using an overlap extension technique. After PCR amplifications, the gene was purified using agarose gel electrophoresis and then the gel piece was purified. In the following step, the gene was successfully double digested using

endonucleases that have cut sites at both ends of the gene. This sample was cloned into the double digested and purified expression vector, pET20b and then transformed into the *E.Coli* host strain. After overnight transformation, colonies grown on the agar plates were selected and expressed overnight in liquid cell culture medium (LB). Cells grown in the cell culture were collected by centrifugation and their gene was extracted (Miniprep, Qaigen). These DNA samples were tested in additional PCR reactions and successful samples were sequenced. One plasmid having the correct sequence was designated as T1D.

Time course of the samples (before induction and every hour after induction) for both soluble and insoluble fractions were collected and monitored by polyacrylamide gel electrophoresis in order to determine the optimal expression and purification strategy.

In Figure 3.1, six hour time course of the bacterial protein expression is presented. 1 ml samples were taken during the time course and cells were separated by centrifugation. Pellets were then resuspended in 100 µl BPER (Pierce) and centrifuged at 14000 rpm using a table top centrifuge. Supernatant represents the soluble fraction while the pellets are the insoluble fractions. Insoluble fractions were resuspended again in 100 µl BPER solution for electrophoresis. 20 µl samples were run on the tris-tricine gel at a constant voltage (80 V) for two hours [111]. SDS page was then stained using GelCode Blue staining reagent (Pierce) and destained according to the protocol given in the manufacturer's manual.

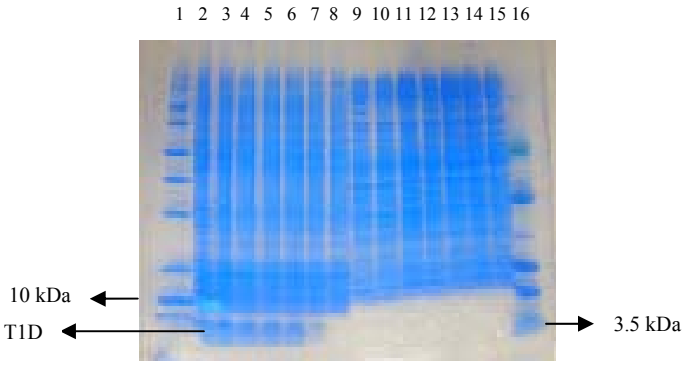

Figure 3.1. Tris-Tricine gel of the time course of T1D expression. Lanes 1 and 16 are the molecular weight markers. Lanes 2-7 are the insoluble fractions of 6 hour postinduction period from 6 hours to 1 hour, respectively. Lane 8 is the insoluble fraction preinduction control. Similarly, lanes 9-14 are the soluble fractions of 6 hour postinduction period and Lane 15 is the soluble fraction preinduction control.

It is clearly seen from Figure 3.1 that T1D is accumulated only in the insoluble fractions. In this case, proteins form aggregates and they are present in inclusion bodies. It is seen that T1D expression starts after induction and expression level increases over a period of 3 hours. After 3 hours T1D expression remains stable up to 6 hours. When compared to the molecular weight markers, the size of T1D is approximately 5000 kDa as expected. It was also determined from the mass spectroscopy data that the actual size of T1D is 5108.6 g/mol.

For site directed bioconjugation purposes, an isoform of T1D was designed. In order to conjugate this protein to a polyallyamine through its carboxy terminus, T1D was modified by replacing the two acidic residues at the N-terminus. This modified protein was named as T1N and a similar procedure was used to create the gene for producing

T1N except that a slightly modified forward extension primer was designed to replace aspartic acid residues with asparagines. After successfully obtaining the T1N gene following the similar protocol as in the case of T1D, 1L culture of T1N was inoculated with 5 ml overnight culture and protein expression time course was monitored.

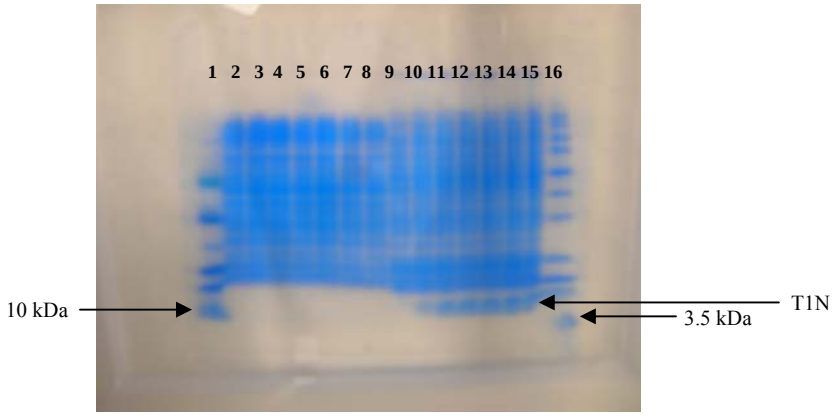

Figure 3.2. Tris-tricine gel of the time course of T1N expression. Lanes 1 and 16 are the molecular weight markers. Lane 2 is the soluble fraction preinduction control. Lanes 3-8 are the soluble fractions of 6 hour postinduction period from 1 hour to 6 hours, respectively. Similarly, lane 9 is the insoluble fraction preinduction control and lanes 10-15 are the insoluble fractions of 6 hour postinduction period.

In Figure 3.2, six hour time course of the bacterial protein expression is presented. 1 ml samples were taken during the time course and cells were separated by centrifugation. It is clearly seen from Figure 3.2 that T1N is also accumulated only in the insoluble fractions. T1N expression starts after induction and expression level increases over a period of 3 hours. After 3 hours T1N expression remains stable up to 6 hours. The size of this protein can be compared with the molecular weight markers. It is seen that the

size of the T1N is also approximately 5000 kDa. It was determined from the mass spectroscopy analysis that the actual size of the T1N is 5105.6 g/mol as expected.

After expressing T1D and T1N, samples were purified using ethanolic extraction. This was possible because the samples were soluble in ethanol. For this, cell pellets were solubilized in ethanol and heated at 75 ^{o}C. Since the proteins are soluble in ethanol, insoluble proteins could be removed by centrifugation. Protein solutions were then mixed with acetone for precipitation. Precipitated protein was recovered by centrifugation and and solubilized. Final solutions were dialyzed against 10 mM ammonium bicarbonate using 1000 Da cutoff membrane and then lyophilized. Details of this procedure is given in Appendix (A.5).

Purified samples were run on the tris-tricine polyacrylamide gel. It is clearly seen from Figure 3.3 that T1D and T1N samples were successfully purified as there are no additional protein bands visible on the gel.

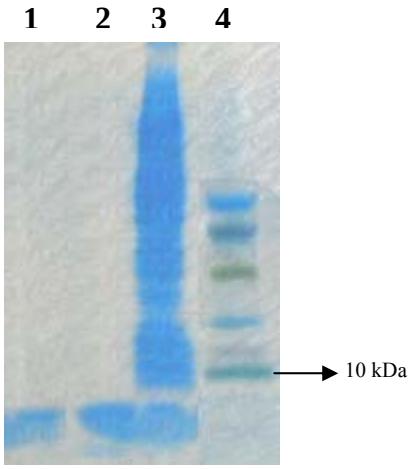

Figure 3.3. Tris-tricine gel of the purified T1D and T1N. Lane 4 is the molecular weight marker. Lane 3 is the T1N sample before purification and lanes 1 and 2 are the purified T1D and T1N, respectively.

Purity of the samples was also confirmed by reverse phase HPLC (Figure 3.4). Two different solutions having different levels of hydrophobicities (solution A: 950 ml double distilled water, 50 ml acetonitrile (HPLC grade, Sigma-Aldrich), 1 ml TFA and solution B: 600 ml acetonitrile, 300 ml isopropanol, 100 ml double distilled water, 0.75 ml TFA) were pumped to the C18 column (150x10 mm) (Restek) with 0.5% gradient of 85% to 100% solution B between 6 and 36 minutes followed by 100% solution B for an additional 5 minutes to ensure that the proteins were eluted from the column.

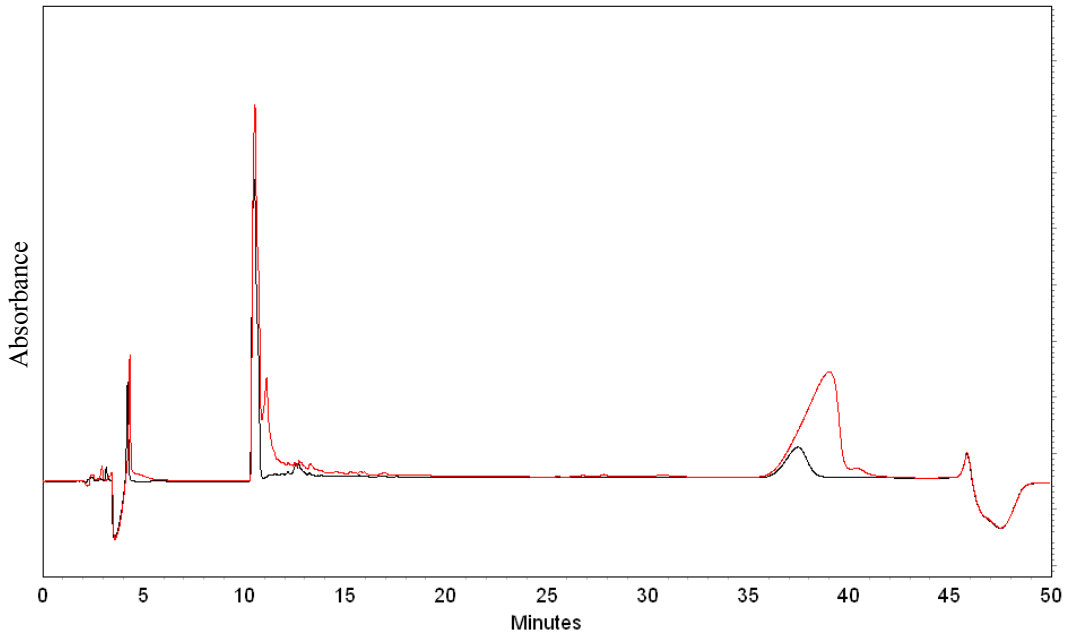

Figure 3.4. Reverse phase HPLC results for T1D (black) and T1N (red).

Since T1D and T1N are highly hydrophobic proteins containing 70% alanine residues in their amino acid sequence, they have a strong interaction with the hydrophobic C18 column. Type I AFPs longer than the HPLC6 have shown to exhibit significant interaction with the C18 columns [112]. Hence, it requires using high

concentration of hydrophobic solvents to elute the proteins from the column. In Figure 3.4, the peak around 10 minutes corresponds to acetonitrile, while the proteins started to be eluted from the column at 36 minutes. Since there is no additional peaks observed in the chromatogram, no further purification was performed.

3.1.2 Expression and purification of T1Dfoldon and RD3Nfoldon

T1D gene was used to prepare a trimer (T1Dfoldon) of this protein using foldon domain. Foldon domain from bacteriophage T4 fibritin is known to form three stranded triple helix which allowed us to make a trimer of α-helical T1D. To facilitate the folding of the protein, a 9 residue linker was designed and used to connect the foldon domain to the carboxy-terminus of T1D. This was a multi-step process involving point mutations and the preparation of the individual components of the plasmid. After successful preparation of the gene, T1Dfoldon was expressed in 1L culture. It was determined that the protein goes into the insoluble fractions as in the case of its precessors.

A time course for the expression of T1Dfoldon was monitored using tris-glycine gel electrophoresis for optimal expression. As can be seen from Figure 3.5 that recombinant T1Dfoldon expression started after induction and no increase in the level of expression was observed after 2 hours. From the DNA sequences the molecular weight of this protein was calculated as 9525.6 g/mol, which seems to be in good agreement with the gel electrophoresis.

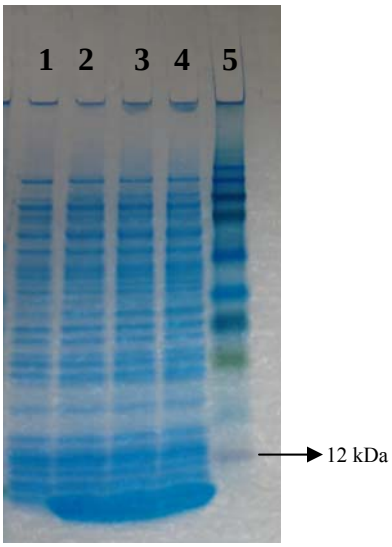

Figure 3.5. Tris-glycine gel of the T1Dfoldon. Lane 5 is the molecular weight marker. Lane 1 is the preinduction control and lanes 2-4 are the postinduction samples collected every 2 hours.

T1Dfoldon was purified from the inclusion bodies using BPER bacterial protein extraction reagent (Pierce) following the general protein extraction and purification protocol given in Appendix. In the final stage of the purification, T1Dfoldon in the pellet form was solubilized using a denaturant, Guanidine hydrochloride (6M) and then refolded in PBS (phosphate buffered saline) for 3 days at 4 ^{o}C to ensure complete refolding of the protein. Refolded protein was then concentrated using a concentrator (ICON, Pierce) until it starts precipitating, which indicates that the solubility limit is reached. A small fraction from this purified sample was then run on the tris-glycine gel to confirm its purity.

Figure 3.6. Tris-glycine gel of the purified T1Dfoldon. Lane 1 is the molecular weight marker. Lanes 2 and 3 are the purified T1Dfoldon samples with and without boiling in SDS, respectively.

In polyacrylamide gel electrophoresis, samples are boiled at 100 ^{o}C for 5 minutes in sodium dodecyl sulfate (SDS) for complete denaturation of the protein. As a control purified T1Dfoldon sample was injected into the gel without boiling. It seems from Figure 3.6 that the sample is still in the denatured monomer form even without boiling prior to injection. This might be the indication of misfolding the T1Dfoldon as it was proved by further characterization studies explained in the following section. The sample seems to be pure enough eliminating the need of further purification.

RD3Nfoldon gene was successfully created as described in T1Dfoldon purification. 1 L culture of RD3Nfoldon was expressed and a time course showing the level of expression was monitored by tris-glycine gel electrophoresis.

As can be seen from Figure 3.7 that RD3Nfoldon expression started after induction and no significant increase in the level of expression was observed after 2 hours. Molecular weight of this protein was calculated from the DNA sequence as 11640.6 g/mol, which seems to be in good agreement with the gel electrophoresis.

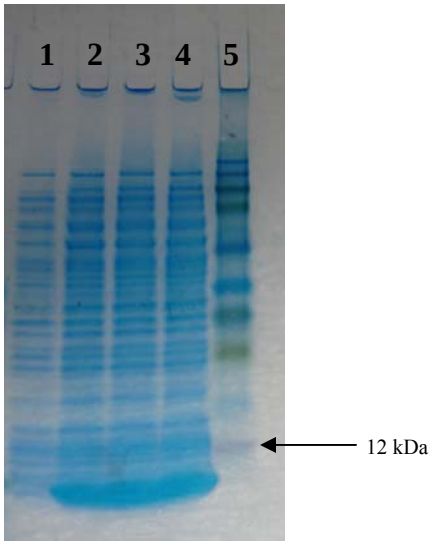

Figure 3.7. Tris-glycine gel of the RD3Nfoldon. Lane 5 is the molecular weight marker. Lane 1 is the preinduction control. Lanes 2-5 are the postinduction samples collected every 2 hours.

After 6 hour expression RD3Nfoldon was purified and concentrated following the same procedure as in the case of T1Dfoldon. In order to test the folding of the RD3Nfoldon, purified samples were run on tris-glycine gel by heating the sample at different temperatures prior to injection. Also, the effect of exposure time of this sample at 100 ^{o}C was investigated.

It is seen in Figure 3.8 that RD3Nfoldon sample that was injected without heating showed more than 90% folding indicated by a darker band at around 30 kDa level which is three times more mass than the monomer. Upon heating at 50 ^{o}C, trimer to monomer ratio decreased to approximately 50%. Increasing the temperature to 60 ^{o}C led the formation of almost 90% monomer in denatured form whereas about 10% of the sample remained folded. For the samples that were heated to 70, 80 and 90 ^{o}C, complete disruption of the folding was observed. These results are consistent with the circular dichroism (CD) spectroscopy analysis data for foldon samples heated from 40 to 90 ^{o}C [88]. In their study, the stability of foldon was assessed by thermal unfolding profiles recorded by CD at the characteristic wavelength for the foldon, 228 nm and the transition temperature was found to be around 60 ^{o}C.

Only the sample heated for 30 seconds at 100 ^{o}C (lane 7 in Figure 3.8) showed some degree of folding, however increased exposure time completely disrupted the stability of the foldon domain.

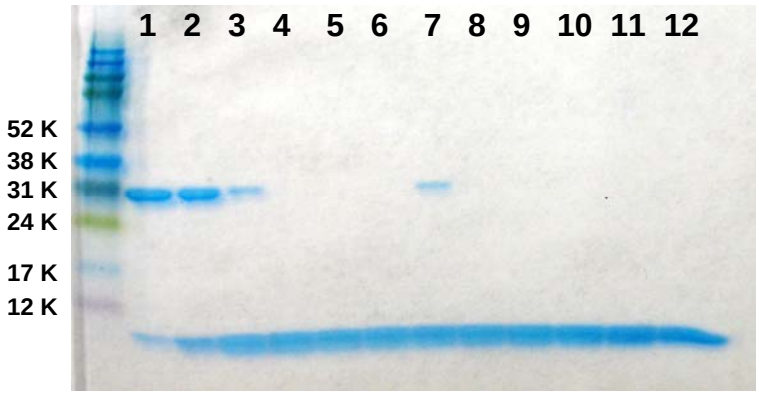

Figure 3.8. Tris-glycine gel of the purified RD3Nfoldon. Lane 1 is the molecular weight marker. Lanes: 1) sample injected without heating. 2-6) sample injected after heating at 50, 60, 70, 80, 90 ^{o}C for five minutes, respectively. 7-12) sample injected after heating at 100 ^{o}C for 30 seconds and 1, 2, 3, 4, 5 minutes.

3.1.3 Circular dichroism spectroscopy studies

The secondary structures of T1D, T1Dfoldon and RD3Nfoldon samples were assessed using CD spectroscopy analysis. Single runs of these samples yielded CD spectra at 25 ^{o}C between 190 and 250 nm as shown in Figure 3.9.

For the T1D and T1Dfoldon samples CD spectra showed a α-helical spectrum with a maximum at short wavelength followed by two minima at longer wavelengths. These results are in accordance with the typical α-helical protein spectra showing that T1D and T1Dfoldon samples were able to fold into a helical structure [113].

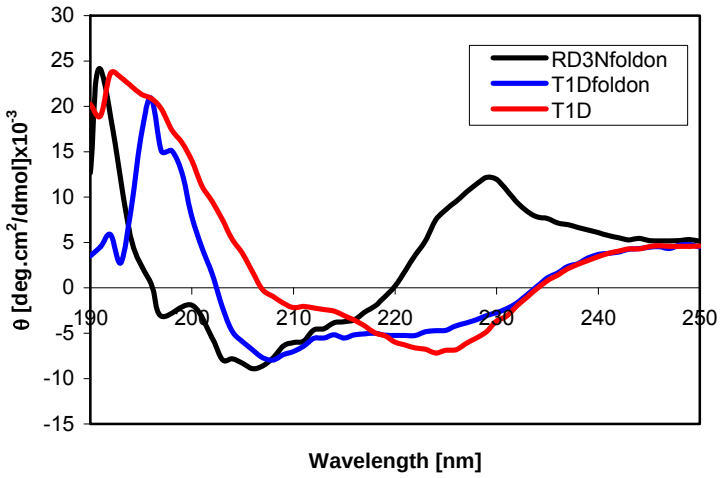

Figure 3.9. Circular dichroism spectra of the α-helical T1D and foldon samples. T1D, T1Dfoldon and RD3foldon samples are colored as red, blue and black, respectively.

CD spectra for RD3Nfoldon showed a minimum at about 208 nm which is a characteristic of the β structure [114]. Foldon domain has a finger print at 228 nm and RD3Nfoldon sample revealed a pronounced maximum at this wavelength showing that this protein is correctly folded [88]. However, for T1Dfoldon sample this characteristic peak for the foldon domain was absent indicating that foldon domain could not trimerize T1D AFP. This was also consistent with the thermal hysteresis results where we have seen that T1Dfoldon was not even as active as the T1D itself showing the incorrect folding of the T1Dfoldon sample (Figure 19).

3.1.4 Expression and purification of RD3CCys and nfe8EGFPCys

One other protein, RD3-C-Cys, was expressed after producing and transforming the gene into the host strain. 1 L culture of RD3CCys expression time course showed that the protein was accumulated in inclusion bodies and the level of protein expression was

slightly increased from 2 to 6 hours as can be seen from Figure 3.10. Molecular weight of this protein was calculated as 7536.8 g/mol from the DNA sequence and it is in good agreement with the SDS-page results.

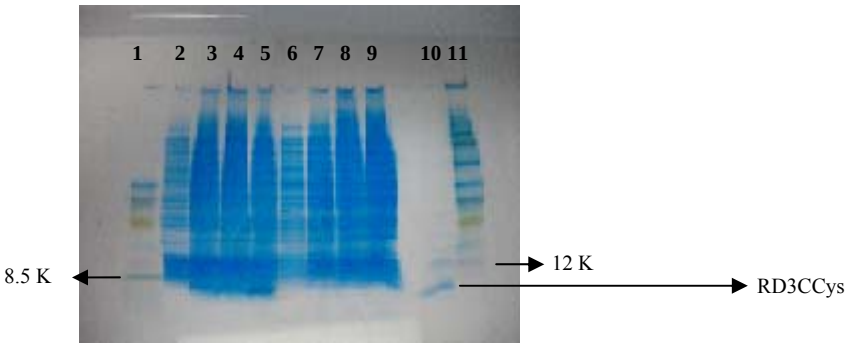

Figure 3.10. Tris-tricine gel of the time course of RD3CCys expression. Lanes 1 and 16 are the molecular weight markers. Lanes 1 and 2 are the low and high range molecular weight markers. Lane 2 is the is the insoluble fraction preinduction control. Lanes 3-5 are the insoluble fractions of 6 hour postinduction period from 2 to 6 hours, respectively. Similarly, lane 6 is the soluble fraction preinduction control and lanes 7-9 are the soluble fractions of 6 hour postinduction period. Lane 10 corresponds to the purified protein.

nfe8EGFPCys was also found to be in the inclusion bodies as can be seen from Figure 3.11. Protein expression slightly increased from 2 to 4 hours and remained the same afterwards.

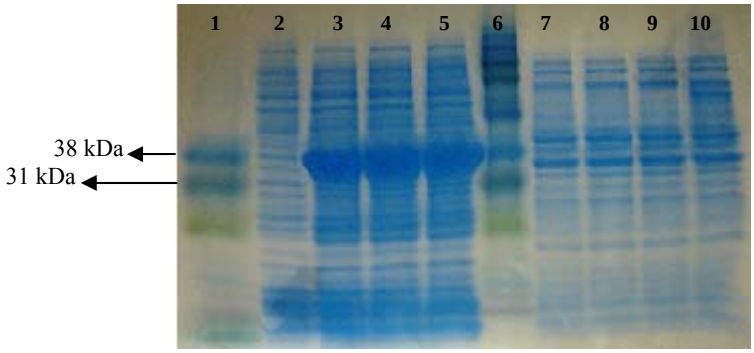

Figure 3.11. Tris-tricine gel of the time course of nfe8EGFPCys expression. Lanes 1 and 6 are the low and high range molecular weight markers. Lane 2 is the insoluble fraction preinduction control. Lanes 3-5 are the insoluble fractions of 6 hour postinduction period from 2 to 6 hours, respectively. Similarly, lane 7 is the soluble fraction preinduction control and lanes 8-10 are the soluble fractions of 6 hour postinduction period.

It is important to note that both RD3CCys and nfe8EGFPCys have cysteine residues that are prone to disulfide bond formation leading to dimerization. In order to prevent this, tris[2-carboxyethyl] phosphine (TCEP) was added to the solutions in the purification steps [96]. TCEP is not stable in phosphate buffers. In fact, a small fraction of RD3CCys was dimerized even after addition of TCEP, explaining the necessity of performing disulfide bond reducing reaction immediately before use [115].

3.2 Characterization of the protein constructs

Type I and type III AFPs produced in this study were characterized using several methods such as size exclusion HPLC, thermal hysteresis measurements and circular dichroism spectroscopy. Following section describes the size exclusion HPLC studies of the reaction products.

3.2.1 Size exclusion studies of the reaction products

3.2.1.1 T1N/PAA reaction

T1N was reacted with PAA through its carboxy terminus using EDC/sulfoNHS chemistry. After the reaction is completed, 500 µl aliquot of the reaction mixture was injected to the size exclusion column to see the size distribution of the conjugated proteins. In size exclusion, molecules are separated by the differences in their sizes. Bigger molecules elute from the column first, followed by small molecules. The reason for this is that bigger molecules can not enter into the pores of the column material having only the void volume excluded by the packing material to travel throughout the column. On the other hand, small ones can access the additional volume of the small pores and eluted later. This method has been used to isolate antifreeze molecules [6, 116, 117]. Figure 3.12 shows the size exclusion profile of the reaction mixture. The first peak corresponds to the reacted product which has a much higher molecular weight than the reactants, which are 17 kDa PAA and 5.1 kDa T1N. The second peak is the unreacted protein peak (labeled as 4) as there is no significant signal showing the presence of PAA. It is seen that the reaction product initially elutes closely behind the void volume (6 ml),

while unreacted T1N eluted 14 minutes after the injection. Samples were fractionated as labeled in Figure 3.12 and analyzed to determine the thermal hysteresis activities and the ice crystal morphologies and discussed in the following sections.

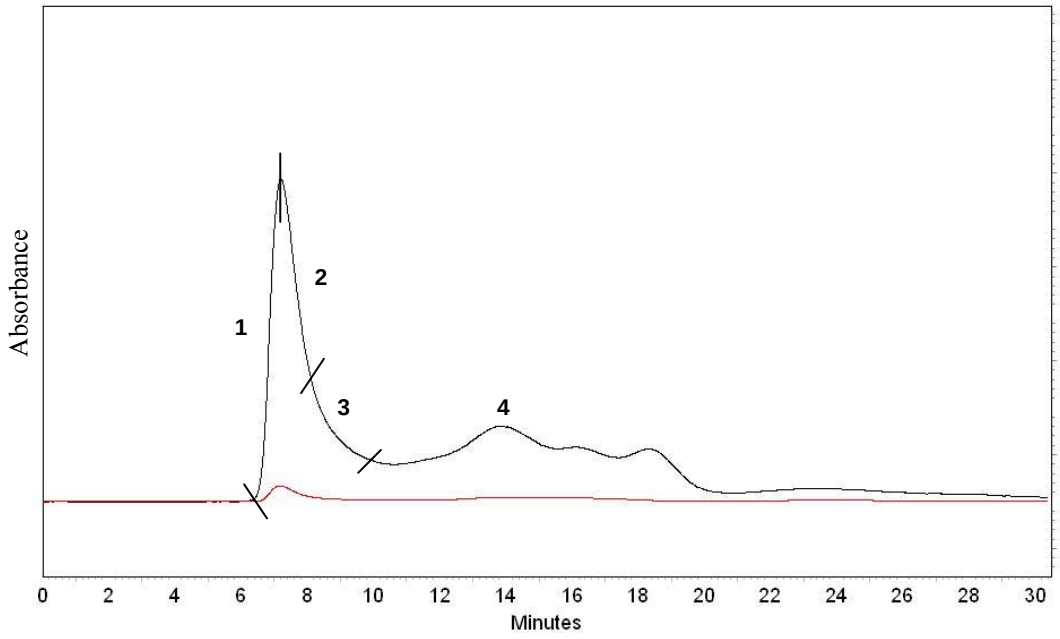

Figure 3.12. Size exclusion HPLC results of the T1N/PAA reaction mixture. Black line: 230 nm, red line: 280 nm.

3.2.1.2 RD3CCys/PAA reaction

RD3CCys was reacted with PAA through its N-terminus cysteine. After the reaction is completed, 500 µl aliquot of the reaction mixture was injected to the size exclusion column to see the size distribution of the conjugated proteins at both 230 and 280 nm. Figure 3.13 shows the size exclusion profile of the reaction mixture. The first peak corresponds to the reacted product which has a much higher molecular weight than the reactants, which are 17 kDa PAA and 7.5 kDa RD3CCys. The second peak is the

unreacted protein peak as can also be understood from the increased absorbances at 280 nm because RD3CCys has a stronger signal at this wavelength as compared to the PAA.

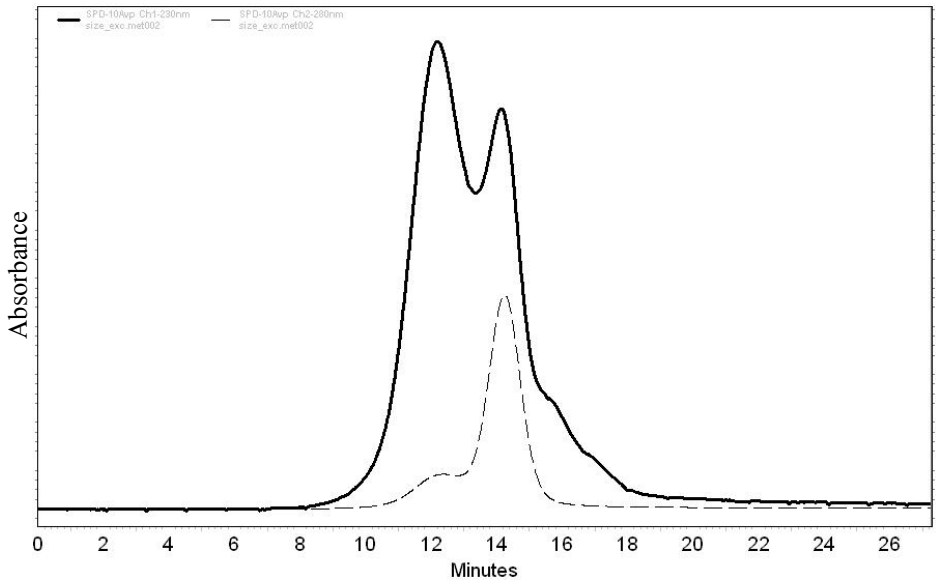

Figure 3.13. Size exclusion HPLC results of the RD3CCys/PAA reaction mixture. Solid line: 230 nm, dashed line: 280 nm.

It is seen from Figure 3.13 that the reaction product started to be eluted shortly after the void volume, while unreacted RD3CCys eluted 14 minutes after the injection. Fractions corresponding to the peaks 1 and 2 were collected for thermal hysteresis activity determinations and discussed in the following sections.

3.2.1.3 nfe8EGFPCys/PAA reaction

nfe8EGFPCys was reacted with PAA through its C-terminus cysteine. After the reaction is completed, 100 µl aliquot of the reaction mixture was injected to the size

exclusion column to see the size distribution of the conjugated proteins at both 230 and 280 nm. Figure 3.14 shows the size exclusion profile of the reaction mixture. The first peak corresponds to the reacted product which has a much higher molecular weight than the reactants, which are 17 kDa PAA and 36.3 kDa nfe8EGFPCys. The second peak is the unreacted protein peak as can also be understood from the increased absorbances at 280 nm because nfe8EGFPCys has a stronger signal at this wavelength as compared to the PAA.

It is seen from Figure 3.14 that the reaction product started to be eluted shortly after the void volume similar to what was observed with the RD3CCys reaction, while unreacted nfe8EGFPCys eluted 14 minutes after the injection. Fractions corresponding to the peaks 1 and 2 were collected for thermal hysteresis activity determinations and discussed in the following sections.

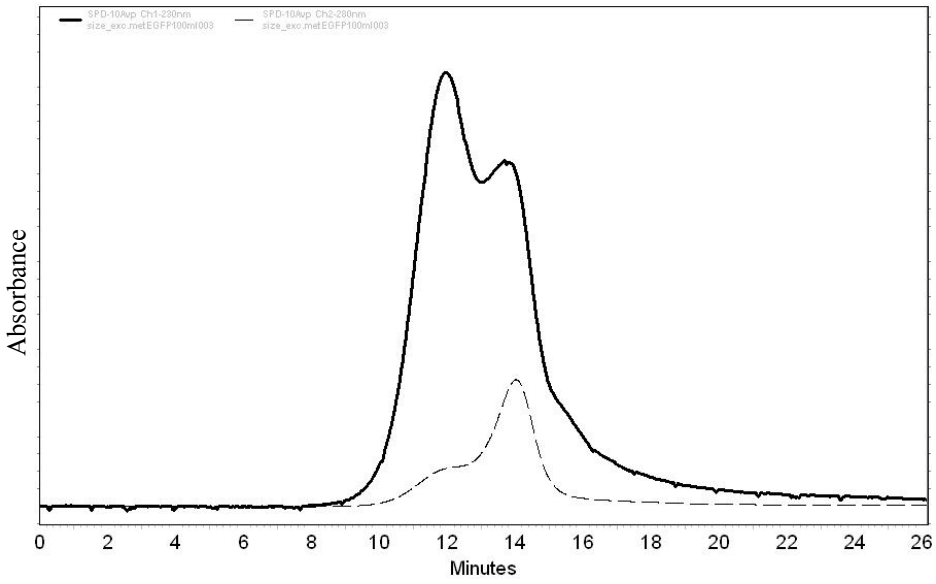

Figure 3.14. Size exclusion HPLC results of the nfe8EGFPCys/PAA reaction mixture. Solid line: 230 nm, dashed line: 280 nm.

3.2.2 Thermal hysteresis studies

The most common way to characterize the AFP activity is to test thermal hysteresis of the protein. Thermal hysteresis is given by the difference between melting and freezing temperatures of an AFP solution. The greater the thermal hysteresis value, more active the AFP is. Unlike colligative properties of the other solutes where their effect is directly proportional to their concentration, AFPs show a noncolligative effect lowering the freezing point. This property allows them to act as antifreeze at much lower concentrations than the other antifreezes such as methanol and polyethylene glycol [5, 118].

Figure 3.15 shows the concentration dependency of the thermal hysteresis for T1D, T1N and T1N/PAA reaction product. All three protein constructs exhibited thermal hysteresis activities. Although T1D and T1N have comparable activities up to 0.2 mM, the activity for T1N was reduced at high concentrations. The reason for reduced thermal hysteresis activity of T1N may be due to the lack of aspartic acid residues that were removed to facilitate site directed conjugation reactions. This protein became highly insoluble after the removal of the acidic residues which seems to play a role affecting the thermal hysteresis activity. When compared to reported thermal hysteresis values of its shorter isoform HPLC-6, T1D is more active for the concentrations lower than 2 mM [58]. As can be seen from Figure 3.15, in low concentration region, T1N/PAA reaction product was approximately twice as active when compared to T1D or T1N. This is consistent with our hypothesis that the addition of multiple AFPs to a polymer chain would increase the concentration of the surface bound proteins especially at low concentrations thereby increasing the activity of the product also by decreasing the

probability of these molecules being desorbed from the ice surface. Hence, we would need to use lesser amount of protein to obtain the same activity in the case of the reaction product.

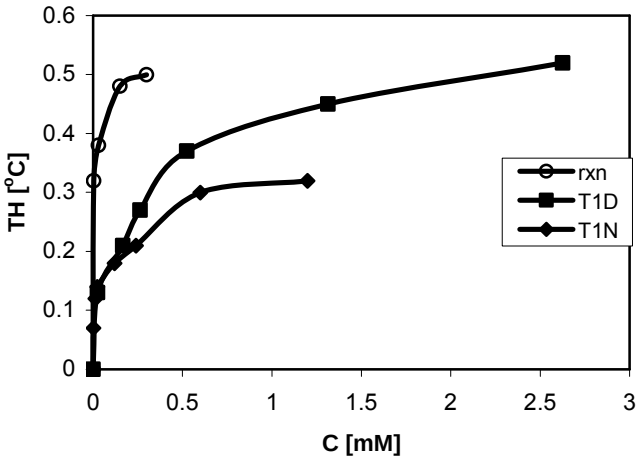

Figure 3.15. Concentration dependence of thermal hysteresis for T1D, T1N and the T1N/PAA reaction product measured at a rate of 0.01 ^{o}C/min.

In Figure 3.16, thermal hysteresis activities of T1D and T1Dfoldon were compared. It was observed that having a foldon domain lowered the thermal hysteresis activity of T1D. This is consistent with CD and gel electrophoresis data showing that the folding of the foldon is interrupted. The reason for this may be that the highly hydrophobic residues of the T1D protein causes them to interact with each other especially when they are in close proximity caused by the foldon domain attached to them which prevents poor association with the surrounding solvent required for folding. We also note that, this construct was designed to have a 9-residue linker which would allow enough space between them for proper folding by estimating the minimum linker

length limited by the diameter of the alpha helix (~1.2 nm). This linker can be kept longer to facilitate proper folding of the T1Dfoldon construct.

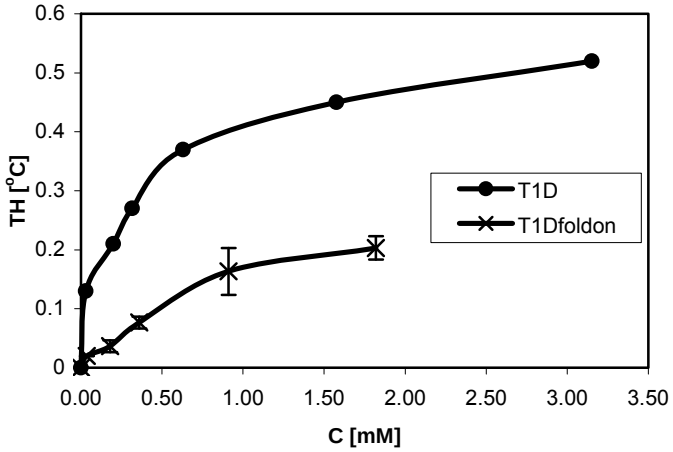

Figure 3.16. Concentration dependence of thermal hysteresis for T1D and T1Dfoldon measured at a rate of 0.01 ^{o}C/min. Error bars represent the standard deviation values calculated from 3 different measurements.

This was not the case for the type III AFPs. RD3Nfoldon showed significantly increased activity as compared to its monomer, RD3N (Figure 3.17). This increase was more pronounced for the low concentration region where the foldon sample was 8 times as active as the monomer. The difference in their activities was lowered to approximately 2.5 fold for concentrations greater than 1 mM. This is due to the decreased number of ice surface sites available for protein adsorption leading to the diminishing effect of having a trimer instead of a monomer.

RD3N thermal hysteresis data was consistent with literature [47]. In a study performed by Nishimiya et al., they have showed that multimers of type III AFP showed

improved thermal hysteresis activity. They have designed multimers of RD3N by tandem repetition of these molecules connected by the original 9-residue linker of the RD3 [69]. They have observed thermal hysteresis activity of approximately 0.74 ^{o}C for 0.5 mM protein concentration, whereas RD3Nfoldon of this study significantly improved this activity and yielded a value of approximately 1.38 ^{o}C at the same protein concentration. The major reason for this improved effect observed in the presence of RD3Nfoldon as compared to previously reported study [47] is due to the uniqueness of the design. RD3N AFPs were trimerized using a foldon domain allowing the individual domains were free to move independently via a flexible 9-residue linker [45] and they were able to engage with the surface more easily as compared to the ones designed in a previous study [47].

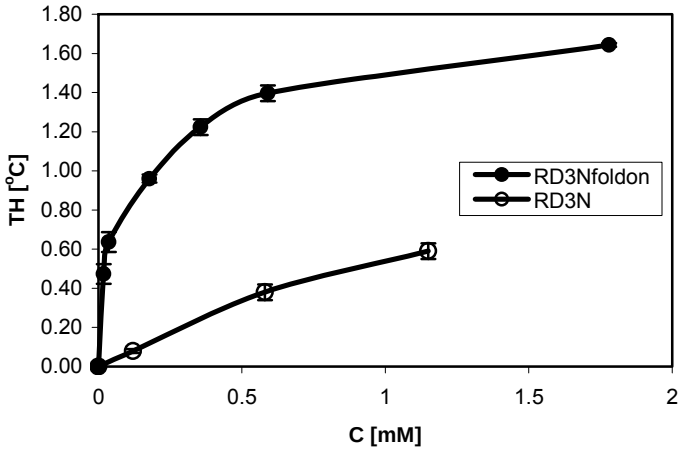

Figure 3.17. Concentration dependence of thermal hysteresis for RD3N and RD3Nfoldon measured at a rate of 0.01 ^{o}C/min. Error bars represent the standard deviation values calculated from 2 and 3 different measurements for RD3N and RD3Nfoldon, respectively.

Conjugation reactions of type III AFPs with PAA worked well in terms of improved thermal hysteresis activities as can be seen from Figure 3.18. nfe8EGFPCys reaction improved the thermal hysteresis activity of the protein from 0.4 to 0.65 ^{o}C at 0.4 mM solution concentration. This improvement was more pronounced at lower concentrations where the thermal hysteresis activity of the protein was approximately doubled and tripled at 0.07 and 0.01 mM, respectively. For RD3CCys reaction, thermal hysteresis activity was increased for only up to 0.15 mM as compared to the protein alone. This might be due to the inability of the C-domain of RD3 to fold when it is connected to another domain. Because the C domain alone shows a typical thermal hysteresis activity for a single domain type III AFP [69].

The activity of the size exclusion fractions from Figure 3.13 and 3.14 was investigated. For both reactions, it was seen that first and second peaks were active showing the presence of the AFPs in both fractions. The activity of the first and second fractions from Figure 3.13 were 0.08 and 0.04 ^{o}C, respectively. Similarly, the activities of the first two fractions from Figure 3.14 were 0.13 and 0.06 ^{o}C, respectively. This proves the presence of the reaction product in the first fraction for both reactions.

It is seen from Figure 3.18 that nfe8EGFPCys yielded slightly higher thermal hysteresis values than RD3CCys. Similar findings were reported for the fusion type III proteins. Introduction of the fusion proteins (maltose binding protein and Thioredoxin) improved the activity of the protein itself [119]. This was explained by the well known Kelvin effect [76]. According to this model, activity increase in the presence of the fusion proteins was attributed to the more ice surface covered by the fusion proteins and it is harder for the ice to grow over them. Hence, if these bigger molecules are covering more

of the surface, they would create larger ice curvatures leading to the lowering of the freezing point due to the increased energy barrier for the addition of the water molecules.

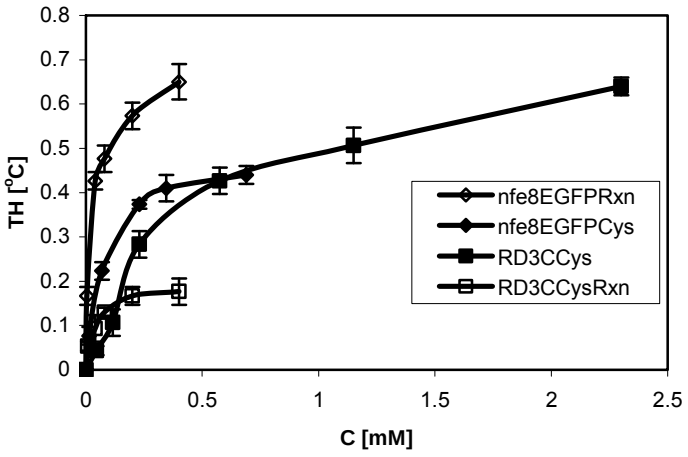

Figure 3.18. Concentration dependence of thermal hysteresis for the type III AFP constructs and their reaction products measured at a rate of 0.01 ^{o}C/min. Error bars represent the standard deviation values calculated from 3 different measurements.

3.2.3 Ice crystal morphologies

Ice crystal morphologies were observed in the presence of the AFPs. It has been previously shown that AFPs of different types produce different ice crystal morphologies which is attributed to their structural differences [63]. Type I AFPs were found to be bound to the bipyramidal (201) plane of ice [76]. Molecular modeling studies revealed that the main source of this interaction was the steric compatibility between the ice plane and the AFP [82]. Type III AFPs were reported to bind to the prism (100) plane of the ice crystal [81]. Similarly, steric contributions and hydrophobic interactions were found to

play an important role in ice binding of these AFPs by molecular dynamics simulations, ice docking and energy minimization studies [42, 76, 80, 120].

In Figure 3.19, ice crystal morphologies in the presence of T1D AFPs for different concentrations were presented. C-axis is shown parallel to the paper plane. In all concentrations, similar ice crystals were obtained (10-15 μm) except at 0.53 mM, where slighlty bigger ice crystals were observed compared to the lower concentrations. It is shown that T1D initially produces truncated bipyramidal ice crystals and then complete bipyramid shape was recovered over time. Hexagonal bipyramidal ice crystal morphologies were reported in the presence of the shorter isoform of T1D [113]. At the burst point, it is observed that ice crystals failed at the tip growing along the c-axis.

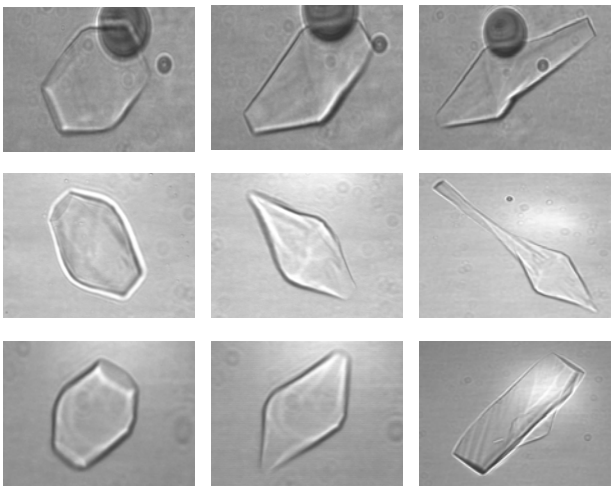

Figure 3.19. Ice crystal morphologies in the presence of T1D. c-axis is parallel to the paper plane. Rows 1 to 3 represent 0.53, 0.26 and 0.02 mM T1D concentrations, respectively.

T1N AFP generally failed to form complete bipyramidal structures especially at low concentrations (Figure 3.20). Truncated ice crystals are clearly visible for 0.24 mM

sample, where the c-axis is perpendicular to the paper plane. Surprisingly, for T1N AFP, burst point morphology was different than its isoform, T1D. Ice crystals were failed at the tip and at the center of the crystal but ice crystal growth was always along the a-axis, which is parallel to the paper plane at 0.24 mM.

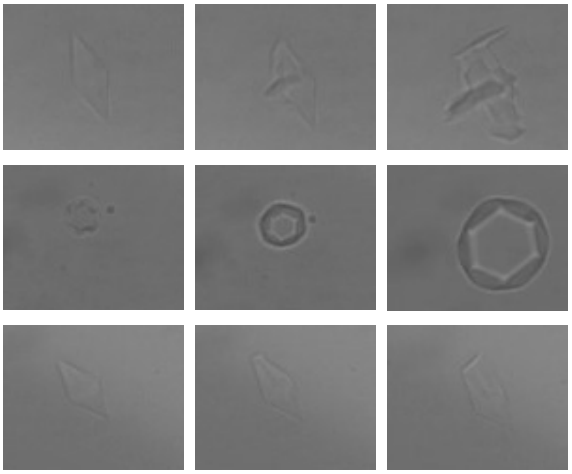

Figure 3.20. Ice crystal morphologies in the presence of T1N. c-axis is parallel to the paper plane except for the second row for which c-axis is perpendicular to the paper plane. Protein concentrations are as follows: Rows 1 to 3: 0.60, 0.24, 0.02 mM, respectively.

Ice crystal morphologies of the T1N/PAA reaction product revealed similar behavior as T1N AFP alone except that much finer ice crystals were obtained even at very low concentrations as can be seen from Figure 3.21. Again, failure occurred at the tip and at the center of the ice crystal carrying similarities from T1N protein.

Figure 3.21. Ice crystal morphologies in the presence of the T1N/PAA reaction mixture. c-axis is parallel to the paper plane. Protein concentrations in rows 1 and 2 are 30 and 3 μM, respectively.

The first and second peaks of T1N with PAA purified by size exclusion HPLC (Figure 3.12) were fractionated and ice crystal morphologies were observed. Thermal hysteresis activities of the samples from first row to the forth row are 0.25, 0.28, 0.2, 0.11 ^{o}C, respectively (Figure 3.22). No ice crystal morphology change was detected for the remainder of the peaks indicating that the first two peaks constitute the majority of the reacted and unreacted protein (data not shown).

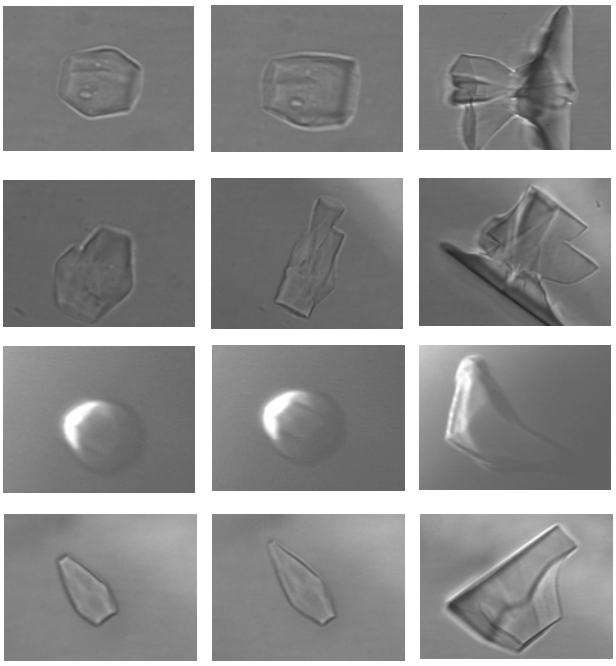

Figure 3.22. Ice crystal morphologies in the presence of the HPLC purified T1N/PAA reaction product. c-axis is parallel to the paper plane except for the third row, which is perpendicular to the paper plane. From left to right: Initial single ice crystal, ice crystal right before growth and right after growth, respectively. First row is the left arm of the first peak in Figure 3.12, while the remaining rows represent the top-right of the first peak, bottom-right of the first peak and the second peak in Figure 3.12, respectively.

Ice crystal morphologies of the other AFP constructs were also investigated. These results are presented in Figure 3.23. Although T1Dfoldon sample does not improve thermal hysteresis activity, it does alter the ice crystal morphology and form perfectly shaped bipyramidal ice crystals (Figure 3.23-A). For this sample, failure occurred along the a-axis which is perpendicular to the paper plane as expected.

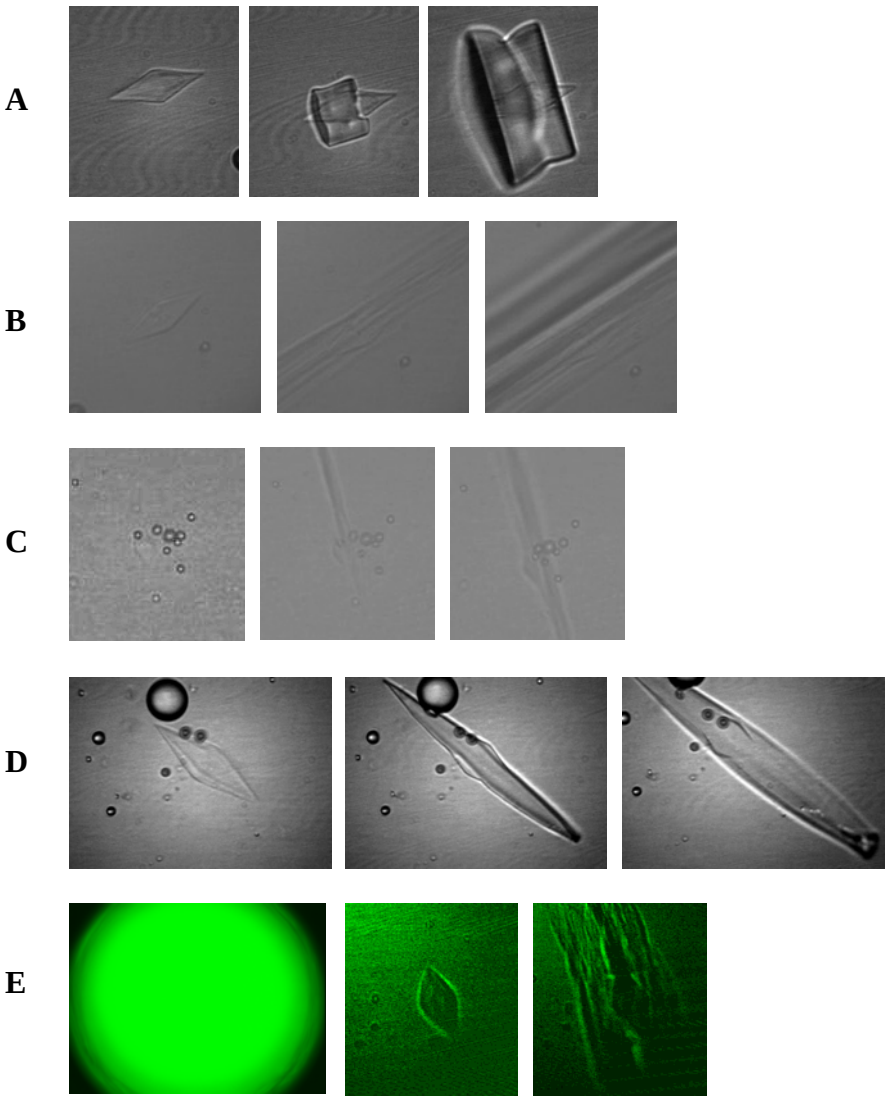

Figure 3.23. Ice crystal morphologies in the presence of the AFP constructs. (A) T1Dfoldon solution (0.91 mM). (B) RD3Nfoldon solution (0.6 mM). (C) RDCCys solution (2.3 mM). (D) RD3CCys reaction mixture. (E) nfe8EGFPCys solution (0.69 mM). In all cases, c-axis is parallel to the paper plane.

For the RD3Nfoldon sample, c-axis to a-axis ratio was decreased significantly forming finer ice crystals (Figure 3.23-B). Very rapid ice growth along the c-axis was observed at the freezing point. RD3CCys was also formed diamond shaped small ice crystals (10 μm) and burst point morphologies were similar to that of RD3Nfoldon (Figure 3.23-C). Similar observations were made in a previous study for a single domain type III AFP [118]. RD3CCys reaction mixture produced bigger ice crystals (~30μm) and the ice crystal growth was observed along the c-axis (Figure 3.23-D).

Ice crystal morphology in the presence of nfe8EGFPCys was investigated using a fluorescence microscope in order to visualize where the fluorescence protein binds to the ice crystal (Figure 26-E). The first column in Figure 3.23-E is the 14 nl nfe8EGFPCys solution suspended in immersion oil. Second column in the same row is the single ice crystal and the last column shows the burst point morphology. It is seen that the protein molecules are surrounding the diamond shaped ice crystal and it fails along the c-axis.

CHAPTER IV

MODELING OF ANTIFREEZE PROTEIN ADSORPTION

Langmuir adsorption isotherm models are used to relate thermal hysteresis and surface coverage values of single-domain and two-domain type III AFP using previously published thermal hysteresis versus concentration data [61]. Surface coverage and binding energy are determined by fitting two independent thermal hysteresis data sets with the classical Langmuir isotherm and a modified isotherm for the one- and two-domain proteins, respectively. Such a comparison is possible because all of the domains have identical structures and should have equivalent binding energies. We first describe the model systems with the governing equations, then derive the isotherms, and finally use these with experimental data to relate thermal hysteresis with surface coverage. This study is also extended to three domain type III AFPs and governing equations are given in the following sections.

4.1 Model systems for a single, two- and three-domain antifreeze protein

We are modeling the reversible adsorption of two different protein configurations onto an ice crystal: a single domain (Figure 4.1-A) and two of the single domains connected by a flexible linker (Figure 4.1-B). For the two domain protein, the adsorbed protein can exist in two states: with one of the domains adsorbed to the ice surface allowing the second domain to freely diffuse only limited by the extent of the linker (*state I*) and with both domains adsorbed to the ice surface (*state II*). Equations used to describe these two processes are given in the following section. It is important to note that NMR analyses of the two-domain type III AFP clearly indicates that the linker is flexible allowing them to move independently of each other [46, 121].

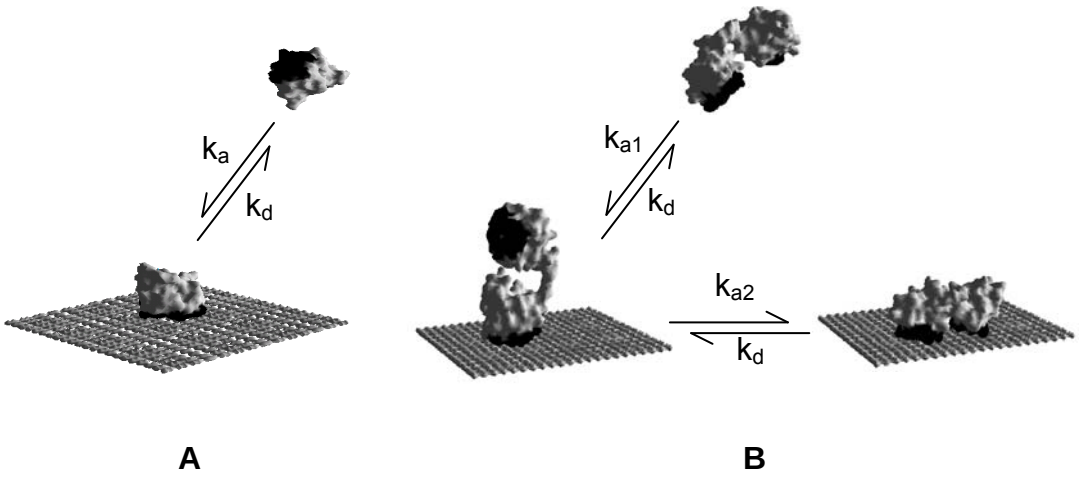

Figure 4.1. Adsorption of proteins to the ice lattice. (A) Single domain type III AFP adsorbs reversibly onto the ice lattice with an adsorption rate constant of k_a. (B) The two-domain type III AFP adsorbs onto the ice lattice in a two-step process. *State I* represents the adsorption of the first domain while *state II* is the two-domain adsorbed state. The corresponding adsorption rate constants are k_{a1} and k_{a2}. In all cases, desorption is governed by the desorption rate constant k_d. Binding faces are shaded.

After modeling two-domain AFP adsorption, we are now modeling the reversible adsorption of three-domain AFP (Figure 4.2-A). RD3Nfoldon is an example of such a molecule where three of the single domains all having linkers are held together by a foldon domain. For the three domain protein, the adsorbed protein can exist in three states: (a) with one of the domains adsorbed to the ice surface (Figure 4.2-B) allowing the other two domains to freely diffuse only limited by the extent of the linkers (*state I*), (b) with two domains adsorbed to the ice surface (Figure 4.2-C) (*state II*), and (c) all three domains adsorbed to the ice surface (Figure 4.2-D) (*state III*). Equations used to describe these three processes are given in the following section.

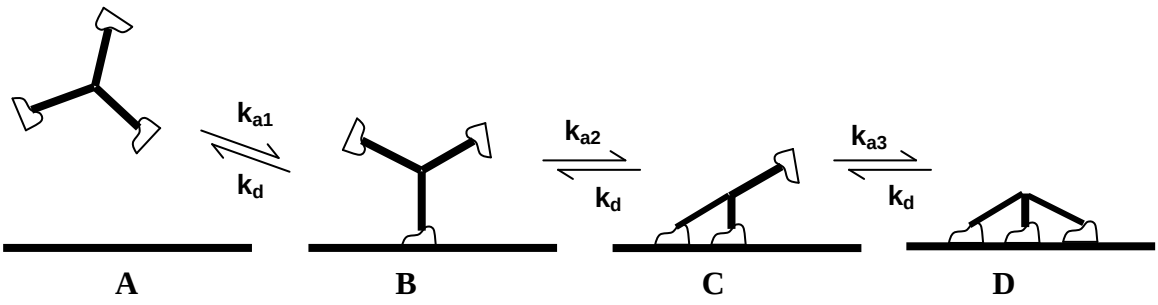

Figure 4.2. Adsorption of three- domain proteins to the ice lattice. (A) Three-domain type III AFP in the solution. (B), (C) and (D) represents three-domain type III AFP adsorption reversibly onto the ice lattice with adsorption rate constants of k_{a1}, k_{a2} and k_{a3}, respectively. *State I* represents the adsorption of the first domain while *state II* and *state III* are the two- and three-domain adsorbed state. In all cases, desorption is governed by the desorption rate constant k_d.

4.2 Langmuir isotherm

Langmuir equilibrium isotherm equation is widely used to describe equilibrium adsorption phenomena. It was developed for gas adsorption but has been extensively applied to adsorption from solution. It has been used previously to describe the adsorption of antifreeze glycoproteins (AFGP) and AFP to ice [62, 78]. The assumption is made that the protein binds as a monolayer to equivalent surface binding sites that are independent, i.e. binding at one site does not affect the binding at other sites. This assumption is consistent with what is known about AFPs.

The kinetic equation for a single domain protein molecule (Figure 4.1-A) can be written as:

$$\frac{d\theta}{dt} = k_a C(1-\theta) - k_d \theta \qquad \textbf{(4.1)}$$

where, θ is the fractional surface coverage, t is time, C is the concentration of the protein in the solution, k_a and k_d are the adsorption and desorption rate constants, respectively. When the adsorption reaches equilibrium (i.e. θ is constant), the Langmuir isotherm equation results [122]:

$$\theta = \frac{KC}{1+KC} \qquad \textbf{(4.2)}$$

where K is the equilibrium binding constant,

$$K = \frac{k_a}{k_d} \qquad \textbf{(4.3)}$$

4.3 Modified Langmuir isotherm for two-domain antifreeze protein

The Langmuir model is modified to account for the two step process of binding a two-domain protein using the same assumptions in the classical Langmuir model with the additional assumptions that the adsorption and desorption rate constants are equivalent for each domain and that the desorption rate constants are not affected by whether the other domain is bound or unbound. When all terms that contribute to formation or elimination of *state I* are considered, the kinetic equation for *state I* is

$$\frac{d\theta_1}{dt} = k_{a1}C(1-\theta_T) - k_d\theta_1 - k_{a2}\theta_1(1-\theta_T) + k_d\theta_2 \qquad \textbf{(4.4)}$$

where θ_1 and θ_2 are the fractional surface coverage values for *state I* and *state II*, respectively, and $\theta_T = \theta_1 + \theta_2$. Increasing θ_1 comes about by either adsorption of one domain from solution with a rate constant of k_{a1} (first term in equation (4.4)) or by desorption of one of the domains of a protein with both domains bound to the surface (*state II*) with a rate constant of k_d (last term in equation (4.4)). Similarly, decreasing θ_1 includes desorption of the singly bound domain into solution with a rate constant of k_d (second term in equation (4.4)) and adsorption of the second domain to the ice surface with a rate constant of k_{a2} resulting in a *state II* protein (third term in equation (4.4)). It should be noted that the adsorption of protein to the surface (the first and third terms) is modulated by the total number of available sites for binding, $1-\theta_T$.

A kinetic equation can similarly be expressed for *state II*:

$$\frac{d\theta_2}{dt} = 2k_{a2}\theta_1(1-\theta_T) - 2k_d\theta_2 \qquad \textbf{(4.5)}$$

where the factors of two arise because the surface coverage of a protein in *state II* is twice as large as a protein in *state I*.

Desorption rate constants for the domains in each state were taken as k_d, since it is assumed that the desorption rate does not depend on the number of domains bound to the surface. At equilibrium, equations (4.4) and (4.5) can be equated to zero, solved for θ_T:

$$\theta_T = \frac{1}{2K_1K_2}\frac{1}{C} + \frac{1}{2K_2} + 1 - \sqrt{\left(\frac{1}{2K_1K_2}\frac{1}{C} + \frac{1}{2K_2}\right)^2 + \frac{1}{K_1K_2}\frac{1}{C}} \qquad \textbf{(4.6)}$$

where K_1 and K_2 are the equilibrium binding constants for *state I* and *state II*, respectively.

4.4 Modified Langmuir isotherm for three-domain antifreeze protein

The Langmuir model is also modified to account for the three-step process of binding a three-domain protein using the same assumptions in the modified Langmuir model.

When all terms that contribute to formation or elimination of *state I* are considered, the kinetic equation for *state I* is

$$\frac{d\theta_1}{dt} = k_{a1}C(1-\theta_T) - k_d\theta_1 - k_{a2}\theta_1(1-\theta_T) + k_d\theta_2 \qquad \textbf{(4.7)}$$

where θ_1 and θ_2 are the fractional surface coverage values for *state I* and *state II*, respectively. Increasing θ_1 comes about by either adsorption of one domain from solution with a rate constant of k_{a1} (first term in equation (4.7)) or by desorption of one of the domains of a protein with two domains bound to the surface (*state II*) with a rate constant

of k_d (last term in equation (4.7)). Similarly, decreasing θ_1 includes desorption of the singly bound domain into solution with a rate constant of k_d (second term in equation (4.7)) and adsorption of the second domain to the ice surface with a rate constant of k_{a2} resulting in a *state II* protein (third term in equation (4.7)). It should be noted that the adsorption of protein to the surface (the first and third terms) is modulated by the total number of available sites for binding, $1-\theta_T$.

A kinetic equation can similarly be expressed for *state II*:

$$\frac{d\theta_2}{dt} = 2k_{a2}\theta_1(1-\theta_T) - 2k_d\theta_2 - 2k_{a3}\theta_2(1-\theta_T) + 2k_d\theta_3 \qquad \textbf{(4.8)}$$

where the factors of two arise because the surface coverage of a protein in *state II* is twice as large as a protein in *state I*.

Similarly, kinetic equation for *state III* is expressed as:

$$\frac{d\theta_3}{dt} = 3k_{a3}\theta_2(1-\theta_T) - 3k_d\theta_3 \qquad \textbf{(4.9)}$$

where, k_{a3} is the adsorption rate constant of the third domain and θ_3 is the fractional surface coverage for *state III* and $\theta_T = \theta_1 + \theta_2 + \theta_3$. Here, the factor of 3 is embedded into the equation 4.9 because the protein in *state III* has three times larger surface area than the protein in *state I*. Also, in this case there are three possible detachments of any of the three domains bound to the surface leading to the formation of *state II*.

At equilibrium, equations (4.7), (4.8) and (4.9) are equated to zero, and after appropriate substitutions, an algebraic cubic equation for θ_T is obtained, where K_1, K_2 and K_3 are the equilibrium binding constants for *states I, II and III,* respectively.

$$(1-\theta_T)^3 + \frac{1}{K_3}(1-\theta_T)^2 + \frac{1+K_1C}{K_1K_2K_3C}(1-\theta_T) - \frac{1}{K_1K_2K_3C} = 0 \qquad \textbf{(4.10)}$$

Solution for θ_T is given by:

$$\theta_T = 1 - \sqrt[3]{-\frac{q}{2} + \sqrt{\frac{q^2}{4} + \frac{p^3}{27}}} - \sqrt[3]{-\frac{q}{2} - \sqrt{\frac{q^2}{4} + \frac{p^3}{27}}} + \frac{a}{3} \qquad \textbf{(4.11)}$$

where,

$q = c + \frac{2a^3 - 9ab}{27}$ and $p = b - \frac{a^2}{3}$. Here, a, b and c are the coefficients of the second, third and the last term in equation 4.10, respectively.

4.5 Relating surface coverage to thermal hysteresis activity

Experimental data is measured as thermal hysteresis versus concentration, yet the equilibrium isotherm equations provide surface coverage (θ) versus concentration. It is necessary to relate thermal hysteresis to θ. This has been done previously by defining a fractional thermal hysteresis activity, which is the ratio between the thermal hysteresis temperature at a given concentration and the maximum attainable thermal hysteresis temperature of that solution [62, 78]. It was suggested that this ratio should be a function of surface coverage, which barring any experimental data the values were simply approximated to be proportional.

In our analysis we do not assume any the relationship between thermal hysteresis and surface coverage. We instead explicitly determine it based on the adsorption isotherms described above (equations (4.2) and (4.6)). We directly relate surface coverage (θ) to thermal hysteresis (TH) through the concentration dependencies. The adsorption isotherm relationships provide the surface coverage as a function of concentration, $\theta(C)$, and experimental data gives us thermal hysteresis as a function of concentration, $TH(C)$. Combining these functions, we can eliminate concentration and

determine the function $TH(\theta)$. One issue with this approach is that the Langmuir equation is dependent on an unknown equilibrium binding constant (K), leaving us with two unknowns, K and θ. However, since we have two independent data sets (the one- and two-domain proteins), so we can solve for both equilibrium constant and surface coverage.

For this procedure to work, the relationship between surface coverage and thermal hysteresis should not be affected by the coupling of domains with the nine-residue linker. As discussed below this may not hold for very low surface coverage, but should hold at higher surface coverage where there is significant binding at neighboring binding sites.

Equation (4.2) was used to calculate the surface coverage with respect to the concentration values that correspond to the experimental thermal hysteresis values reported [61]. Similarly, θ_T values were calculated for the two-domain adsorption from equation (4.6) from equivalent data. These data sets are in themselves ambiguous, because the equilibrium binding constants are not known. Thermal hysteresis versus total surface coverage data were then fit to each other so that they would coincide using the equilibrium constants K_1 and K_2 as fitting parameters. In this procedure, we define an objective function F, which is in essence a function of K_1 and K_2:

$$F_i(K_1, K_2) = \theta_1(K_1, TH_i) - \theta_2(K_1, K_2, TH_i) = 0 \qquad \textbf{(4.12)}$$

where, subscript i denotes the i^{th} experimental point and θ_1 and θ_2 represent the fractional surface coverage values for *state 1* and *state II*, respectively. Equation (4.12) was solved by minimizing the sum of the squares of the function F_i.

In order to fit the two isotherm equations, a relationship between the equilibrium constants (K, K_1, and K_2) needs to be established. The ice binding regions of the protein are identical and in the two domain protein the domains are linked well outside the binding region, it is assumed that the binding energies for each domain are equivalent, and therefore, all else being equivalent, the binding constants for each domain are the same. However, for the two domain protein, K_1 and K_2 are affected by the coupling of the domains.

For K_1, the protein has two independent binding domains, either of which could bind to the ice surface contributing to the binding described by the k_{1a} rate constant in equation 4. This would result in an effective doubling of the equilibrium binding constant suggesting that $K_1 = 2K$, equivalent to double the concentration of the single domain protein. The two domains, however, are not completely independent; they are confined to be within the nine-residue linker length apart. This means that they may not behave as though there is twice single domain concentration. The adsorption of a protein consists of two steps: the Brownian motion (diffusion) of the protein to the surface, followed by one or more collisions with the surface with some probability of sticking upon each collision. For a very low sticking probability, the rate of binding is limited by the number of collisions, which will be determined by the short-range Brownian movement of the domains once it is near to the surface. In this case having two domains with independent local mobility will give you twice the collision frequency, and double the equilibrium binding constant. However, for a high sticking probability, the rate will be limited by the bulk Brownian diffusion that brings the protein close enough to the surface to initiate a collision. In this case, having two domains is not advantageous, because the two domains

will diffuse to the surface as one species. In this case the equilibrium binding constant K_1 will be equivalent to K (or even slightly lower due to the smaller diffusion constant for the two domain protein). If the sticking and diffusion occur with similar rates, K_1 would lie somewhere between K and $2K$.

Although the equilibrium constants K_1 and K_2 were calculated as independent fitting parameters (equation 4.12), they can be related to each other by defining an "effective concentration" that can be used to interpret the data resulting from the curve fitting procedure. Since in *state I* the free domain is confined by the linker to a specific volume, an "effective concentration" of this domain can be calculated. This effective concentration (C_{eff}) can be used to relate the equilibrium constants:

$$K_2 = C_{eff} K_1 \qquad \textbf{(4.13)}$$

To calculate the effective concentration an estimation of the volume available for the free domain to diffuse is needed. In Figure 4.3, four possible orientations of the second domain are shown with the first domain attached to the ice surface. The volume that maps all possible orientations of the second domain can be approximated as a hemisphere, whose volume was taken as a basis to calculate the effective concentration. Radius of the hemisphere was approximated as ~ 4 nm by adding the size of one domain and the full length of the nine residue linker. Then calculating the concentration of one domain in the volume of the hemisphere results in 2.3 mM as the effective concentration.

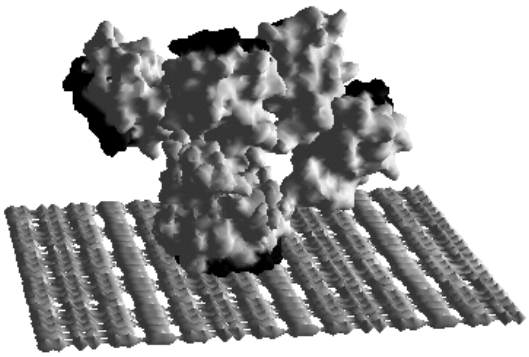

Figure 4.3. Illustration of the origin of the effective concentration. Four possible orientations of the two-domain type III AFP are shown adsorbed onto the ice lattice in *state I* for visualization of effective concentration. Shaded surfaces correspond to the ice binding faces.

Equilibrium constants K_1 and K_2 were calculated for the two extreme situations described above: collision limited ($K_1 = 2K$) and diffusion limited ($K_1 = K$) adsorption. In both cases the fits described the data well for fractional surface coverages greater than 0.2. The effective concentration (K_2/K_1) for diffusion and collision limited cases were calculated to be 2.6 and 0.6 mM, respectively. When these values are compared to the estimated value for the effective concentration, 2.3 mM, it is seen that the diffusion limited case fits the data more closely. For this reason, our calculations are based on the diffusion limited case and hence the equilibrium constants K_1 and K_2, were calculated as 1.9 mM^{-1} and 5, respectively.

The results of the fitting the data (Figure 4.4) illustrates that there is a good agreement between experimental thermal hysteresis values and surface coverage calculated from the isotherm equations. The thermal hysteresis values for surface

coverage greater than 0.2 are the same for the single domain and the two-domain type III AFPs. However, at surface coverage below 0.2, it is observed that the single domain type III AFP gives higher thermal hysteresis for equivalent surface coverage.

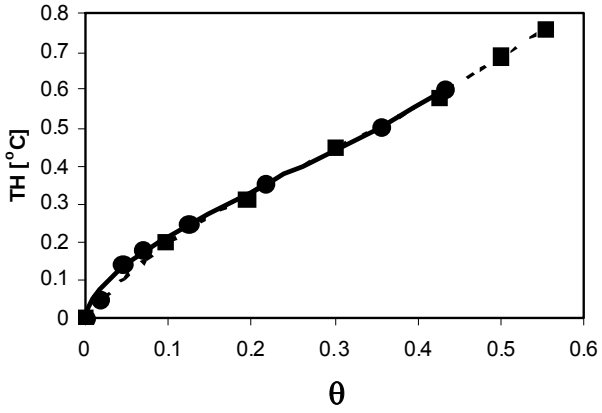

Figure 4.4. Thermal hysteresis as a function of surface coverage. Experimental thermal hysteresis data for the single domain (●) and the two-domain type III AFPs (■). Solid and dashed lines represent the classical and modified Langmuir isotherms, respectively.

With a binding constant for the protein, the energetics of binding a single domain can be determined in terms of the Gibbs free energy:

$$\Delta G^o = -RT \ln K \qquad \textbf{(4.14)}$$

where, K is the adsorption equilibrium constant. Using this relationship, Gibbs free energy of binding for type III AFP at 0˚C is -4.1 kcal/mol (-7.6 *kT)*. It should be noted that Gibbs free energy was calculated using the binding constant of the one domain protein, which is equivalent to the individual domains in the two-domain protein, i.e $K = K_1 = K_2/C_{eff}$.

Classical and modified Langmuir isotherms were applied to one- and two-domain type III AFPs using the equilibrium constants calculated for *state I* and *state II*,

which are 1.9 mM^{-1} and 5, respectively (Figure 4.5). Equilibrium constant for one-domain protein was taken as 1.9 mM^{-1}. It is clearly seen from Figure 4.5 that two-domain protein surface coverage values are greater than the ones for the one-domain protein at low concentrations and the difference between them becomes smaller for higher concentrations.

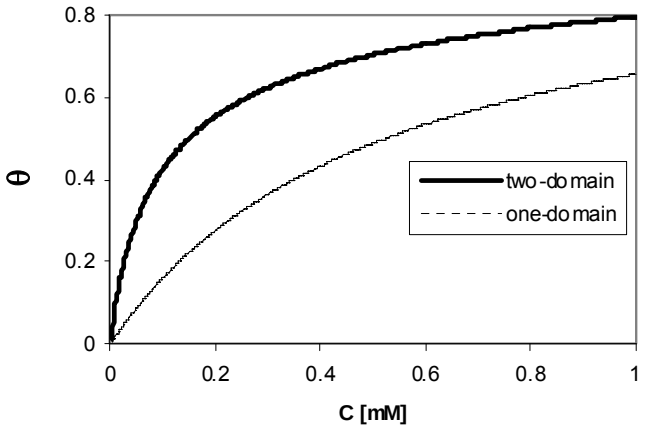

Figure 4.5. Classical and modified Langmuir isotherms applied to one- and two-domain type III AFP adsorption, respectively.

For the three- domain antifreeze protein adsorption, equilibrium constant K_3 was calculated using a similar data mapping technique applied for one- and three-domain proteins. RD3N and RD3Nfoldon thermal hysteresis data were used in the one- and three-domain calculations, respectively. As a result of the fitting procedure, K_1, K_2 and K_3 were calculated as 0.49 mM^{-1}, 7.8 and 31.1, respectively. It is seen from Figure 4.6 that three-domain protein surface coverage values are greater than the ones for the one- domain protein especially at low concentrations and the difference between them becomes smaller for higher concentrations. The same data were plotted against domain concentration in order to see the effect of the multiple domains more clearly. For this,

surface coverage values were plotted against the solution concentration multiplied by 3 for the three-domain AFP. The improved surface coverage values of the three-domain AFP are observed from Figure 4.7 when compared to one- domain AFP. The effect of multimerization is more pronounced when the data are plotted against the solution concentration. The improved effect of three-domain AFP is slightly diminished but is still significantly greater at low concentrations when it is plotted against domain concentration which means that the surface coverage in the presence of three-domain AFP is significantly enhanced at per domain level.

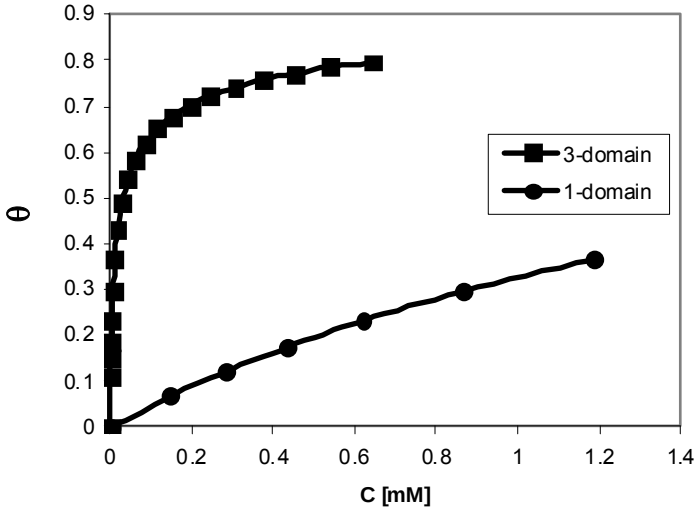

Figure 4.6. Classical and modified Langmuir isotherms applied to one- and three-domain type III AFP adsorption, respectively.

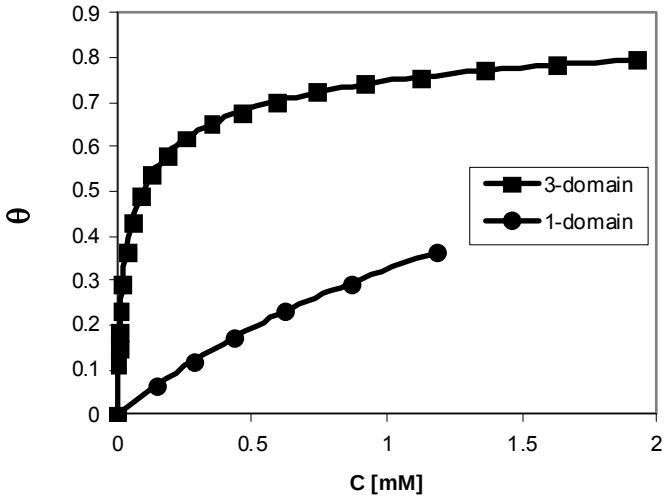

Figure 4.7. Classical and modified Langmuir isotherms applied to one- and three-domain (per domain) type III AFP adsorption, respectively. Surface coverage values were calculated as per domain basis where, concentration for three-domain AFP was multiplied by three.

The results of the fitting data (Figure 4.8) illustrates that there is a good agreement between experimental thermal hysteresis values and surface coverage calculated from the isotherm equations. In the case of three-domain AFPs we have obtained more data for higher surface coverage and thermal hysteresis values than we have obtained for one- and two-domain AFPs. The fitting curve bends up for high surface coverage values and approaches to a limiting thermal hysteresis value of about 2 ^{o}C determined by the number of surface sites left that are available for adsorption.

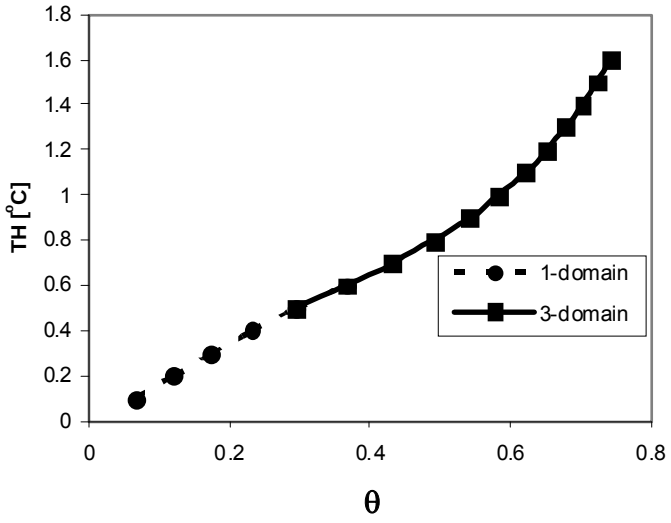

Figure 4.8. Thermal hysteresis as a function of surface coverage. Experimental thermal hysteresis data for the single domain (●) the three-domain type III AFPs (■).

4.6 Kinetic analyses

Time related information about one and two-domain protein adsorption was obtained by rewriting equations (4.1), (4.4) and (4.5) by dividing both sides of the equations by k_d:

$$\frac{d\theta}{d(tk_d)} = KC(1-\theta) - \theta \qquad \textbf{(4.15)}$$

$$\frac{d\theta_1}{d(tk_d)} = K_1C(1-\theta_T) - \theta_1 - K_2\theta_1(1-\theta_T) + \theta_2 \qquad \textbf{(4.16)}$$

$$\frac{d\theta_2}{d(tk_d)} = 2K_2\theta_1(1-\theta_T) - 2\theta_2 \qquad \textbf{(4.17)}$$

where, tk_d is dimensionless time. The term, k_d, is the desorption rate constant, which is combined with time, t, in order to calculate the surface coverage values with respect to dimensionless time. Since the value of the equilibrium constant is known, determining

the adsorption or desorption rate constant would permit the calculation of the real time from the dimensionless time term. This data is not readily available, and so only the dimensionless time data is presented. Equation (4.15) was solved numerically to give $\theta(tk_d)$ and equations (4.16) and (4.17) were solved simultaneously to determine $\theta_1(tk_d)$ and $\theta_2(tk_d)$, where the summation of the last two yielded $\theta_T(tk_d)$ (Figure 4.9). The equilibrium surface coverage are obtained at high tk_d and have been used to corroborate the analytical expression derived for surface coverage. Additionally, a comparison of two-domain AFP in *states I* and *II* gives us a picture of the density of the protein at the ice surface. As the surface has higher coverage, there is a higher proportion of proteins with only one domain bound (*state I*).

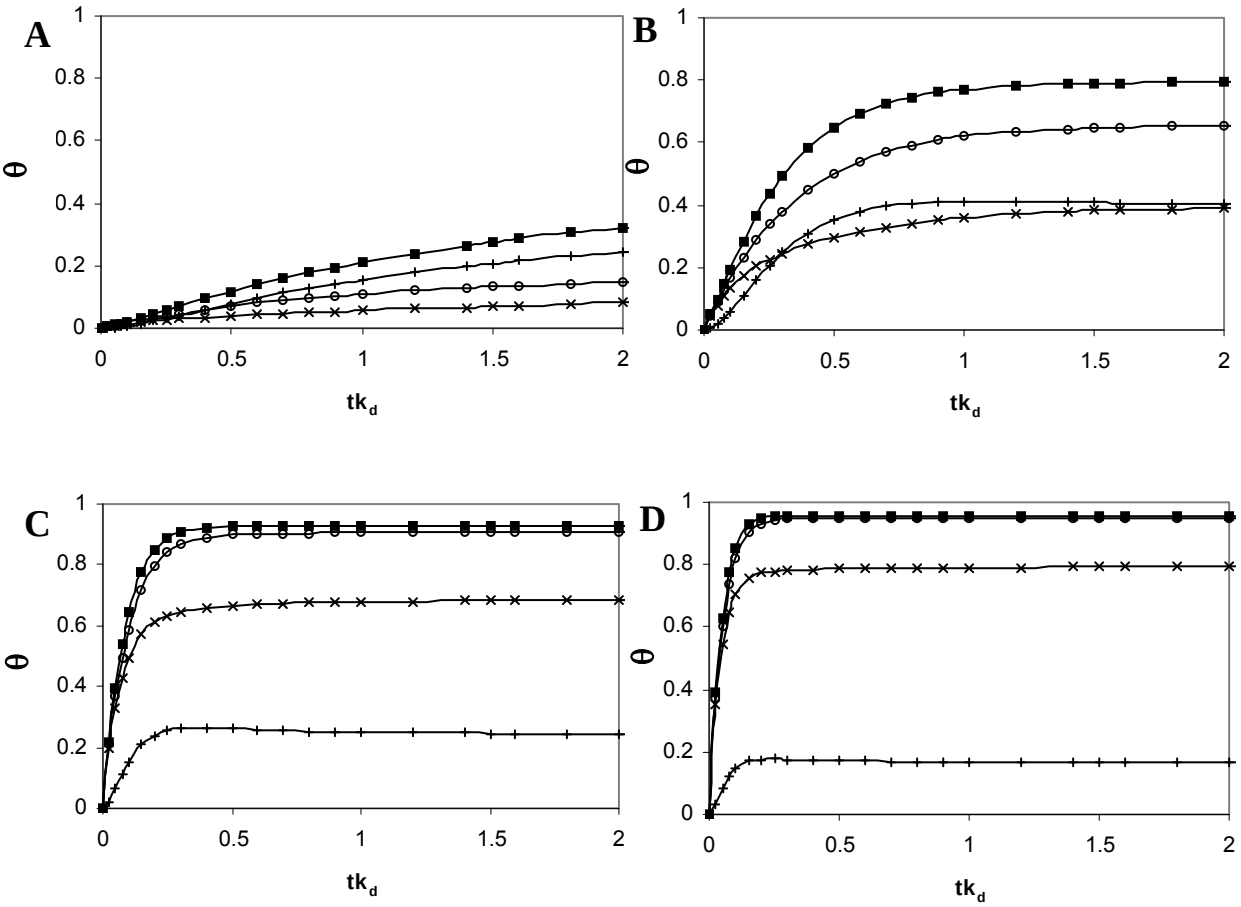

Figure 4.9. Surface coverage values with respect to dimensionless time at different solution concentrations. (A) C= 0.1 mM, (B) C= 1 mM, (C) C= 5 mM, (D) C= 10 mM. Surface coverage values are given for *state I* (x), *state II* (+), *state I* and *state II* total (■), and single domain (●).

The interaction of antifreeze proteins with ice crystal surfaces has been compared to the interaction between a receptor (AFP) and ligand (ice) [9]. However, determining the corresponding binding affinity (equilibrium binding constant) and fraction of ligands bound (surface coverage) is experimentally difficult because of the dynamic nature of the ice-water interface. Within this study, we determined the binding

affinity and relationship between surface coverage and thermal hysteresis for a type III antifreeze protein.

This was accomplished because of the availability of data on a unique two-domain construct of this protein [61]. The two domains of the protein are identical in structure and are connected by a nine-residue flexible linker, resulting in enhanced thermal hysteresis activity at low solution concentrations [61]. The two domains of an identically linked naturally found protein (RD3) have been shown to move independent of each other, enabling the domains to bind to the surface independently, indicating that the observed increase in activity comes from an increased avidity rather than increased affinity of protein [46]. Because the binding of the two domain protein can include a second binding step, the concentration dependence of surface coverage is governed by a different relationship than the single domain protein. However, the relationship between surface coverage and thermal hysteresis should be the same because the AFP domains binding to the ice surface are identical in structure. Since the binding affinities of the domains of the one- and two-domain proteins are the same, the independent thermal hysteresis data for the one- and two-domain proteins can be used to determine the two unknowns of the binding affinity and surface coverage.

This is different than other instances where the activity of AFP has been altered. For several different types of AFP, it has been demonstrated that increasing the ice binding surface area of the protein increases the antifreeze activity. For instance, the helical proteins such as those from winter flounder and *Tenebrio molitor*, have exhibited increased thermal hysteresis by extending the length of the protein [68, 71]. The activity increase is attributed to an increased affinity for the surface by increasing the binding

face or size of the protein [123, 124]. Point mutations have also been shown to affect the thermal hysteresis by reducing the geometric fit of the protein to the ice surface [56, 125]. This also is attributable to a change in the affinity for the ice surface. In these cases, each time a new set of thermal hysteresis data is added, an additional unknown binding affinity is also introduced. This always leaves one more unknown than sets of data. The two domain constructs are the only AFPs known to alter activity through avidity.

The first step in obtaining the binding constants and surface coverage was to modify the Langmuir adsorption isotherm to include the two-step binding process of the two-domain protein. It should be noted that this isotherm may be of more general use for the adsorption of other molecules that have two independent adsorbing regions, such as bolaform surfactants [126] or tri-block copolymers [127]. In fact, the same principle could be generalized to calculate an isotherm for multi-domain adsorbates such as the three- and four-domain AFPs developed by Nishimiya et al. [69], comb-like polymer surfactants [128], or other molecular architectures with multiple independent binding regions.

The fit of the experimental data sets results in the master thermal hysteresis versus surface coverage plot (Figure 4.5). The thermal hysteresis values obtained for a given surface coverage are the same for the single domain and the two-domain type III AFPs for surface coverage values greater than 0.2, showing a very good fit for the two sets of data. However, as noted above, there is a deviation between one- and two-domain type III AFP at low surface coverage. The single domain protein yields higher thermal hysteresis for the same surface coverage. One might initially attribute this to larger errors in the measurement of low thermal hysteresis values. But looking deeper, this can be

explained by the average spacing between adsorbates on the ice crystal lattice. Thermal hysteresis is attributed to the Kelvin effect, where the ice crystal growth is inhibited by the increased curvature of ice growing between adsorbed proteins [129]. The smaller the distance between proteins, the larger the thermal hysteresis is. Figure 4.10 shows examples of 10 and 50% surface coverage for one- and two-domain proteins. At 10% coverage, the surface is sparsely populated with protein. It makes sense that molecular spacing between adsorbed protein molecules would be higher for two-domain AFP molecules at the same surface coverage, because the two domains of the two-domain protein will adsorb on neighboring sites, leaving more open space for a given surface coverage. However, having a second domain will no longer have a significant effect at higher surface coverage where there is a similarly high probability of single domain proteins occupying neighboring sites. This transition occurs around 20-25% surface coverage.

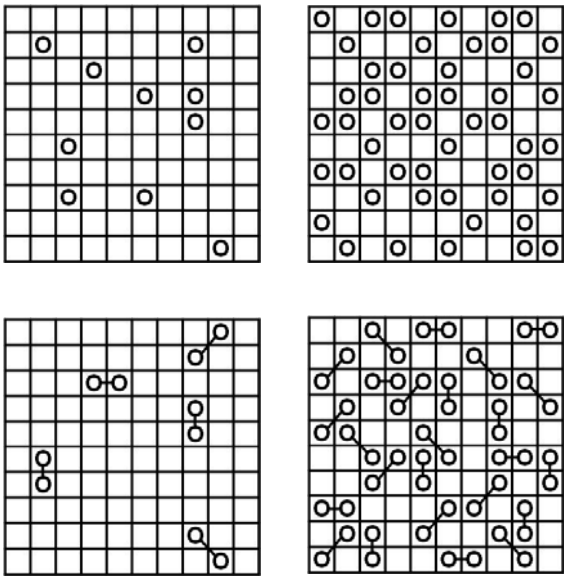

Figure 4.10. One- and two-domain protein adsorption on an ice lattice. Circles and connected circles represent the surface sites that are occupied by one- and two-domain protein molecules, respectively. The first column is an example of 10% surface coverage, the second column has 50% surface coverage.

In previous work, the Langmuir equation was used to model thermal hysteresis data [78] and estimate the binding energy of type I winter flounder AFP [62]. Since the relationship between thermal hysteresis and the surface coverage of protein was not available, they made the approximation that the thermal hysteresis is proportional to fractional surface coverage with a proportionality constant of the estimated maximum thermal hysteresis. This presumed linear relationship fit the thermal hysteresis data to a first approximation. Our data (Figure 4.5) illustrates that their approximation was adequate (particularly for higher surface coverage), but breaks down at lower surface coverage where we observe significant deviation from linearity.

The binding constant for the type III AFP domain was determined to be 1.9 mM^{-1}. This corresponds to an equilibrium dissociation constant (K_d) of 0.53 mM, which is very weak in terms of typical receptor-ligand interactions. The corresponding -4.1 kcal/mol (7.6 *kT)* binding energy is indicative of a significant, but relatively weak interaction compared to the expected energy of interaction for an "irreversibly" bound protein. This is consistent with theoretical predictions for the type I AFPs that exhibit similar thermal hysteresis activities [62].

The reversible process with weak binding is compatible with the reversible step of AFP interaction with ice as described by Kristiansen and Zachariassen [6]. However, instead of a simple partitioning of the protein into an interfacial region as proposed in their model, our data analysis is consistent with direct AFP interact with the ice crystal during this reversible step. It has been shown that two linked AFP domains are not sufficient to increase the thermal hysteresis, but that the domains must be able to have an orientation where they can both bind to the surface [61]. If AFPs were not interacting with the ice crystal surface during the reversible step, having an additional domains in the protein structure would not have any effect on the activity. However, it has been shown that multimers of type III AFPs significantly enhance thermal hysteresis activity [61, 69]. Therefore, AFPs must interact with the ice surface in order to justify the differences in the activities.

CHAPTER V

SUMMARY

We have succesfully expressed and characterized several type I and type III AFP constructs in order to increase the thermal hysteresis activity. These proteins were modified to create AFP multimers using genetic engineering and bioconjugation techniques. Our results revealed that type III AFP trimer, RD3Nfoldon sample was the most active yielding 1.65 ^{o}C thermal hysteresis activity at 1.8 mM. Many of the reaction products of these protein constructs gave rise to a much better thermal hysteresis activities than the AFPs alone. This improvement in the thermal hysteresis activities were more pronounced especially at low concentrations.

In addition, we have successfully developed new relationships to describe two- and three-domain protein adsorption based on classical Langmuir model. These modified isotherms were used successfully to characterize the adsorption of two- and three-domain antifreeze proteins onto an ice surface, illustrating that the Langmuir adsorption model is sufficient to describe AFP adsorption to an ice crystal. Using classical and modified Langmuir model, the relationship between surface coverage and thermal hysteresis

activity was obtained for a type III antifreeze protein, as well as equilibrium binding constants. It should be noted that modified Langmuir isotherms derived in this study can be of general use and can be further modified and extended to other molecular constructs with multiple independent binding regions.

It is crucial to further investigate the role of the AFP multimers for their increased thermal hysteresis activities in order to make them better candidates for cryopreservation and heat transfer fluid additives. It has been shown in this study that the novel AFP constructs have increased activities which should lead to other studies to find possibly more active AFPs. Perhaps originally hyperactive insect AFPs can be oligomerized to broaden the thermal hysteresis window. More importantly, designing superior AFP constructs which would have considerable thermal hysteresis activities at significantly low concentrations would make it much more economical to use them as an additive in these systems. Bioreactor systems can be designed and optimized to produce AFPs in large quantities along with the optimized down stream conjugation reactions and purification methodologies. Developing molecular biology techniques and bioconjugation technology will shed light to designing novel synthetic materials that are suitable to use in such applications.

BIBLIOGRAPHY

[1] A. L. Devries, *Antarctic Communities – Species, Structure and Survival*, Cambridge University Press: 1997.

[2] M. Griffith, K. V. Ewart, Antifreeze Proteins and Their Potential Use in Frozen Foods, *Biotechnology Advances.* 13 (**1995)** 375.

[3] G. L. Fletcher, C. L. Hew, P. L. Davies, Antifreeze proteins of teleost fishes, *Annual Review of Physiology.* 63 (**2001)** 359.

[4] J. Baardsnes, P. L. Davies, Contribution of hydrophobic residues to ice binding by fish type III antifreeze protein, *Biochimica Et Biophysica Acta-Proteins And Proteomics.* 1601 (**2002)** 49.

[5] S. Venketesh, C. Dayananda, Properties, potentials, and prospects of antifreeze proteins, *Critical Reviews in Biotechnology.* 28 (**2008)** 57.

[6] E. Kristiansen, K. E. Zachariassen, The mechanism by which fish antifreeze proteins cause thermal hysteresis, *Cryobiology.* 51 (**2005)** 262.

[7] A. D. J. Haymet, L. G. Ward, M. M. Harding, C. A. Knight, Valine substituted winter flounder 'antifreeze': preservation of ice growth hysteresis, *Febs Letters.* 430 (**1998)** 301.

[8] W. Zhang, R. A. Laursen, Structure-function relationships in a type I antifreeze polypeptide - The role of threonine methyl and hydroxyl groups in antifreeze activity, *Journal of Biological Chemistry.* 273 (**1998)** 34806.

[9] Z. C. Jia, P. L. Davies, Antifreeze proteins: an unusual receptor-ligand interaction, *Trends in Biochemical Sciences.* 27 (**2002)** 101.

[10] H. M. Young, G. L. Fletcher, Antifreeze protein gene expression in winter flounder pre-hatch embryos: Implications for cryopreservation, *Cryobiology.* 57 (**2008)** 84.

[11] K. A. Soltys, A. K. Batta, B. Koneru, Successful nonfreezing, subzero preservation of rat liver with 2,3-butanediol and type I antifreeze protein, *Journal of Surgical Research.* 96 (**2001)** 30.

[12] G. Amir, L. Horowitz, B. Rubinsky, B. S. Yousif, J. Lavee, A. K. Smolinsky, Subzero nonfreezing cryopresevation of rat hearts using antifreeze protein I and antifreeze protein III, *Cryobiology.* 48 (**2004)** 273.

[13] G. Amir, B. Rubinsky, Y. Kassif, L. Horowitz, A. K. Smolinsky, J. Lavee, Preservation of myocyte structure and mitochondrial integrity in subzero cryopreservation of mammalian hearts for transplantation using antifreeze proteins - an electron microscopy study, *European Journal of Cardio-Thoracic Surgery.* 24 (**2003)** 292.

[14] H. M. Chao, P. L. Davies, J. F. Carpenter, Effects of antifreeze proteins on red blood cell survival during cryopreservation, *Journal of Experimental Biology.* 199 (**1996)** 2071.

[15] G. Amir, B. Rubinsky, L. Horowitz, L. Miller, J. Leor, Y. Kassif, D. Mishaly, A. K. Smolinsky, J. Lavee, Prolonged 24-hour subzero preservation of heterotopically transplanted rat hearts using antifreeze proteins derived from arctic fish, *Annals of Thoracic Surgery.* 77 (**2004)** 1648.

[16] K. A. R. Ismail, M. M. Radwan, Modeling of ice crystal growth in laminar falling films for the production of pumpable ice slurries, *Energy Conversion and Management.* 44 (**2003)** 65.

[17] J. W. Meewisse, C. A. I. Ferreira, Validation of the use of heat transfer models in liquid/solid fluidized beds for ice slurry generation, *International Journal of Heat and Mass Transfer.* 46 (**2003)** 3683.

[18] P. W. Egolf, A. Kitanovski, D. Ata-Caesar, E. Stamatiou, M. Kawaji, J. P. Bedecarrats, F. Strub, Thermodynamics and heat transfer of ice slurries, *International Journal of Refrigeration-Revue Internationale Du Froid.* 28 (**2005)** 51.

[19] D. W. Lee, A. Sharma, Melting of ice slurry in a tube-in-tube heat exchanger, *International Journal of Energy Research.* 30 (**2006)** 1013.

[20] A. Saito, Recent advances in research on cold thermal energy storage, *International Journal of Refrigeration-Revue Internationale Du Froid.* 25 (**2002)** 177.

[21] H. Inaba, T. Inada, A. Horibe, H. Suzuki, H. Usui, Preventing agglomeration and growth of ice particles in water with suitable additives, *International Journal of Refrigeration-Revue Internationale Du Froid.* 28 (**2005)** 20.

[22] T. Inada, P. R. Modak, Growth control of ice crystals by poly(vinyl alcohol) and antifreeze protein in ice slurries, *Chemical Engineering Science.* 61 (**2006)** 3149.

[23] P. W. Egolf, M. Kauffeld, From physical properties of ice slurries to industrial ice slurry applications, *International Journal of Refrigeration-Revue Internationale Du Froid.* 28 (**2005)** 4.

[24] V. Ayel, O. Lottin, H. Peerhossaini, Rheology, flow behaviour and heat transfer of ice slurries: a review of the state of the art, *International Journal of Refrigeration-Revue Internationale Du Froid.* 26 (**2003)** 95.

[25] T. Inada, A. Yabe, S. Grandum, T. Saito, Control of molecular-level ice crystallization using antifreeze protein and silane coupling agent, *Materials Science and Engineering A-Structural Materials Properties Microstructure and Processing.* 292 (**2000)** 149.

[26] T. M. Hansen, M. Radosevic, M. Kauffeld, T. Zwieg, Investigation of ice crystal growth and geometrical characteristics in ice slurry (RP-1166), *Hvac&R Research.* 9 (**2003)** 19.

[27] P. Pronk, T. M. Hansen, C. A. I. Ferreira, G. J. Witkamp, Time-dependent behavior of different ice slurries during storage, *International Journal of Refrigeration-Revue Internationale Du Froid.* 28 (**2005)** 27.

[28] S. Grandum, K. Nakagomi, Characteristics of ice slurry containing antifreeze protein for ice storage applications, *Journal of Thermophysics and Heat Transfer.* 11 (**1997)** 461.

[29] S. Grandum, A. Yabe, K. Nakagomi, M. Tanaka, F. Takemura, Y. Kobayashi, P. E. Frivik, Analysis of ice crystal growth for a crystal surface containing adsorbed antifreeze proteins, *Journal of Crystal Growth.* 205 (**1999)** 382.

[30] H. Inaba, New challenge in advanced thermal energy transportation using functionally thermal fluids, *International Journal of Thermal Sciences.* 39 (**2000)** 991.

[31] E. Norgaard, T. A. Sorensen, T. M. Hansen, M. Kauffeld, Performance of components of ice slurry systems: pumps, plate heat exchangers, and fittings, *International Journal of Refrigeration-Revue Internationale Du Froid.* 28 (**2005)** 83.

[32] J. Guilpart, E. Stamatiou, L. Fournaison, The control of ice slurry systems: an overview, *International Journal of Refrigeration-Revue Internationale Du Froid.* 28 (**2005)** 98.

[33] Y. H. Cheng, Z. Y. Yang, H. W. Tan, R. Z. Liu, G. J. Chen, Z. C. Jia, Analysis of ice-binding sites in fish type II antifreeze protein by quantum mechanics, *Biophysical Journal.* 83 (**2002)** 2202.

[34] Z. C. Jia, C. I. DeLuca, H. M. Chao, P. L. Davies, Structural basis for the binding of a globular antifreeze protein to ice, *Nature.* 384 (**1996)** 285.

[35] K. V. Ewart, Q. Lin, C. L. Hew, Structure, function and evolution of antifreeze proteins, *Cellular and Molecular Life Sciences.* 55 (**1999)** 271.

[36] F. Sicheri, D. S. C. Yang, Ice-Binding Structure and Mechanism of An Antifreeze Protein from Winter Flounder, *Nature.* 375 (**1995)** 427.

[37] R. W. R. Crevel, J. K. Fedyk, M. J. Spurgeon, Antifreeze proteins: characteristics, occurrence and human exposure, *Food and Chemical Toxicology.* 40 (**2002)** 899.

[38] D. J. Brown, in: *Fish Antifreeze Proteins*, 2002; pp 109.

[39] G. J. Chen, Z. C. Jia, Ice-binding surface of fish type III antifreeze, *Biophysical Journal.* 77 (**1999)** 1602.

[40] F. D. Sonnichsen, B. D. Sykes, H. Chao, P. L. Davies, The Nonhelical Structure of Antifreeze Protein Type-Iii, *Science.* 259 (**1993)** 1154.

[41] C. I. DeLuca, H. Chao, F. D. Sonnichsen, B. D. Sykes, P. L. Davies, Effect of type III antifreeze protein dilution and mutation on the growth inhibition of ice, *Biophysical Journal.* 71 (**1996)** 2346.

[42] F. D. Sonnichsen, C. I. DeLuca, P. L. Davies, B. D. Sykes, Refined solution structure of type III antifreeze protein: Hydrophobic groups may be involved in the energetics of the protein-ice interaction, *Structure.* 4 (**1996)** 1325.

[43] A. Chakrabartty, V. S. Ananthanarayanan, C. L. Hew, Structure-function Relationship in a Winter Flounder Antifreeze Polypeptide. 1. Stabilization of an alpha-

helical Antifreeze Polypeptide by Charged-group and Hydrophobic Interactions, *Journal of Biological Chemistry.* 264 (**1989)** 11307.

[44] B. Wathen, M. Kuiper, V. Walker, Z. C. Jia, New simulation model of multicomponent crystal growth and inhibition, *Chemistry-A European Journal.* 10 (**2004)** 1598.

[45] X. Wang, A. L. Devries, C. H. C. Cheng, Antifreeze Peptide Heterogeneity in an Antarctic Eel Pout Includes an Unusually Large Major Variant Comprised of 2 7-Kda Type-III Afps Linked in Tandem, *Biochimica Et Biophysica Acta-Protein Structure and Molecular Enzymology.* 1247 (**1995)** 163.

[46] N. B. N. Holland, Y.; Tsuda, S.; Sönnichsen, F. D., Two Domains of RD3 Antifreeze Protein Diffuse Independently, *Biochemistry.* 47 (**2008)** 5935.

[47] K. Miura, S. Ohgiya, T. Hoshino, N. Nemoto, T. Suetake, A. Miura, L. Spyracopoulos, H. Kondo, S. Tsuda, NMR analysis of type III antifreeze protein intramolecular dimer - Structural basis for enhanced activity, *Journal of Biological Chemistry.* 276 (**2001)** 1304.

[48] W. Gronwald, M. C. Loewen, B. Lix, A. J. Daugulis, F. D. Sonnichsen, P. L. Davies, B. D. Sykes, The solution structure of type II antifreeze protein reveals a new member of the lectin family, *Biochemistry.* 37 (**1998)** 4712.

[49] T. P. Ko, H. Robinson, Y. G. Gao, C. H. C. Cheng, A. L. DeVries, A. H. J. Wang, The refined crystal structure of an eel pout type III antifreeze protein RD1 at 0.62-A

resolution reveals structural microheterogeneity of protein and solvation, *Biophysical Journal.* 84 (**2003)** 1228.

[50] N. Guex, M. C. Peitsch, SWISS-MODEL and the Swiss-PdbViewer: An environment for comparative protein modeling, *Electrophoresis.* 18 (**1997)** 2714.

[51] P. L. Davies, B. D. Sykes, Antifreeze proteins, *Current Opinion in Structural Biology.* 7 (**1997)** 828.

[52] C. A. Knight, A. L. Devries, L. D. Oolman, Fish Antifreeze Protein and the Freezing and Recrystallization of Ice, *Nature.* 308 (**1984)** 295.

[53] G. M. Mueller, R. L. McKown, L. V. Corotto, C. Hague, G. J. Warren, Inhibition of Recrystallization in Ice by Chimeric Proteins Containing Antifreeze Domains, *Journal of Biological Chemistry.* 266 (**1991)** 7339.

[54] C. A. Knight, J. G. Duman, Inhibition of Recrystallization of Ice by Insect Thermal Hysteresis Proteins - A Possible Cryoprotective Role, *Cryobiology.* 23 (**1986)** 256.

[55] M. E. Urrutia, J. G. Duman, C. A. Knight, Plant Thermal Hysteresis Proteins, *Biochimica Et Biophysica Acta.* 1121 (**1992)** 199.

[56] H. Chao, F. D. Sonnichsen, C. I. Deluca, B. D. Sykes, P. L. Davies, Structure-Function Relationship In The Globular Type-Iii Antifreeze Protein - Identification of A Cluster of Surface Residues Required for Binding to Ice, *Protein Science.* 3 (**1994)** 1760.

[57] C. I. DeLuca, R. Comley, P. L. Davies, Antifreeze proteins bind independently to ice, *Biophysical Journal.* 74 (**1998)** 1502.

[58] J. Baardsnes, L. H. Kondejewski, R. S. Hodges, H. Chao, C. Kay, P. L. Davies, New ice-binding face for type I antifreeze protein, *Febs Letters.* 463 (**1999)** 87.

[59] H. M. Chao, M. E. Houston, R. S. Hodges, C. M. Kay, B. D. Sykes, M. C. Loewen, P. L. Davies, F. D. Sonnichsen, A diminished role for hydrogen bonds in antifreeze protein binding to ice, *Biochemistry.* 36 (**1997)** 14652.

[60] J. Baardsnes, M. Jelokhani-Niaraki, L. H. Kondejewski, M. J. Kuiper, C. M. Kay, R. S. Hodges, P. L. Davies, Antifreeze protein from shorthorn sculpin: Identification of the ice-binding surface, *Protein Science.* 10 (**2001)** 2566.

[61] J. Baardsnes, M. J. Kuiper, P. L. Davies, Antifreeze protein dimer - When two ice-binding faces are better than one, *Journal of Biological Chemistry.* 278 (**2003)** 38942.

[62] A. Jorov, B. S. Zhorov, D. S. C. Yang, Theoretical study of interaction of winter flounder antifreeze protein with ice, *Protein Science.* 13 (**2004)** 1524.

[63] H. Chao, C. I. Deluca, P. L. Davies, Mixing Antifreeze Protein Types Changes Ice Crystal Morphology without Affecting Antifreeze Activity, *Febs Letters.* 357 (**1995)** 183.

[64] E. Kristiansen, S. A. Pedersen, K. E. Zachariassen, Salt-induced enhancement of antifreeze protein activity: A salting-out effect, *Cryobiology.* 57 (**2008)** 122.

[65] L. Tong, Q. S. Lin, W. K. R. Wong, A. Ali, D. Lim, W. L. Sung, C. L. Hew, D. S. C. Yang, Extracellular expression, purification, and characterization of a winter flounder

antifreeze polypeptide from Escherichia coli, *Protein Expression and Purification.* 18 (**2000)** 175.

[66] H. Chao, R. S. Hodges, C. M. Kay, S. Y. Gauthier, P. L. Davies, A natural variant of type I antifreeze protein with four ice-binding repeats is a particularly potent antifreeze, *Protein Science.* 5 (**1996)** 1150.

[67] S. Y. Gauthier, C. B. Marshall, G. L. Fletcher, P. L. Davies, Hyperactive antifreeze protein in flounder species, *Febs Journal.* 272 (**2005)** 4439.

[68] C. B. Marshall, A. Chakrabartty, P. L. Davies, Hyperactive antifreeze protein from winter flounder is a very long rod-like dimer of alpha-helices, *Journal of Biological Chemistry.* 280 (**2005)** 17920.

[69] Y. Nishimiya, S. Ohgiya, S. Tsuda, Artificial multimers of the type III antifreeze protein - Effects on thermal hysteresis and ice crystal morphology, *Journal of Biological Chemistry.* 278 (**2003)** 32307.

[70] E. K. Leinala, P. L. Davies, D. Doucet, M. G. Tyshenko, V. K. Walker, Z. C. Jia, A beta-helical antifreeze protein isoform with increased activity - Structural and functional insights, *Journal of Biological Chemistry.* 277 (**2002)** 33349.

[71] C. B. Marshall, M. E. Daley, B. D. Sykes, P. L. Davies, Enhancing the activity of a beta-helical antifreeze protein by the engineered addition of coils, *Biochemistry.* 43 (**2004)** 11637.

[72] C. B. Marshall, G. L. Fletcher, P. L. Davies, Hyperactive antifreeze protein in a fish, *Nature.* 429 (**2004)** 153.

[73] A. Chakrabartty, C. L. Hew, The Effect of Enhanced Alpha-Helicity on The Activity of A Winter Flounder Antifreeze Polypeptide, *European Journal of Biochemistry.* 202 (**1991)** 1057.

[74] D. G. Hall, A. Lips, Phenomenology and mechanism of antifreeze peptide activity, *Langmuir.* 15 (**1999)** 1905.

[75] B. Wathen, M. Kuiper, V. Walker, Z. C. Jia, A new model for simulating 3-D crystal growth and its application to the study of antifreeze proteins, *Journal of The American Chemical Society.* 125 (**2003)** 729.

[76] C. A. Knight, C. C. Cheng, A. L. Devries, Adsorption of Alpha-helical Antifreeze Peptides on Specific Ice Crystal Surface Planes, *Biophysical Journal.* 59 (**1991)** 409.

[77] N. Pertaya, C. B. Marshall, C. L. DiPrinzio, L. Wilen, E. S. Thomson, J. S. Wettlaufer, P. L. Davies, I. Braslavsky, Fluorescence microscopy evidence for quasi-permanent attachment of antifreeze proteins to ice surfaces, *Biophysical Journal.* 92 (**2007)** 3663.

[78] T. S. Burcham, D. T. Osuga, Y. Yeh, R. E. Feeney, A Kinetic Description of Antifreeze Glycoprotein Activity, *Journal of Biological Chemistry.* 261 (**1986)** 6390.

[79] Y. G. Mao, Y. Ba, Ice-surface adsorption enhanced colligative effect of antifreeze proteins in ice growth inhibition, *Journal of Chemical Physics.* 125 (**2006)**.

[80] A. D. J. Haymet, L. G. Ward, M. M. Harding, Winter flounder "antifreeze" proteins: Synthesis and ice growth inhibition of analogues that probe the relative importance of hydrophobic and hydrogen-bonding interactions, *Journal of the American Chemical Society.* 121 (**1999)** 941.

[81] J. D. Madura, K. Baran, A. Wierzbicki, Molecular recognition and binding of thermal hysteresis proteins to ice, *Journal of Molecular Recognition.* 13 (**2000)** 101.

[82] M. Lal, A. H. Clark, A. Lips, J. N. Ruddock, D. N. J. White, Inhibition of Ice Crystal-Growth By Preferential Peptide Adsorption - A Molecular Modeling Study, *Faraday Discussions.* (**1993)** 299.

[83] A. L. Cheng, K. M. Merz, Ice-binding mechanism of winter flounder antifreeze proteins, *Biophysical Journal.* 73 (**1997)** 2851.

[84] H. Xu, S. Perumal, X. B. Zhao, N. Du, X. Y. Liu, Z. C. Jia, J. R. Lu, Interfacial adsorption of antifreeze proteins: A neutron reaction study, *Biophysical Journal.* 94 (**2008)** 4405.

[85] Y. Z. Tao, S. V. Strelkov, V. V. Mesyanzhinov, M. G. Rossmann, Structure of bacteriophage T4 fibritin: A segmented coiled coil and the role of the C-terminal domain, *Structure.* 5 (**1997)** 789.

[86] D. N. Woolfson, T. Alber, Predicting Oligomerization States of Coiled Coils, *Protein Science.* 4 (**1995)** 1596.

[87] J. Engel, R. A. Kammerer in: *What are oligomerization domains good for?*, 2000; 2000; pp 283.

[88] S. Frank, R. A. Kammerer, D. Mechling, T. Schulthess, R. Landwehr, J. Bann, Y. Guo, A. Lustig, H. P. Bachinger, J. Engel, Stabilization of short collagen-like triple helices by protein engineering, *Journal of Molecular Biology.* 308 (**2001)** 1081.

[89] J. Stetefeld, S. Frank, M. Jenny, T. Schulthess, R. A. Kammerer, S. Boudko, R. Landwehr, K. Okuyama, J. Engel, Collagen stabilization at atomic level: Crystal structure of designed (GlyProPro)(10)foldon, *Structure.* 11 (**2003)** 339.

[90] J. Nicolas, E. Khoshdel, D. M. Haddleton, Bioconjugation onto biological surfaces with fluorescently labeled polymers, *Chemical Communications.* (**2007)** 1722.

[91] Z. P. Tolstyka, J. T. Kopping, H. A. Maynard, Straightforward synthesis of cysteine-reactive telechelic polystyrene, *Macromolecules.* 41 (**2008)** 599.

[92] J. F. Lutz, H. G. Borner, Modern trends in polymer bioconjugates design, *Progress in Polymer Science.* 33 (**2008)** 1.

[93] J. C. M. Van Hest, Biosynthetic-synthetic polymer conjugates, *Polymer Reviews.* 47 (**2007)** 63.

[94] G. H. Chen, D. Huynh, P. L. Felgner, Z. B. Guan, Tandem chain walking polymerization and atom transfer radical polymerization for efficient synthesis of dendritic nanoparticles for bioconjugation, *Journal of the American Chemical Society.* 128 (**2006)** 4298.

[95] M. A. Gauthier, H. A. Klok, Peptide/protein-polymer conjugates: synthetic strategies and design concepts, *Chemical Communications.* (**2008)** 2591.

[96] G. T. Hermanson, *Bioconjugate Techniques*. Second edition ed.; Elsevier: 2008.

[97] S. Moelbert, E. Emberly, C. Tang, Correlation between sequence hydrophobicity and surface-exposure pattern of database proteins, *Protein Science.* 13 (**2004)** 752.

[98] H. O. Villar, R. T. Koehler, Amino acid preferences of small, naturally occurring polypeptides, *Biopolymers.* 53 (**2000)** 226.

[99] L. Nobs, F. Buchegger, R. Gurny, E. Allemann, Surface modification of poly(lactic acid) nanoparticles by covalent attachment of thiol groups by means of three methods, *International Journal of Pharmaceutics.* 250 (**2003)** 327.

[100] J. Kalia, R. T. Raines, Catalysis of imido group hydrolysis in a maleimide conjugate, *Bioorganic & Medicinal Chemistry Letters.* 17 (**2007)** 6286.

[101] O. K. Farha, R. L. Julius, M. F. Hawthorne, Synthesis of a homotrifunctional conjugation reagent based on maleimide chemistry, *Tetrahedron Letters.* 47 (**2006)** 2619.

[102] R. A. Bednar, Reactivity and PH-Dependence of Thiol to N-ethylmaleimide-Detection of a Conformational Change in Chalcone Isomerase, *Biochemistry.* 29 (**1990)** 3684.

[103] J. Kubler-Kielb, V. Pozsgay, A new method for conjugation of carbohydrates to proteins using an aminooxy-thiol heterobifunctional linker, *Journal of Organic Chemistry.* 70 (**2005)** 6987.

[104] T. C. Liu, J. H. Wang, H. Q. Wang, H. L. Zhang, Z. H. Zhang, X. F. Hua, Y. C. Cao, Y. D. Zhao, Q. M. Luo, Bioconjugate recognition molecules to quantum dots as tumor probes, *Journal of Biomedical Materials Research Part A.* 83A (**2007)** 1209.

[105] Y. Luo, G. D. Prestwich, Hyaluronic acid-N-hydroxysuccinimide: A useful intermediate for bioconjugation, *Bioconjugate Chemistry.* 12 (**2001)** 1085.

[106] R. G. Solomon, R. Appels, Stable, high-level expression of a type antifreeze protein in Escherichia coli, *Protein Expression and Purification.* 16 (**1999)** 53.

[107] D. E. Meyer, A. Chilkoti, Genetically encoded synthesis of protein-based polymers with precisely specified molecular weight and sequence by recursive directional ligation: Examples from the elastin-like polypeptide system, *Biomacromolecules.* 3 (**2002)** 357.

[108] Y. Nishimiya, R. Sato, M. Takamichi, A. Miura, S. Tsuda, Co-operative effect of the isoforms of type III antifreeze protein expressed in Notched-fin eelpout, Zoarces elongatus Kner, *Febs Journal.* 272 (**2005)** 482.

[109] S. C. Gill, P. H. Vonhippel, Calculation of Protein Extinction Coefficients from Amino Acid Sequence Data, *Analytical Biochemistry.* 182 (**1989)** 319.

[110] R. R. Chapleau, R. Blomberg, P. C. Ford, M. Sagermann, Design of a highly specific and noninvasive biosensor suitable for real-time in vivo imaging of mercury(II) uptake, *Protein Science.* 17 (**2008)** 614.

[111] G. v. J. Hermann Schagger, Tricine-Sodium Dodecyl Sulfate-Polyacrylamide Gel Electrophoresis for the separation of Proteins in the Range from 1 to 100 kDa, *Analytical Biochemistry.* 166 (**1987)** 368.

[112] G. J. Warren, C. M. Hague, L. V. Corotto, G. M. Mueller, Properties of Engineered Antifreeze Peptides, *Febs Letters.* 321 (**1993)** 116.

[113] R. P. Evans, G. L. Fletcher, Isolation and characterization of type I antifreeze proteins from Atlantic snailfish (Liparis atlanticus) and dusky snailfish (Liparis gibbus), *Biochimica Et Biophysica Acta-Protein Structure and Molecular Enzymology.* 1547 (**2001)** 235.

[114] S. M. Kelly, T. J. Jess, N. C. Price, How to study proteins by circular dichroism, *Biochimica Et Biophysica Acta-Proteins and Proteomics.* 1751 (**2005)** 119.

[115] J. C. Han, G. Y. Han, A Procedure for Quantitative Determination of Tris(2-Carboxyethyl)Phosphine, an Odorless Reducing Agent More Stable and Effective than Dithiothreitol, *Analytical Biochemistry.* 220 (**1994)** 5.

[116] Y. M. Jin, A. L. DeVries, Antifreeze glycoprotein levels in Antarctic notothenioid fishes inhabiting different thermal enviroments and the effect of warm acclimation, *Comparative Biochemistry and Physiology B-Biochemistry & Molecular Biology.* 144 (**2006)** 290.

[117] B. P. Duncker, S. Y. Gauthier, P. L. Davies, Evidence for a proprotein intermediate during maturation of Type II antifreeze protein in sea raven, Hemitripterus

americanus, *Biochimica Et Biophysica Acta-Protein Structure and Molecular Enzymology.* 1292 (**1996)** 312.

[118] P. L. Davies, J. Baardsnes, M. J. Kuiper, V. K. Walker, Structure and function of antifreeze proteins, *Philosophical Transactions of The Royal Society of London Series B-Biological Sciences.* 357 (**2002)** 927.

[119] C. I. DeLuca, P. L. Davies, Q. L. Ye, Z. C. Jia, The effects of steric mutations on the structure of type III antifreeze protein and its interaction with ice, *Journal of Molecular Biology.* 275 (**1998)** 515.

[120] M. C. Loewen, H. M. Chao, M. E. Houston, J. Baardsnes, R. S. Hodges, C. M. Kay, B. D. Sykes, F. D. Sonnichsen, P. L. Davies, Alternative roles for putative ice-binding residues in type I antifreeze protein, *Biochemistry.* 38 (**1999)** 4743.

[121] N. B. Holland, Y. Nishimiya, S. Tsuda, F. D. Sonnichsen, Activity of a two-domain antifreeze protein is not dependent on linker sequence, *Biophysical Journal.* 92 (**2007)** 541.

[122] A. W. Adamson, Gast, A. P., *Pyhsical Chemistry of Surfaces*. Sixth Edition ed.; John Wiley & Sons, Inc.: 1997.

[123] J. J. Liu, Q. Z. Li, Theoretical model of antifreeze protein-ice adsorption: Binding of large ligands to a two-dimensional homogeneous lattice, *Chemical Physics Letters.* 422 (**2006)** 67.

[124] Q. Z. Li, Y. Yeh, J. J. Liu, R. E. Feeney, V. V. Krishnan, A two-dimensional adsorption kinetic model for thermal hysteresis activity in antifreeze proteins, *Journal of Chemical Physics.* 124 (**2006)**.

[125] C. B. Marshall, M. M. Tomczak, S. Y. Gauthier, M. J. Kuiper, C. Lankin, V. K. Walker, P. L. Davies, Partitioning of fish and insect antifreeze proteins into ice suggests they bind with comparable affinity, *Biochemistry.* 43 (**2004)** 148.

[126] B. Song, G. Q. Liu, R. Xu, S. C. Yin, Z. Q. Wang, X. Zhang, Interfacial self-organization of bolaamphiphiles bearing mesogenic groups: Relationships between the molecular structures and their self-organized morphologies, *Langmuir.* 24 (**2008)** 3734.

[127] T. Haliloglu, D. C. Stevenson, W. L. Mattice, Monte Carlo simulation of the adsorption from a nonselective solvent of symmetric triblock copolymers with sticky end blocks, *Journal of Chemical Physics.* 106 (**1997)** 3365.

[128] N. B. Holland, Y. X. Qiu, M. Ruegsegger, R. E. Marchant, Biomimetic engineering of non-adhesive glycocalyx-like surfaces using oligosaccharide surfactant polymers, *Nature.* 392 (**1998)** 799.

[129] P. W. Wilson, Explaining Thermal Hysteresis By The Kelvin Effect, *Cryo-Letters.* 14 (**1993)** 31.

APPENDIX

A.1 Protein expression/purification protocol

Protein expression:

- Make 5 ml starter culture with (100 μg amplicilin per ml) and grow cells at 37 ^{o}C overnight.

- Put entire culture into 1L LB (Lysogeny broth) and grow cells at 37 ^{o}C until the optical density reaches 0.6 at 600 nm UV wavelength.

- Induce protein expression with 120 mg IPTG.

- Centrifuge the cell culture after six hours and freeze the pellet.

Protein extraction:

- Resuspend the cell pellet in 10 ml BPER.

- Centrifuge at 27000g for 15 minutes.

- Pour off supernatant and resuspend the pellet in BPER.

- Add 10 mg/ml lysozyme and incubate at room temperature for five minutes.

- Add 20 ml 1:10 diluted BPER and centrifuge at 27000g for 15 minutes.

- Pour off supernatant and resuspend the pellet in 30 ml 1:20 diluted BPER.

- Centrifuge at 27000g for 15 minutes.

- Repeat resuspension and centrifugation steps two more times.

- Resuspend the final pellet in 6M Guanadine HCl.

- Dilute the solution 20 fold using refolding buffer (50 mM K_2PO_4, 100 mM NaCl).

- Chill solution at 4^{o}C for 3 days.

Purification and desalting:

- Dialyze the solution against acetic acid (pH 3.7) for 2-3 days with subsequent repetitions.
- After final dialysis, centrifuge at 27000g for 15 minutes.
- Retain supernatant for lyophilizing.

A.2 PCR protocol

Resuspend oligonucleotides in TE buffer to a concentration of 100 μM.

Prepare 10 μM stock solutions for future use (keep the original solution in -80 ^{o}C freezer).

50 μl reaction prepared in PCR tubes:

- 1 μl template primer
- 5 μl forward primer
- 5 μl reverse primer
- 25 μl PCR master mix
- 14 μl nuclease free water

Place PCR tubes in a thermocycler.

Adjust the desired program.

Sample program:

- 2 minutes at 95 ^{o}C for melting the DNA
    - 30 cycles of:
        - 1 minute at 72 ^{o}C for annealing the primers to the DNA.
        - 30 seconds at approximately 5 ^{o}C below the melting point of the primers for primer extension.
        - 1 minute at 72 ^{o}C for the primer extention.
- Refrigeration at 4 ^{o}C for several hours until the sample is removed form the thermocycler.

A.3 Agarose gel electrophoresis protocol

Preparing 1.5% agarose gel:

- Add 1.125 g agarose (molecular biology grade) in a beaker containing 75 ml 1X TAE buffer (cover with aluminum foil).
- Stir and heat until clean liquid is formed.
- Allow it to cool down.
- Add 7.5 µl ethidium bromide and mix by swirling.
- Pour the solution in a cassette and place the appropriate combs for sample injection.
- Allow it to cool down to room temperature.
- Remove the combs and place the gel in a gel box.
- Fill the gel box with 1X TAE solution.

A.4 Polyacrylamide gel electrophoresis running protocol

Tris-tricine gel electrophoresis:

1. Prepare 10X Tris-tricine SDS running buffer stock solution (pH 8.3).
    - 10X solution (1 L):
        - 1M Tris base
        - 1M Tricine
        - 1% SDS

Tris-glycine gel electrophoresis:

2. Prepare 10X Tris-glycine SDS running buffer stock solution (pH 8.3).
    - 10X solution (1 L):
        - 0.25 M Tris base
        - 1.92 M Glycine
        - 1% SDS

Protocol for running the gel:

3. Dilute 10X either Tris-tricine or Tris-glycine running Buffer to 1X in double distilled water
4. Prepare samples in 6X sample buffer
        - 6X sample buffer:
            - 375 mM Tris-HCl (pH 6.8)
            - 9 w% SDS
            - 50% Glycerol
            - 0.02% Bromophenol blue
            - 375 mM DTT

5. Prepare molecular weight markers in 2X sample buffer
6. Electrophorese the gel at 100 volts until the dye front is near the bottom of the gel (approximately 2 hours).

A.5 Type I AFP purification protocol

1. Dissolve cell pellets from 1 L culture in 60 ml, 70% ethanol.
2. Heat this suspension in water bath at 75 ^{o}C for 30 minutes with occasional shaking.
3. Centrifuge at 14000g for 20 minutes.
4. Discard the pellet and keep the ethanol soluble protein.
5. Add four volume of chilled acetone and store the solution at 20 ^{o}C overnight.
6. Centrifuge at 14000g for 45 minutes.
7. Discard the solution and allow the acetone precipitate to dry at room temperature.
8. Resuspend the pellet in 40 ml of 100 mM ammonium bicarbonate.
9. Add 40 ml of saturated ammonium sulfate.
10. Centrifuge at 6300g for 30 minutes.
11. Discard the solution and resuspend the pellet in 40 ml of 100 mM ammonium bicarbonate.

A.6 Protein concentration determination

Protein concentrations (except T1D and T1N. Amino acid analysis was used to determine the concentrations of these two proteins) were determined by calculating the molar extinction coefficients by following the procedure given by Gill and Hippel [109] as explained in the Experimental section. The calibration curves are presented in the following figures.

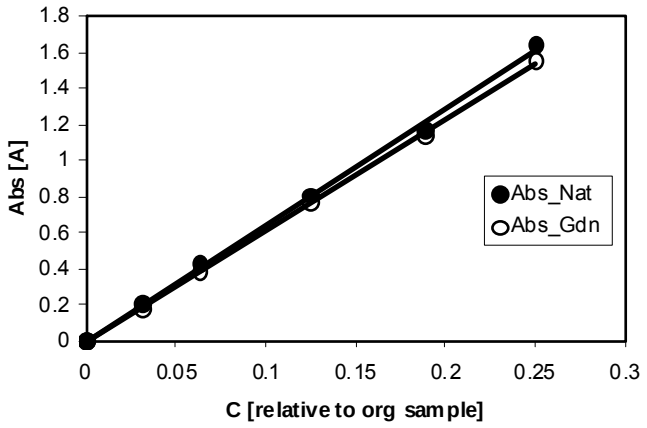

Figure A.1. Calibration curve for RDCCys concentration determination. C is the concentration of the unknown sample relative to the original sample prepared. Lines represent the linear fit to the UV^{280} absorbance versus concentration data.

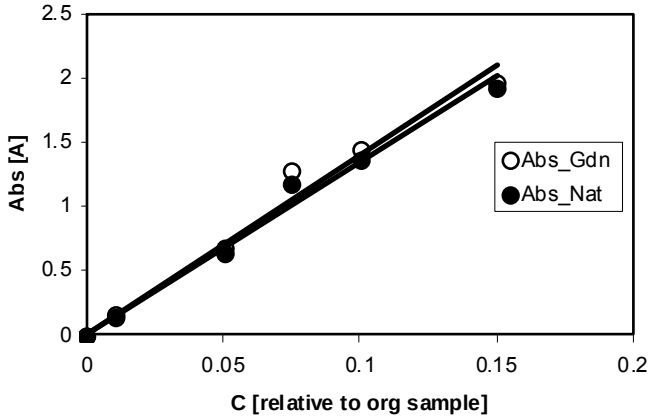

Figure A.2. Calibration curve for nfe8EGFPCys concentration determination. C is the concentration of the unknown sample relative to the original sample prepared. Lines represent the linear fit to the UV^{280} absorbance versus concentration data.

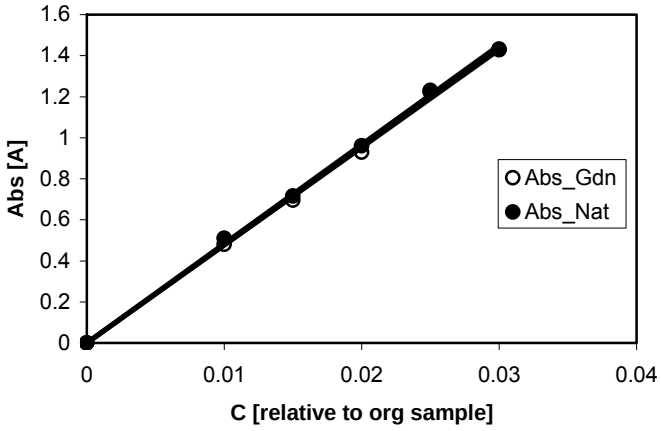

Figure A.3. Calibration curve for RD3Nfoldon concentration determination. C is the concentration of the unknown sample relative to the original sample prepared. Lines represent the linear fit to the UV^{280} absorbance versus concentration data.

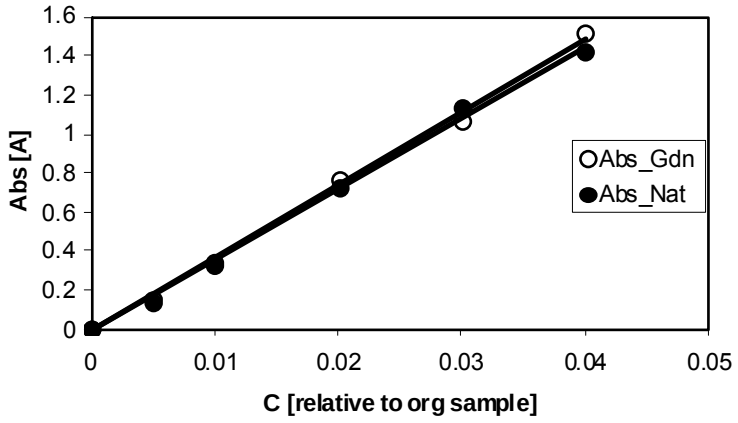

Figure A.4. Calibration curve for T1Dfoldon concentration determination. C is the concentration of the unknown sample relative to the original sample prepared. Lines represent the linear fit to the UV^{280} absorbance versus concentration data. Equations and correlation coefficients (R^2) of the linear fit are presented near the corresponding data.

A.7 Thermal hysteresis measurement protocol

1. Prepare the protein sample at different concentrations.
2. Inject immersion oil into one of the sample wells using a plastic tubing-Pasteur pipette-bulb assembly.
3. Place the nanoliter osmometer assembly onto the microscope stage.
4. Fill the needle attached to the automatic injector with immersion oil.
5. Fill the tip of the needle with the sample.
6. Inject approximately 14 nl sample (for 300 μm droplet) into the oil.
7. Assemble cooling water tubing.
8. Turn on the video controller, light source, computer and VCR.
9. Cover and seal the entire microscope with plastic bag.
10. Connect adsorbent column to the pump and other end onto the sample stage
11. Operate the pump for 15 minutes prior to start cooling the stage.
12. Start flowing chilled water through plastic tubing.
13. Turn on the osmometer temperature controller and bring it to the "freeze" mode.
14. After freezing, switch to the normal mode.
15. Disconnect chilled water line and connect to the tap water line.
16. Wait for 5 minutes for thermal equilibrium and start thawing the sample slowly until obtaining one single ice crystal.
17. Start taking pictures either using the computer or VCR.
18. Wait for 5 minutes for thermal equilibrium and decrease the temperature by 0.01 ^{o}C every minute until ice crystal starts growing.
19. Repeat the experiment three times for each sample.